DECLASSIFIED

AEDC-TR-65-233

cy 1

[redacted]

FEB 9 1966

UNCLASSIFIED

(U) SIMULATED ALTITUDE TESTING OF THE APOLLO SERVICE MODULE PROPULSION SYSTEM (REPORT I, PHASE II DEVELOPMENT TEST)

G. H. Schulz and J. F. DeFord
ARO, Inc.

January 1966

~~In addition to security requirements which must be met, this document is subject to special export controls and each transmittal to foreign governments or foreign nationals may be made only with prior approval of National Aeronautics and Space Administration-Manned Spacecraft Center.~~ (EP-2)

ROCKET TEST FACILITY
ARNOLD ENGINEERING DEVELOPMENT CENTER
AIR FORCE SYSTEMS COMMAND
ARNOLD AIR FORCE STATION, TENNESSEE

[redacted]

DECLASSIFIED

UNCLASSIFIED

NOTICES

When U. S. Government drawings specifications, or other data are used for any purpose other than a definitely related Government procurement operation, the Government thereby incurs no responsibility nor any obligation whatsoever, and the fact that the Government may have formulated, furnished, or in any way supplied the said drawings, specifications, or other data, is not to be regarded by implication or otherwise, or in any manner licensing the holder or any other person or corporation, or conveying any rights or permission to manufacture, use, or sell any patented invention that may in any way be related thereto.

Qualified users may obtain copies of this report from the Defense Documentation Center.

This document contains information affecting the national defense of the United States within the meaning of the Espionage Laws (Title 18, U.S.C., sections 793 and 794) the transmission or revelation of which in any manner to an unauthorized person is prohibited by law.

References to named commercial products in this report are not to be considered in any sense as an endorsement of the product by the United States Air Force or the Government.

Do not return this copy. When not needed, destroy in accordance with pertinent security regulations.

(U) SIMULATED ALTITUDE TESTING OF THE APOLLO SERVICE MODULE PROPULSION SYSTEM (REPORT I, PHASE II DEVELOPMENT TEST)

G. H. Schulz and J. F. DeFord
ARO, Inc.

FOREWORD

(U) The contents of this report are the results of a test program sponsored by the National Aeronautics and Space Administration-Manned Spacecraft Center (NASA-MSC). Technical liaison was provided by the Aerojet-General Corporation (AGC), which is subcontractor for the development of the Apollo Service Propulsion System engine (AJ10-137). The prime contractor to NASA-MSC for the Apollo Service Module is North American Aviation, Space and Information Division (NAA-S&ID). The test program was requested to support the Apollo Project under Air Force Systems Command (AFSC) System 921E.

(U) Testing was conducted by ARO, Inc. (a subsidiary of Sverdrup and Parcel, Inc.), Arnold Engineering Development Center (AEDC), AFSC, Arnold Air Force Station, Tennessee, under Contract AF40(600)-1200. The results reported herein were obtained in Propulsion Engine Test Cell (J-3) of the Rocket Test Facility (RTF), during the period between December 15, 1964, and April 7, 1965, under ARO Project No. RM1356, and the manuscript was submitted for publication on October 15, 1965.

(U) The authors wish to acknowledge invaluable collaboration in the preparation of this report by their associates in the J-3 Projects Section: C. R. Bartlett, E. S. Gall, M. W. McIlveen, C. E. Robinson, and R. B. Runyan.

(U) This report contains no classified information extracted from other classified documents.

(U) This technical report has been reviewed and is approved.

Ralph W. Everett
Major, USAF
AF Representative, RTF
DCS/Test

Jean A. Jack
Colonel, USAF
DCS/Test

UNCLASSIFIED ABSTRACT

(U) The Apollo Service Module (S/M) propulsion system, tested at AEDC, consisted of the Aerojet-General Corporation AJ10-137 flight-type rocket engine and a North American Aviation ground test replica of the Apollo S/M propellant system and was subjected to simulated altitudes up to 120,000 ft during engine firing operation. The testing reported herein was conducted with the first three engine assemblies of the AEDC Phase II development program and included seventy-four test firings with an accumulated duration of 1561.2 sec. The primary objectives of the test were to check out system operation, define propulsion system altitude performance, and prove engine structural endurance over ranges of propellant mixture ratio and combustion chamber pressure. Engine gimbaling operations were performed during certain firings. Ballistic performance of the three engine assemblies tested is presented. Engine temperature data, the effect of ablation on the thrust vector, and a discussion of engine gimbal operation are also presented.

CONTENTS

ILLUSTRATIONS

TABLES

NOMENCLATURE

A/A^*	Area ratio
A_t	Throat area, in.^{2}
$A_{t_{calc}}$	Calculated throat area, in.^{2}
A_{t_m}	Measured throat area, in.^{2}

C_F	Thrust coefficient
C_{F_v}	Vacuum thrust coefficient
$C_{i,j}$	Calibration constants
c*	Characteristic velocity, ft/sec
c^*_i	Characteristic velocity calculated at the beginning of a test which used a new combustion chamber, ft/sec
F_a	Axial thrust, lb_f
$F_{a_{cal}}$	Calibrate axial thrust, lb_f
F_m	Measured thrust, lb_f
$F_{P_{1cal}}$	Upper pitch force calibrate, lb_f
$F_{P_{1data}}$	Upper pitch force data, lb_f
$F_{P_{2cal}}$	Lower pitch force calibrate, lb_f
$F_{P_{2data}}$	Lower pitch force data, lb_f
$F_{R_{cal}}$	Roll force calibrate, lb_f
F_v	Vacuum thrust, lb_f
$F_{Y_{1cal}}$	Upper yaw force calibrate, lb_f
$F_{Y_{1data}}$	Upper yaw force data, lb_f
$F_{Y_{2cal}}$	Lower yaw force calibrate, lb_f
$F_{Y_{2data}}$	Lower yaw force data, lb_f
f_{corr}	Correction factor based on mixture ratio, oxidizer to fuel
g	Dimensional constant, $32.174 \frac{lb_m\text{-ft}}{lb_f\text{-sec}^2}$
I_{sp}	Specific impulse, lb_f-sec/lb_m
I_{sp_v}	Vacuum specific impulse, lb_f-sec/lb_m
I_t	Total impulse, lb_f-sec
K_{fm}	Flowmeter constant, lb-H_2O/cycle
$K_{j,i}$	Balance constants
L_j	Applied load
MR	Mixture ratio, oxidizer to fuel
P_a	Test cell pressure, psia
P_c	Combustion chamber pressure, psia

P_{c_m}	Measured combustion chamber pressure, psia
P_{fj}	Fuel injector pressure, psia
P_{ftca}	Fuel interface pressure, psia
P_{oj}	Oxidizer injector pressure, psia
P_{otca}	Oxidizer interface pressure, psia
R_i	Data load cell output, lb_f
$\dot{W}_f$	Fuel weight flow, lb_m/sec
$\dot{W}_o$	Oxidizer weight flow, lb_m/sec
$\dot{W}_t$	Total propellant weight flow, lb_m/sec
$\dot{W}_{tm}$	Measured total propellant weight flow, lb_m/sec
θ	Pitch angle, deg
ϕ	Yaw angle, deg

SECTION I
INTRODUCTION

(U) The Apollo spacecraft and Lunar Excursion Modules (LEM) are the "life supporting" modules of the "man-on-the-moon" mission. The Apollo spacecraft consists of a Command Module (three-man capsule) and an attached Service Module (S/M). The S/M houses the propulsion system which provides energy for midcourse velocity correction and injection into and ejection from lunar orbit. The Apollo S/M will remain in a lunar orbit while lunar exploration takes place with the LEM. After LEM rendezvous with the S/M and ejection from lunar orbit, the S/M is used for final, return, midcourse correction.

(U) Three phases of Apollo S/M development and qualification testing at altitude pressure conditions were planned for conduct at AEDC. Phase I, completed in April 1964, was concerned with developmental testing of the S/M rocket engine. Phase II was a systems test for extended developmental testing of the engine with a heavy-duty model of the S/M propellant tankage (F-3 fixture) and with flight-vehicle-type propellant feed lines. The Phase III altitude qualification program for the Aerojet-General Corporation AJ10-137 liquid-propellant rocket engine is also to be done with the F-3 fixture.

(U) Presented in this report are the results obtained during the initial 10 test periods of Phase II, which include 74 test firings with a total duration of 1561.2 sec on three different engine assemblies. The primary objective of Phase II development tests was to establish the operating characteristics and performance level of the Apollo S/M engine at simulated altitudes above 110,000 ft. Specific objectives include the following:

1. Engine ballistic performance at design operating conditions,
2. Engine ballistic performance and durability at off-design chamber pressures, mixture ratios, and propellant temperatures,
3. Effect of thrust chamber valve alternate passage selection on engine ballistic performance,
4. Gimbal system operation,
5. Minimum impulse bit operation,
6. Thrust vector determination,
7. Ablation characteristics,
8. Start and shutdown impulse characteristics, and
9. Restart capability.

SECTION II
APPARATUS

2.1 TEST ARTICLE – GENERAL

(U) The AJ10-137 rocket engine and an Apollo S/M version propellant system (tankage and plumbing, designated the F-3 fixture) constituted the test article for the AEDC tests. Three different flight-type engine assemblies, designated engines S/N 9, 9-1, and 11, were tested during this report period. The engine configurations included three different nozzle extension designs, two injector types, and one configuration with gimbal actuators.

(U) The F-3 fixture, provided by NAA-S&ID, was a heavy-duty version of the Service Module propellant storage and supply system. The boilerplate tanks were of spacecraft size, shape, and volume; the propellant lines duplicated spacecraft size, hydrodynamics, and approximate routing, and the spacecraft propellant feed pressurization system was duplicated, except for the helium pressurant supply storage. A heavy structural steel frame supported the tanks and plumbing and provided a base mount for the engine mount/thrust balance cage.

2.2 ENGINE

2.2.1 General Description

(U) The AJ10-137 engine tested during this report period is a pressure-fed, liquid-propellant rocket engine consisting of a thrust chamber assembly, a bipropellant valve assembly, and a gimbal actuator-ring mount assembly. The overall height of the engine is approximately 13 ft, and the diameter of the nozzle exit is approximately 8 ft.

(U) The design vacuum performance of the engine is 21,900-lb_f thrust at a propellant weight mixture ratio of 2.0 and a chamber pressure (measured at the injector face) of 100 psia. The engine is designed to be capable of a minimum of 50 restarts over the design operating life of 750 sec (Ref. 1). The engine burns hypergolic, storable propellants; nitrogen tetroxide (N_2O_4) is the oxidizer, and the fuel is a 50-50 weight blend of hydrazine (N_2H_4) and unsymmetrical dimethylhydrazine (UDMH).

(U) The thrust chamber assembly consists of a propellant injector, ablatively cooled combustion chamber, and a radiation-cooled nozzle

extension. The bipropellant valve is mounted on top of the injector dome. The thrust chamber assembly is mounted in a ring mount assembly and is gimbaled in two orthogonal planes by two electrically operated gimbal actuators.

(U) Two of the three engine assemblies tested during this report period are shown without the nozzle extension in Figs. 1a and b. The engine assembly components were:

Engine Serial Number	Injector Serial Number	Propellant Valve (TCV) Serial Number	Combustion Chamber Serial Number	Nozzle Extension Serial Number
9	AFF-78	0000020	A-11	0000001
9-1	AFF-78	0000020	0000050	0000039
11	0000046	0000032	0000047	0000026

2.2.2 Propellant Injector

(U) Two types of injectors were used during these tests; both had doublet orifice impingement in a concentric-ring pattern. The injector used on engines S/N 9 and 9-1 was unbaffled, whereas the injector used on engine S/N 11 was baffled (Fig. 2) for improved combustion stability. A pulse charge was placed in the combustion chamber for test firings G-25, H-29, and J-40 to investigate the ability of the injector to suppress induced combustion instability. The pulse charge was a No. 8 blasting cap and 2.46 gm of C-4 explosive in a Teflon® holder, which was screwed into the center of the injector face (Fig. 3). The pulse charge was located on the centerline of the combustion chamber about 6 in. downstream of the injector face. Pulse charge detonation was by combustion heat.

(U) The injector baffles were regeneratively cooled with fuel, which was routed through the baffles and back to the injection ring passages. Fuel coolant was not discharged directly from the baffles. Film cooling of the combustion chamber was provided by fuel flow from orifices in the outer fuel ring of the injector, adjacent to the injector mounting flange. Approximately 5 percent of the engine fuel flow was injected for film cooling.

2.2.3 Combustion Chamber

(U) The combustion chamber was constructed with an ablative liner, an asbestos insulating layer, and an external structural wrap (Fig. 4). The ablative material consists of a silica glass fabric tape impregnated with a phenolic resin compound. The chambers were constructed so that

the maximum ablative thickness was obtained at the throat section. Several layers of resin impregnated fiber glass wrap (glass fabric and glass filament) were bonded over the asbestos. The mounting flanges for the injector and nozzle extension were attached to the chamber by bonding the flange lips to the ablative material and structural wrap. Figure 4 also details the combustion chamber dimensions.

(U) Three combustion chambers were used during these tests (see section 2.2.1). Although the exit cone of each chamber extended to the 6:1 divergent area ratio, two different chamber-to-nozzle attachment flange designs were utilized. Engine S/N 9 used obsolescent J-flange components (shown in Fig. 4) for initial shakedown firing operations. Rebuilt engine S/N 9-1 used a current prototype modified J-flange combustion chamber (Fig. 4) to complete shakedown firings because no more J-flange nozzle extensions were available.

2.2.4 Exhaust Nozzle Extension

(U) The radiation-cooled nozzle extension is bolted to the ablative chamber at the 6:1 area ratio and extends to the 62.5:1 area ratio. The extension is fabricated from columbium and titanium. The three nozzle extension designs are shown in Fig. 5.

(U) Both engines S/N 9 and 9-1 used extensions with columbium to the 20:1 area ratio and titanium alloy from the 20:1 to the 62.5:1 area ratio (Figs. 5a and b). The nozzle extension used on engine S/N 11 was the first of the flight-type nozzles with columbium to the 40:1 area ratio and titanium alloy to the 62.5:1 area ratio (Fig. 5c). The columbium section thickness is 0.30 in. to area ratio 20:1 and 0.022 in. from area ratio 20:1 to the columbium-titanium joint. The titanium portion is fabricated from 0.025-in.-thick titanium alloy (5 Al - 2.5 Sn). The columbium section is coated to prevent oxidation, and the titanium section is coated to improve emissivity and thus reduce surface temperature.

(U) The nozzle extension of engine S/N 9 (Fig. 5a) had been used during previous testing (Ref. 2). This nozzle was an obsolescent J-flange design used for initial shakedown firing operations. Rebuilt engine S/N 9-1 used an intermediate design exit nozzle extension with a modified J-flange (Fig. 5b) to complete shakedown firings because no more J-flange nozzle extensions were available.

(U) The current prototype nozzle extension, used on engine S/N 11, was a modified J-flange design with columbium to area ratio 40 and a simplified stiffener arrangement (Fig. 5c).

2.2.5 Thrust Chamber Propellant Valve (TCV)

(U) The engine propellant valves, used during these tests, were actuated by fuel pressure with electrical command opening and signal-off closing (Figs. 1 and 6). The propellant valving system consisted of eight ball valves: two each in the two parallel fuel passages and two each in the two parallel oxidizer passages as shown in Fig. 6. Each of four fuel-pressure actuators operated one fuel and one oxidizer ball valve. Each of two solenoid pilot valves operated a pair of actuators (designated banks A and B). Thus, either bank, A or B, or both, could fire or shut down the engine. An auxiliary system, supplying gaseous nitrogen to the actuators, was installed at AEDC to effect TCV operation for checks and to actuate the TCV in the event normal fuel pressure actuation malfunctioned.

(U) Orifices at the TCV inlets were provided to balance the parallel passages, so engine operation on either bank A or B was intended to produce the same engine ballistic performance for given propellant interface pressures (Ref. 1). Engine ballistic performance was expected to change about two percent from "single bank" to "both banks" operation for given propellant interface pressures.

2.3 NAA F-3 FIXTURE

2.3.1 General

(U) The F-3 fixture (Fig. 7) was designed to reproduce the propellant system hydrodynamics of the S/M spacecraft with necessary modifications incorporated to facilitate ground test operations. The fixture structural frame, tanks, and plumbing had overall dimensions of 100 by 153 in. laterally and 15 ft high. The fixture weighed approximately 27,500 lb. A schematic diagram of the F-3 fixture propellant and pressurization plumbing is presented in Fig. 8.

2.3.2 Propellant System

(U) The propellant tanks were of spacecraft size, shape, and volume, consisting of two 1050-gal fuel tanks and two 1310-gal oxidizer tanks, but were designed and fabricated to meet the specifications of the ASME pressure vessel code. As in the S/M spacecraft, the two oxidizer and two fuel tanks of the F-3 fixture were series connected with propellant crossover lines; the engine propellant feed lines were connected to the sump tanks, and propellant force feed pressurization was through the storage tanks. The tandem tanks and crossover line arrangement

resulted in variations of propellant feed pressures with changes in propellant level although force feed pressurization was constant.

(U) The fixture propellant feed lines were modified to accommodate AEDC flowmeters and bypass connections for flowmeter calibration. Duplication of spacecraft line pressure losses was retained by changing the fixture line balance orifices. A detailed analysis of the flowmeter calibrations and techniques is presented in Appendix I.

2.3.3 Propellant Feed Pressurization System

(U) The pneumatic pressurization system of the F-3 fixture used equivalent components and schematic configuration but did not duplicate the spacecraft system. Fixture flight-type regulators could not be remotely controlled for the frequent testing at off-design mixture ratios or chamber pressures, so AEDC facility helium pressurization regulators were located in the test cell and were used instead of the fixture regulators. As in the spacecraft, the regulator discharges were manifolded with a connecting line. An array of doubly redundant check valves was located in each propellant tank pressurization line, downstream of the connecting line, to prevent mixing of hypergolic propellant vapors. A valve was provided in the connecting line to accommodate off-design mixture ratio testing.

2.3.4 Heat Shield

(U) The heat shield was an early model shield, designed for the protection of the spacecraft propellant plumbing and tankage from nozzle extension thermal radiation. A 120-deg sector of this heat shield was supplied by NAA for use during part of this testing. The shield was composed of a rigid bell of corrosion resistant steel and fiber-glass-type material and flexible boot of high-silica glass cloth and batting, as shown in Fig. 9. The bell outer edge was cut away for plumbing clearance and mounting on the lower framework of the F-3 fixture.

2.4 INSTALLATION

(U) The Apollo S/M propulsion system F-3 fixture and the AJ10-137 engine were installed in the Propulsion Engine Test Cell (J-3), a vertical test cell for testing rocket engines at pressure altitudes in excess of 100,000 ft (Fig. 10 and Ref. 3). An aluminum test cell capsule, which is 18 ft in diameter and 40 ft high, was installed over the test article to form the pressure-sealed test chamber.

(U) The engine was installed in a multicomponent force balance. This balance was mounted in the F-3 fixture by six flexure-mounted load cells for thrust vector measurement (Figs. 11a, b, and c). The installation is represented schematically in Fig. 11d. Figures 11e, f, and g provide location dimensions of the six load cells, which are used to determine the six components, three forces and three moments, generated by the thrust vector. The three forces are axial, pitch, and yaw, and the three moments are pitch, yaw, and roll.

(U) Pressure altitudes were maintained, prior to and following test engine firing, with a steam-driven ejector in the test cell exhaust duct in series with the facility exhaust compressors and during the steady-state portion of the test by a supersonic engine exhaust diffuser (Fig. 10). Ejector steam was supplied by the AEDC stationary boiler plant, supplemented by a steam-gas mixture from a rocket-type combustion steam generator. Facility systems included ground level propellant storage; helium for test article propellant tank pressurization; gaseous nitrogen for test article pressure/leak checking, purging, and valve operation; F-3 fixture helium pressurization controls, operable from the J-3 control room (also see section 2.3.3); and electrical power in both 28v dc and 110v, 60-cycle ac. Equipment for test article operation, located in the J-3 control room, included the gimbal system checkout and control consoles and the firing control and combustion stability monitor (CSM) console.

2.5 INSTRUMENTATION

(U) Instrumentation was provided to measure engine thrust (including axial and side forces); chamber pressure; propellant system pressures, temperatures, and flow rates; nozzle extension and combustion chamber case temperatures; test cell pressures and wall temperatures; gimbal system electrical signals; and various vibrations and accelerations. Schematic diagrams of relative locations of the test article and test cell instrumentation are shown in Figs. 10b and 12. A compendium of the more important parameters and the means of data acquisition are given in Table I.

2.5.1 Force Measuring System

2.5.1.1 Axial Force

(U) The axial thrust force (F_a) was measured with a dual-bridge, strain-gage-type load cell of 50,000-lb_f rated capacity. In-place calibration was accomplished with a hydraulic actuator axial loading system

containing a calibration load cell (Fig. 10b and Ref. 4). The calibration load cell was periodically laboratory calibrated with traceability to the National Bureau of Standards (NBS).

2.5.1.2 Side and Roll Forces

(U) Two yaw forces, two pitch forces, and one roll force were measured with strain-gage-type load cells of 500-lbf rated capacity. These forces complete the complement of the six-component system for engine thrust vector determination. In-place loading calibration with NBS traceability was provided for these load cells also (Fig. 11d and Ref. 4).

2.5.2 Pressures

2.5.2.1 Combustion Chamber Pressure

(U) Chamber pressure was measured using two strain-gage-type pressure transducers. One transducer was close-coupled to optimize response to pressure transients; the other transducer was provided with the capability for in-place applied pressure calibration (Fig. 13). The calibration transducer was a precision reluctance type, which was laboratory calibrated with NBS traceability.

2.5.2.2 Cell Pressure

(U) Test cell pressure was measured with two capacitance-type precision pressure transducers located outside the cell capsule in a self-contained, controlled-temperature environment. These transducers were laboratory calibrated periodically with a precision mercury manometer. In-place calibrations were made by electrical voltage substitutions only.

(U) Test cell pressure was also measured with two auxiliary strain-gage-type transducers. These were situated in the test cell behind the F-3 fixture support structure to minimize exposure to thermal radiation.

2.5.2.3 Propellant Pressures

(U) Propellant pressures in the F-3 fixture lines, engine lines, thrust chamber valve, and injector manifolds were measured with strain-gage-type pressure transducers.

2.5.3 Temperatures

2.5.3.1 Engine Assembly Temperatures

(U) Exhaust nozzle extension, combustion chamber, and injector surface temperatures were measured with Chromel®-Alumel® thermocouples (Fig. 12). Combustion chamber case temperature thermocouples were welded or bonded to the structure surface as appropriate for the base material.

2.5.3.2 Propellant Temperatures

(U) Propellant temperatures in the F-3 fixture tanks and engine line inlets were measured with copper-constantan thermocouple immersion probes. Propellant temperatures in the F-3 fixture propellant lines were measured with resistance temperature transducer (RTT) immersion probes.

2.5.3.3 Test Cell Wall Temperature

(U) Cell wall interior surface temperatures were sensed with copper-constantan thermocouples welded to the cell capsule wall surface.

2.5.4 Propellant Flow Rates

(U) Propellant flow rates were measured with one flowmeter in each F-3 fixture propellant feed line, upstream of the engine interface. The flowmeters are rotating permanent magnet, turbine-type, axial flow, volumetric flow sensors with two induction coil signal generators. The flowmeter in-place calibration technique and the calibrations performed during this report period are detailed in Appendix I.

2.5.5 Engine Vibration and Acceleration

(U) Engine injector, combustion chamber, and mount structure vibration were measured in three perpendicular planes with piezoelectric-type accelerometers (Fig. 12). Any engine vibration caused by combustion instability was sensed by one of the accelerometers mounted on the engine injector (Fig. 12). The accelerometer output signal was analyzed by the AGC Combustion Stability Monitor (CSM) to automatically initiate engine shutdown in the event of rough combustion (defined as engine acceleration exceeding 60 g's peak-to-peak at a frequency above 600 cps for longer than 0.040 sec).

2.5.6 Gimbal System Electrical Signals

(U) Electrical voltage and current signals from the gimbal control and actuation systems were tapped to indicate gimbal actuator position, actuator position change rate, actuator drive motor voltage and current, and actuator clutch currents.

2.5.7 Data Conditioning and Recording

(U) A continuous recording of analog data on magnetic tape was recorded from analog instrument signals by (1) analog-to-frequency converters and (2) magnetic tape, frequency modulated (FM) recording with a saturation-level pulse technique. Instrument signals produced in a proportionate frequency form were amplified for continuous FM recording on magnetic tape. Magnetic tape recording in digital form used a recorder system that both produces and tape-records an analog signal in a binary-coded decimal form. Various instrument analog signals were (1) amplified and converted to a common range of analog base-level and amplitude, (2) commutated for sequential scanning, and (3) converted to the binary code for magnetic tape recording.

(U) Light-beam oscillographs were used for continuous graphic recordings of analog and proportionate frequency signals. Proportionate frequency signals of the propellant flowmeters were recorded on the oscillograph with a divided frequency to improve record readability.

(U) Direct-inking, strip-chart recorders were used for immediate access, continuous, graphic recordings. Analog signals produced pen deflections with a null-balance potentiometer mechanism. Proportionate frequency signals were converted to analog for strip-chart recording.

2.5.8 Visual Coverage

(U) Two closed-circuit television systems permitted visual monitoring of the test article during testing operations. Permanent visual documentation of engine test firings was provided by 16-mm color motion pictures. An oscilloscope enabled visual observation of the CSM accelerometer signal during testing operations. Various engine and F-3 fixture parameters were recorded on strip-chart recorders with visual indicators in addition to the direct-inking feature to provide control room indications of test article operation, performance, and environment during testing operations.

SECTION III
PROCEDURE

3.1 PRE-TEST OPERATIONS

(U) Prior to each test period, the following functions were performed at sea-level pressure:

1. The F-3 fixture was loaded with propellants.
2. Flowmeters were in-place calibrated using the J-3 flowmeter calibration system described in Appendix I.
3. Propellant samples were taken to determine the specific gravity and a particulate contamination count of foreign matter in the propellants.
4. Propellant tanks were pressurized.
5. Instrumentation systems were calibrated.
6. A functional/sequence check of all systems was made.
7. An in-place calibration of the six-component thrust system was made (Ref. 4 provides a detailed explanation of the calibration procedures).
8. Axial thrust and chamber and cell pressures were in-place calibrated.

(U) After the above procedures, the test cell pressure was reduced to approximately 0.4 psia with the facility exhaust compressors for altitude calibrations and items 5, 6, and 8 above were repeated.

(U) After completion of instrumentation altitude calibrations, the steam ejector was used to reduce the test cell pressure to about 0.2 psia. All pre-fire operations, 60 sec prior to firing, and all immediate post-fire operations were automatically sequenced. These operations included instrumentation and camera starts, engine firing, engine shutdown, instrumentation and camera stops, and steam generator firing and shutdown. Steam augmentation by operation of the steam generator further reduced the test cell pressure to a level between 0.05 and 0.1 psia prior to ignition of the test engine. Simulated altitudes were maintained during engine coast periods by the facility exhaust compressors.

(U) After the final firing of a test period,

1. The steam ejector was shut down and the cell pressure maintained at about 0.4 psia by the facility exhaust compressors,
2. Pre-test steps 5 and 8 were repeated for post-test altitude calibration,

3. The F-3 fixture propellant tanks were drained and depressurized,
4. The engine propellant valves were opened for approximately an hour to aspirate the propellant lines (occasionally F-3 tanks also),
5. The propellant valves were closed, and the test cell pressure was raised to one atmosphere, and
6. Pre-test steps 5, 7, and 8 were performed for post-test, sea-level calibration.

(U) Installation of instrumentation on the test engines and engine rebuilding was accomplished by AGC and ARO technicians in an engine assembly room where the particle size was maintained below 500 microns. Engine rebuilding was accomplished in accordance with procedures supplied by AGC.

3.2 PERFORMANCE DATA ACQUISITION AND REDUCTION

3.2.1 General

(U) Engine performance data were acquired as shown in Table I. Digital computers were used to recover data from magnetic tape records, produce data printouts in engineering units, and perform computations to produce engine performance information as follows:

1. Rocket engine ballistic performance (vacuum thrust, thrust coefficient, specific impulse, and characteristic velocity),
2. Total impulse of start and shutdown transients,
3. Total impulse of minimum impulse bit operation, and
4. Thrust vector determination.

(U) The equations used for engine performance calculations were according to general standard practice, except for adaptations in usage, which were made to account for area changes of the ablative combustion chamber throat. Performance calculations were based on combustion chamber pressure measured at the injector. No correction was made for total pressure loss due to heat addition. Steady-state performance calculations were made from measured data which were averaged over 2-sec time periods.

3.2.2 Ballistic Performance

(U) Because of the nonuniform variations of the effective nozzle throat area during a firing and the physical impossibility of measuring

the throat area between firings, characteristic velocity and nozzle throat area were calculated during firing series using the following assumptions:

1. Characteristic velocity, corrected to a mixture ratio of 2.0, is constant for a given injector and is independent of chamber geometry.
2. Characteristic velocity is a function of mixture ratio and chamber pressure only. (However, because of a paucity of experimental data, c* is assumed to vary linearly with chamber pressure.)
3. The slope of the c* versus MR curve conforms to previous experimental data.

(U) Characteristic velocity (c^*_i) for a given injector was calculated using (1) the engine data between 2 and 4 sec of the initial firing on a new chamber, (2) the pre-test measured nozzle throat area, and (3) the relationship: $c^*_i = P_{cm} A_{tm} g/W_t$. The c* for a mixture ratio (MR) of 2.0 was derived using a curve slope factor (shown below) supplied by AGC (which was based on data from tests with the known throat area of a steel combustion chamber):

$$f_{corr} = 5592.0 / [5277.91 + 691.846 (MR) - 267.12 (MR^2)]$$

$$c^*_i (\text{at MR} = 2) = (c^*_i)(f_{corr})$$

This c^*_i for MR = 2 was retained as the standard for the given injector to be used for subsequent data reduction. The c* for any other MR, during subsequent firing, was derived by reversing the process and applying the MR slope factor (f_{corr}) to the standard c^*_i for MR = 2.

(U) The throat area of the nozzle for subsequent firings was calculated using the c* derived above, the measured chamber pressure, measured propellant flow rates, and the relationship: $A_{tcalc} = c^* \dot{W}_{tm}/g\, P_{cm}$. This calculated nozzle throat area was used with axial thrust corrected to vacuum conditions and measured chamber pressure to determine the vacuum thrust coefficient.

3.2.3 Total Impulse of Start and Shutdown Transients

(U) The total impulse (lb-sec) of the start transient covered the time period from FS-1 to 100 percent of steady-state combustion chamber pressure. The impulse integral was derived using calculated thrust based on chamber pressure; that is,

$$I_t = C_F A_t \int_0^t P_c dt$$

Intermediate impulse values were also derived for levels of chamber pressure at intervals of 10 percent up to the steady-state level. The

total impulse of the shutdown transient covered the time period from 100 to 1 percent of steady-state combustion chamber pressure. Vacuum thrust, computed from measured thrust, was not used because system dynamics invalidate thrust data during the starting and shutdown transients. In addition, at chamber pressures below about 60 psia, during the shutdown transient, the nozzle no longer flows full with the existing chamber-to-cell pressure ratio.

(U) Measured combustion chamber pressure was reduced at 0.005-sec intervals (200 intervals/sec) from the continuous magnetic tape recording of close-coupled transducer data. The combustion chamber pressure was used with calculated steady-state vacuum thrust coefficient and calculated nozzle throat area to compute vacuum thrust. The values of C_{F_V} and A_t, derived at the steady-state operation nearest the transient of interest, were assumed to be constant throughout the transient. The assumption of constant C_{F_V}, during the transients, implies that the nozzle throat is choked throughout the entire transient. Any discrepancies inherent in this assumption occur within a relatively small time period at a very low chamber pressure only and are not, therefore, sufficient to detract from the significance of the results.

(U) A digital computer program determines the time of occurrence, the thrust-rise-rate, and the integrated total impulse at the specific percentage levels of chamber pressure during the start and shutdown transients. The 100-percent chamber pressure basis is that derived from pressure measured during the steady-state data period nearest the transient of interest.

3.2.4 Total Impulse of Minimum Impulse Bit (MIB) Operation

(U) The method used for calculating the total thrust impulse integrals (lb-sec) of the minimum impulse bit firings was like that used for the start and shutdown transients. In the MIB firings, the impulse is totalled for the entire firing from FS-1 through the thrust decay to one percent of engine nominal chamber pressure. As in the transient impulse calculations, thrust was computed from combustion chamber pressure measured at 5-msec intervals. Since the MIB firings are too short to establish steady-state engine performance levels, the vacuum thrust coefficient (C_{F_V}) and exit nozzle throat area (A_t) used were obtained from the nearest previous engine firing which produced steady-state data. The same assumptions of constant C_{F_V} and A_t throughout the MIB firing were retained.

3.2.5 Thrust Vector Determination

(U) The multicomponent force measurement system is shown schematically in Figs. 11b, c, and d, which give the location of the six load cells. These load cells are used to measure the six components of force: forward and aft pitch, forward and aft yaw, roll, and axial. The force balance system employs the premise of a linear, repeatable, mechanical interaction for a given force application. That is, for a given force application (L), the force (R) measured in any load cell can be obtained from the following relationship:

$$R_i = C_{i,j} L_j$$

where $C_{i,j}$ represents the calibration constants based on the slope of the interaction. Because there are six data and six calibrate load cells, both i (which represents the data load cell being observed) and j (which represents the load applicator being used) vary from one to six, and $C_{i,j}$ is a six by six matrix.

(U) To obtain true forces from the thrust system, an equation of the following form is required:

$$L_j = K_{j,i} R_i$$

where $K_{j,i}$ represents the balance constants and is the inverse of the calibration constant matrix ($C_{i,j}$). The true forces are obtained by multiplying the force measured by the inversion of the calibration constants. A complete explanation of the force system and the method of determining balance constants is given in Ref. 4.

(U) Once the forces are determined at the six load cells, the equations of static equilibrium are employed to resolve these forces into a thrust vector at the engine gimbal plane (plane of engine throat). This thrust vector is presented in the form of the angle, from vertical, in the pitch and yaw planes and the offset from the centerline of the inner thrust cage at the point of intersection of the thrust vector with the gimbal plane.

SECTION IV
RESULTS AND DISCUSSION

4.1 GENERAL

(U) The primary objective of these tests was to establish the operating characteristics and performance level of the Apollo S/M propulsion system at simulated altitudes above 110,000 ft. Specific objectives were to determine:

1. Engine performance at design operating conditions,
2. Engine performance at off-design chamber pressures, mixture ratios, and propellant temperatures,
3. Engine ballistic performance using a single bank of thrust chamber propellant valves,
4. Gimbal system operation,
5. Minimum impulse bit operation,
6. Thrust vector determination,
7. Combustion chamber ablation characteristics,
8. Start and shutdown impulse characteristics, and
9. Restart capability.

(U) Seventy-four test firings with an accumulated duration of 1561.2 sec were conducted using three engine assemblies to meet these test objectives. A brief description of each test period (covered by this report) is presented in Appendix II, and a summary of test number, dates, objectives, and durations is listed in Table II. In addition to the objectives stated above, the effects of propellant tank crossover on ballistic performance, the test article temperature during firings, the extended coast periods at simulated high altitudes, and rocket engine durability are also discussed. During this testing, the maximum and minimum propellant temperatures were 100.0 and 45.0°F, respectively, and the test cell wall temperature was maintained near 60°F.

4.2 ENGINE PERFORMANCE

4.2.1 General

(U) Three basic parameters were used to describe engine performance: specific impulse, corrected to vacuum conditions, was used to define overall engine performance; characteristic velocity, computed using injector face pressure, was used to compare the performance of various injectors; and the performance of various nozzles with a given injector/chamber geometry was indicated by the vacuum thrust coefficient. The calculation of I_{sp_V} uses measured data and incorporates no assumptions and therefore should be considered the most accurate performance parameter.

(U) The data from six test firings (G-25 through G-28, H-29 and H-30) are presented in Table III but are not shown in graphical form.

Tests G-25 through G-28 exhibited discrepancies in the measured data used to compute vacuum thrust. During tests H-29 and H-30, cell pressure was higher (P_a = 0.24 psia) than normal (P_a = 0.10 psia) and also higher than the nozzle exit static pressure (0.2 psia). The data from these tests show the effect of high cell pressure on engine C_{F_v} performance.

4.2.2 Overall Engine Performance

(U) The overall engine performance, as defined by the vacuum specific impulse (I_{sp_v}), was obtained for the three engine assemblies by conducting fifty-four test firings over a mixture ratio range from 1.53 to 2.28 and a chamber pressure range from 80 to 127 psia. Performance data from steady-state operation at design and off-design chamber pressure are presented in Table III and in Figs. 14 and 15. Table IV presents the measured operating data during both design and off-design chamber pressure tests. Figure 14 shows that I_{sp_v} varies widely with mixture ratio for the particular hardware design used, whereas Fig. 15 shows that I_{sp_v} is a strong function of the magnitude of chamber pressure.

(U) The data from Table III for all of the design chamber pressure (P_c = 100 psia) tests were used to construct (by digital computer) a second-order, least-squares curve applicable to each engine. The results of this analysis indicated the precision with which the data were acquired, the repeatability of the engine operation, and a mathematical equation for expressing the overall engine performance. Pertinent data are tabulated below.

Engine Serial Number	9	9-1	11
Number of test periods (at design chamber pressure)	3	2	3
Number of test firings (at design chamber pressure)	8	7	18
Number of data samples	30	27	96
Standard deviation of data about second-order, least-squares curve percentage	0.203	0.096	0.087
I_{sp_v} at MR = 2.00	307.91	309.64	311.27

(U) The least-squares computer program indicated that the best fit second-order equations for calculating I_{sp_v} for the three engines tested are:

S/N 9 $\quad I_{sp_v} = 316.118 + 11.082\,MR - 7.592\,MR^2$

S/N 9-1 $\quad I_{sp_v} = 303.304 + 26.613\,MR - 11.722\,MR^2$

S/N 11 $\quad I_{sp_v} = 275.938 + 53.306\,MR - 17.819\,MR^2$

(U) These data indicate that the overall performance of engine S/N 11, utilizing the baffled injector and the flight-type nozzle extension, was 311.2 lb_f-sec/lb_m at an MR = 2.0 and was at least 0.5 percent higher than either of the first two engine assemblies.

(U) The data presented in Fig. 14 also indicate that engine efficiency continually increased with the lower mixture ratios and did not reach an apparent maximum for any of the engines over the range of mixture ratios investigated (1.53 to 2.28).

(U) Seven test firings were conducted at off-design chamber pressures between 80 and 127 psia. These data (presented in Table IIId and Fig. 15) show that overall engine efficiency increased with increasing chamber pressure. Six of these seven tests were conducted on engine S/N 9-1, which utilized the unbaffled injector (Table II). Figure 15 is a plot of I_{sp_v} versus MR for various chamber pressures from 80 to 127 psia for engines S/N 9-1 and 11. For test E-12 (chamber pressure of 127 psia and MR = 2.0), the I_{sp_v} was 311.7 lb_f-sec/lb_m. This is 0.7 percent greater than the I_{sp_v} = 309.6 lb_f-sec/lb_m for the design 100-psia chamber pressure for test E-15, and 1.4 percent greater than the 80-psia chamber pressure for test E-17, I_{sp_v} = 307.4 lb_f-sec/lb_m. This increase in performance, for engine S/N 9-1, is attributed to improved combustion efficiency at the higher chamber pressures; a more detailed discussion is contained in section 4.2.3.

(U) The difference in the performance between engines S/N 9 and 9-1 is believed to have been caused by the small increase in nozzle efficiency for the nozzle used on engine S/N 9-1 and is discussed in section 4.2.4.

(U) It was noted that during long-duration firings (greater than 50 sec), vacuum specific impulse indicated increasing engine performance with time which cannot be explained by mixture ratio changes. This performance increase is thought to be caused by contour changes of the nozzle extension under load at high temperature and is discussed further in section 4.2.4.

(U) From a consideration of ballistic performance only, it appears that more efficient engine operation would be obtained by operation at a lower mixture ratio and at a higher chamber pressure than the design conditions (P_C = 100 psia, MR = 2.0).

4.2.3 Combustion Chamber Performance

(U) Characteristic velocity, an indicator of combustion chamber efficiency, was calculated by using the equations presented in section 3.2.2. The method of calculation derives a representative c* early in the firing (between 2 and 4 sec) of a new chamber by the $P_c/\dot{W}_t$ relation and the prefire measured throat area. The influence of chamber pressure on combustion efficiency was then determined by assuming that c* varied linearly with chamber pressure for the remainder of the firing.

(U) Because of the unknown changes in nozzle throat area which occur during a firing, the only reliable experimental c* data are those calculated for the initial portion of a firing of a new chamber before a significant throat area change results. These initial values are shown in Fig. 16 for the two injector designs used. The baffled injector (engine S/N 11) c* for the design condition of P_C = 100 and MR = 2.0 was 5696 ft/sec, or 3.3 percent higher than the equivalent c* of 5514.0 ft/sec for the unbaffled injector. These values, as stated previously, were based on chamber pressure measured at the injector face and do not account for possible differences in chamber pressure loss between injectors.

(U) Testing of engines S/N 9 and 9-1 encompassed two combustion chambers utilizing the same unbaffled injector. The initial tests were conducted at chamber pressures of 100 and 127 psia, respectively. Characteristic velocity for varying chamber pressure is presented in Fig. 17. It is noted that c* obtained during the 127-psia firing was 5553.9.

4.2.4 Nozzle Performance

(U) Nozzle performance was obtained for three nozzle extensions. The nozzle extensions (Fig. 6) for engines S/N 9 and 9-1 were non-flight type; the nozzle extension for engine S/N 11 (Fig. 5c) was a flight-type design (discussed in section 2.0). Vacuum thrust coefficients are presented in Fig. 18. At design operating conditions (MR = 2.0), C_{F_V} for engines S/N 9, 9-1, and 11 were 1.800, 1.807, and 1.755, respectively. It should again be noted that chamber pressure measured at the injector face was used to calculate the vacuum thrust coefficient. The change in C_{F_V} that occurred between engines S/N 9-1 and 11 may be the result of

different chamber pressure loss factors between the measured pressure and the plenum total pressure for the unbaffled and baffled injectors.

(U) Figure 19, test F-24, shows that, during longer test firings, vacuum thrust coefficient increased with time. The increase during the 177 sec of test F-24 was about 0.5 percent. This increase is attributed to recontouring of the nozzle extension under load at higher temperature. It should be noted that the measured force returned to zero after shutdown, indicating no adverse effect of temperature on the load measuring system. A smaller thrust increase of not more than 0.18 percent occurred because of nozzle extension thermal expansion.

4.2.5 Effect of Propellant Tank Crossover on Engine Ballistic Performance

(U) Figure 8 shows that the storage tank is continually feeding the sump tank throughout a firing. The regulated helium pressure is supplied to the top of the storage tank, and the propellant flow rate to the engine is a function of the pressure at the bottom of the sump tank. As the propellant level of the storage tank drops, for a constant helium pressure, the flow-controlling pressure will drop. When the propellant is depleted in the storage tank (defined as crossover), the pressure in the sump tank will increase suddenly because there is no propellant level difference between the tanks to overcome, and crossover line flow loss becomes very small. As shown in Fig. 20, crossover had a pronounced effect on engine mixture ratio and subsequent engine performance because of the propellant feed pressure variations. These variations are, of course, related to local gravitational effects during vertical ground testing. This effect could be quite different in the space environment.

4.2.6 Effect of Propellant Valve Bank Selection on Engine Ballistic Performance

(U) During engine operation, flow through the propellant valve assembly may be routed through TCV bank A only, through TCV bank B only, or through both banks simultaneously, as discussed in section 2.2. As stated in Table II, engine S/N 9 operation utilized only TCV bank A for all firings; engine S/N 9-1 utilized banks A or A and B; S/N 11 utilized bank A or B selections only. This testing was to indicate whether any propellant flow pattern variations, arising from TCV bank selection, were sufficient to cause variations in engine combustion performance (e. g., c* and I_{sp}). A review of the performance (Tables III and IV) indicates that, within the precision of the data ($\sigma < 0.096$ percent), all of the three selections resulted in essentially the same performance.

4.2.7 Start and Shutdown Transient Characteristics

(U) The total impulse (lb-sec) of several starting and shutdown transients was calculated to document the quality and repeatability of the total impulse associated with the non-steady-state portions of engine firings.

(U) Typical start transients are shown in Fig. 21. The time requirement for thrust buildup and the general repeatability of the time of ignition are shown in Fig. 21a. The start transient total impulse repeatability is shown by the dispersion of the termini of the impulse history curves in Fig. 21b. A summary of start transient impulse data for engine S/N 11 is given in the following table:

Test Number	Rise Time (to 100 percent), sec	Start Impulse, $\left(I_t = C_F A_t \int_0^t P_c dt\right)$, lb-sec
J-40	0.51	3273
J-41	0.54	2715
J-42	0.48	3052
J-43	0.59	2901
J-44	0.55	2716
K-49*	0.51	3572
K-50	0.48	1866
K-51	0.48	2034
K-52	0.49	2178
K-53	0.49	2258
K-54	0.48	2223

*P_c = 125 psia

The repeatability of the total impulse of the start transient was within about ±27 percent for the entire set of data except test No. K-49. The differences between consecutive firings were much smaller, with the exception of an apparent shift following Test K-49. The cause of this shift is unknown; however, Test K-49 was the only firing of this engine series at an off-design combustion chamber pressure (125 psia) and included gimbal operations.

(U) Typical shutdown transients are shown in Fig. 22. The thrust decline repeatability is shown in Fig. 22a. A summary of the shutdown transient impulse data for engine S/N 11 is given in the following table:

Test No.	Shutdown Time (to 1 percent), sec		Shutdown Impulse, lb/sec
J-40	2.31		10089
J-41	1.40	to 2%	7826
J-42	1.53		6977
J-43	2.71		7481
J-44	2.73		7356
K-49*	2.49		8219
K-50	2.63		7905
K-51	2.58		7535
K-52	2.49		7268
K-53	2.41		7366
K-54	2.31		7141

*P_c = 125 psia

The impulse repeatability (Fig. 22a) is mainly a function of the repeatability of the TCV closing, which is indicated in Fig. 22b by the differences in impulse at 0.5 sec from FS-2. Below the 10-percent thrust level, the repeatability is less precise. However, this non-repeatability in the final tailoff has a relatively small effect on the total impulse because the contribution of the tailoff to total impulse is small. This small effect is shown in Fig. 22b by the small slopes of the curves near termination. The repeatability of the total impulse of the shutdown transient was within about ±18 percent.

(U) The shutdown transient impulse is reduced from a chamber pressure corresponding to 100 percent steady-state thrust to a value of 1 percent of the steady-state thrust. These thrust levels correspond to a design chamber pressure of from 100 to 1 psia, respectively. The maximum cell pressure at shutdown was 0.33 psia (test K-49) and is significantly less than the 1.0-psia chamber pressure.

4.2.8 Minimum Impulse Bit Operation

(U) Short firings were made with various durations from 0.2 to 1.0 sec to document the precision of total impulse repeatability (lb-sec).

(U) Typical chamber pressure transients, which occurred during the impulse bit operations, are shown in Fig. 23a. Since the shorter duration firings did not include any steady-state operation, they were more sensitive to the repeatability of propellant valve operation. Repeatability of the total impulse (Fig. 23b) also showed the effects of valve operation. The impulse data of the shorter firings showed a greater percentage of dispersion as firing duration decreased. The increased dispersion indicated the accumulated effects of propellant valve, injection pattern, and combustion irregularities. The nonlinearity of the median of impulse data versus time showed variations in propellant inertial effects, the variations in propellant valve initial opening dead time, and nonlinearity of open area versus valve position. Thus, by extrapolation, the minimum firing duration to obtain any impulse was about 0.19 sec. Minimum firing duration for impulse repeatability within ±10 percent was about 0.5 sec.

4.3 COMBUSTION CHAMBER ABLATION CHARACTERISTICS

(U) Ablative nozzle throats are characterized by an area change during firing. The throat diameter measurements can be taken only prior to engine test and after engine removal. A method was derived to compute the throat area at any time during a test (see section III). Figure 24 shows the comparison, for the three engines tested, between the calculated and the measured throat areas, assuming a linear change between the pre- and post-test measured throat areas. The difference in the two methods for obtaining the throat area was about 1 percent or less.

(U) Figure 25 shows the combustion chamber ablation after test C-9 on engine S/N 9, F-24 on engine S/N 9-1, and test K-54 on engine S/N 11. No areas of nonuniform or localized ablation (streaks or gouging) of the interior ablation surface were experienced with the three engines tested and reported herein.

4.4 NOZZLE EXTENSION AND COMBUSTION CHAMBER TEMPERATURES

4.4.1 Nozzle Extension

(U) Figures 26a and b present the temperature history for the longest duration tests on engines S/N 9-1 and 11, respectively. The extension reached near steady-state temperatures after about 60 sec of operation. Figure 26b indicates that the nozzle extension temperature data did not show a significant increase when the 120-deg heat shield was installed

with engine S/N 11. However, the temperature at the 10:1 area ratio (Fig. 26b) may have been invalid since the thermocouple fastening on the columbium section was unreliable, and the thermocouples frequently lifted off the nozzle surface. This may explain the apparent decay in the temperature level ($A/A^* = 10$) at approximately 45 sec of firing time.

(U) Figures 26c and d present the nozzle extension temperature during the mixture ratio tests for engines S/N 9-1 and 11 and shows that mixture ratios between 1.7 and 2.2 have, in general, less than 100°F influence on measured temperature. Figure 26d does show a significant increase in temperature across the columbium-titanium joint at the 40:1 area ratio, for engine S/N 11, which did not exist (Fig. 26c) at the 20:1 joint on engine S/N 9-1.

(U) Chamber pressures between 80 and 127 psia influenced the temperature level of the nozzle extension as shown in Figs. 26e and f. On engine S/N 9-1, the temperature was about 200°F higher for the 127-psia test than for the 80-psia test.

(U) A comparison of the nozzle temperature for the two nozzle extension designs is presented in Fig. 26g for design engine operation ($P_c = 100$ and MR = 2.0) for the time of 40 sec after ignition. No significant temperature difference was indicated by the comparison of the two different nozzle designs.

4.4.2 Combustion Chamber

(U) The combustion chamber surface temperature reached maximum values during the altitude coast periods between 20 and 50 min after shutdown. Figure 27 shows that the maximum surface temperature was located in the plane of the throat and was approximately 430°F on engine S/N 9-1 after a 177-sec test and was 300°F on engine S/N 11 after a 160-sec test firing.

(U) The rapid rise in surface temperature during the firings was believed to be caused by radiation from the nozzle, conduction from the nozzle extension to the attachment flanges, and thermal reflection from the cell components. Radiation from the nozzle extension was indicated by the temperature of the test cell inner wall surface where a direct view of the nozzle extension existed (Fig. 27b). Figure 27b also shows that the cell wall temperature did not exceed 70°F in areas shielded from the view of the nozzle extension.

4.5 GIMBAL SYSTEM OPERATION

(U) Gimbaling operations were conducted during six firings of engine S/N 9-1 and during one firing of engine S/N 11 (Table I). The gimbal amplitude was limited to 1.5 deg during these operations to preclude spilling the nozzle exhaust over the inlet edge of the exhaust diffuser and into the test cell (see Fig. 10b). The gimbal operations included ramp, step, and sine function command signals of various frequencies to document gimbal system mechanical and electrical dynamics. These gimbal operations of the engine complete with nozzle extension at altitude pressure conditions were done to provide data amenable to mathematical treatment in order to define the engine mount/gimbal system vibration characteristics (e. g., system spring rate, effective mass, and damping). Analysis of the gimbal data was done by AGC and NAA.

(U) The examples of oscillograph data, reproduced in Fig. 28, are typical of gimbal operation conducted during this test period. The position and rate traces are analogs of engine angular position and rate of change of position (angular velocity), which were derived from the electrical signal of the gimbal actuator position potentiometers.

(U) The engine position and rate traces show the gimbal system response and precision capabilities; linearity of the position trace in following a linear ramp command signal shows gimbal system precision (Fig. 28a). The position trace slope and rate trace amplitude following a step command signal show gimbal system response (Fig. 28b). The absence of position "overtravel" and slackening of drive rate, as the commanded position was attained, shows the integration of position error and rate used by the gimbal control system to maintain system stability and "anticipate" zero position error. The gimbal system response limitation was indicated by the reduction of position excursion amplitude as the sine function command frequency was increased (Figs. 28c and d).

4.6 THRUST VECTOR DETERMINATION

(U) The multicomponent force measurement system was employed to determine the thrust vector and the excursion of this vector during steady-state non-gimbaling test firings on engine S/N 11 (Table II). A complete description of the multicomponent force measurement system (force balance), which was used during these tests, is given in Ref. 4.

(U) The thrust vector angle is presented in Fig. 29 as a function of time. Pitch and yaw components of the thrust vector angle, as shown by

the point of intersection of the vector with the gimbal plane, are presented in Fig. 30. The thrust vector angle in pitch (θ) displayed a net increase throughout the progression of firings with increasing engine firing time. The deviation during individual firings, however, showed a more complex behavior. For an individual firing, the vector angle decreased with time from ignition until a minimum value was obtained. This minimum was obtained only after a firing time of approximately 50 sec in test H-32 as shown in Fig. 29. After the minimum value was obtained in test H-32, the vector angle increased until engine shutdown. Test H-32 was the only firing of sufficient length to observe the vector angle increase.

(U) The thrust vector angle in yaw (ϕ) displayed a net decrease throughout the progression of firings. The behavior of the yaw angle displayed a similar pattern to the pitch angle; however, it was less pronounced (Fig. 29).

(U) Figure 30 presents the variation of the location of the thrust vector intersection with the gimbal plane relative to the axial centerline for the engine tested. The thrust vector location showed random migration with time. The two separate groups of data can again be explained by engine realignment with the gimbal actuator installation. The data appearing in quadrant two are from the J period (with gimbal actuators installed), but the data in quadrant one are from the G and H periods (stiff links installed). At the end of a firing the throat area changes because of the cooling of the ablative material. This throat area change accounts for the shift of the thrust vector from the end of one firing to the beginning of the next.

(U) Thrust vector excursion was believed to be primarily related to the chamber and throat ablation. Figures 25 and 31 show typical pre- and post-fire condition of engine combustion chambers. For a perfectly aligned engine with a symmetrical exit nozzle extension and thrust chamber, and with the gimbal ring mechanical deflection properly compensated, the initial thrust vector would be zero ($t = 0$ and $\theta = 0$ deg). The high initial value of the thrust vector ($t = 0$ and $\theta = 1.11$ deg) indicates that one or more of the above criteria were not fully satisfied. For the G and H test periods, stiff links were used in place of gimbal actuators to fix the engine in the null position. For the J and K periods, however, gimbal actuators were installed and the engine was aligned differently. This realignment is the reason for the two widely separate levels of vector angle and location.

4.7 OPERATIONAL PERFORMANCE AND RELIABILITY

4.7.1 Propellant Injector

(U) Prior to three tests (G-25, H-29, and J-40) a small explosive charge (No. 8 blasting cap and 2.46 gm of C-4 explosive) was installed as shown in Fig. 3. This was done to test the ability of the baffled injector to recover from induced combustion instability. Heat from engine combustion fired the pulse charge at about 1 sec after engine ignition. Figure 32 shows the combustion chamber pressure traces from oscillograph data during detonation of tests G-25 and J-40, respectively. It is suspected that the charge did not detonate during test H-29 since no pressure pulse was noted on the oscillograph record. Combustion stability recovery was satisfactory for tests G-25 and J-40.

4.7.2 Nozzle Extension

(U) Post-test inspection after test G-28 revealed several broad shallow depressions in the columbium section, just below the chamber mating flange (Fig. 33). Motion-picture coverage showed that "oil canning" occurred during all G-series shutdowns and left permanent depressions in the nozzle on test G-28. Because of test cell leakage, the test cell pressure at shutdown was 0.37 psia on that test and is considered to be the cause of the more severe nozzle loading at shutdown. Nominal steady-state cell pressure is 0.1 psia.

4.7.3 Thrust Chamber Valve

(U) At 3.5 sec after FS-2 during test G-28, the fuel line pressure decayed from normal "lock-up" pressure (about 200 psia) to approximately 10 psia. Post-test leak checks indicated flow through the TCV actuator dump line. Further checks isolated the leakage to the broken 1/4-in.-diam line on the TCV enable valve.

4.7.4 Engine Restart

(U) Engine restart capability was demonstrated on engine S/N 11 when an initial firing and 49 successful restarts were conducted at simulated altitudes from 80,000 to 120,000 ft.

SECTION V
SUMMARY OF RESULTS

(U) Significant results obtained during this part of the Apollo Service Module Engine Phase II test program are summarized as follows:

(U) 1. The vacuum specific impulse (I_{sp_v}) of the AJ10-137 engine utilizing a baffled injector and a flight-type nozzle extension (engine S/N 11) was 311.2 lb_f-sec/lb_m at a chamber pressure (P_c) of 100 psia, mixture ratio (MR) of 2.0, and at nominal propellant temperatures. The I_{sp_v} data obtained at normal conditions for this engine exhibited a one standard deviation about a second-order, least-squares curve of 0.088 percent. The I_{sp_v} for this engine was 0.5 percent greater at MR = 2.0 than the I_{sp_v} for either of the other two engines tested (using non-baffled injectors and development-type nozzle extensions).

(U) 2. Characteristic velocity and vacuum thrust coefficient for engine S/N 11 were 5696.7 and 1.755, respectively, at P_c = 100 psia and MR = 2.0.

(U) 3. Vacuum specific impulse as a function of mixture ratio exhibited a negative slope over the entire range of mixture ratios tested (1.53 to 2.28) and did not reach a maximum value ($dI_{sp_v}/dMR = 0$).

(U) 4. Vacuum specific impulse was found to be a strong function of the magnitude of chamber pressure. For the mixture ratio 2.0 tests on engine S/N 9-1, the I_{sp_v} at 127 psia was 311.7 lb_f-sec/lb_m, which was 1.4 percent higher than the I_{sp_v} of 307.4 lb_f-sec/lb_m at 80-psia chamber pressure.

(U) 5. There was no significant difference in engine performance between different thrust chamber valve bank operations within the data scatter (0.088 percent, one standard deviation).

(U) 6. Tests conducted to determine minimum impulse characteristics indicated that no impulse is produced during thrust chamber valve actuation times less than 0.2 sec.

(U) 7. The thrust vector for engine S/N 11 changed in both angle and location as a function of time and indicated a non-symmetrical ablation of the engine throat. The vector/throat plane intercept experienced a random variation between

the limits of 0 and 0.018 in. in the yaw plane and 0.16 and -0.02 in. in the pitch plane. The vector components varied between the limits of 1.05 and 1.65 deg in the pitch angle and 0 and 0.25 deg in the yaw angle.

(U) 8. There was no unusual or nonuniform throat ablation observed on any of the three chambers tested. One chamber experienced 50 starts and shutdowns with total test duration at high altitude of 654.8 sec.

REFERENCES

1. NAA Procurement Specification MC901-0009A. (U) "Apollo Spacecraft Service Module Propulsion System Rocket Engine." November 15, 1962, revised March 8, 1963. [redacted]

2. Vetter, N. R. and DeFord, J. F. (U) "Simulated Altitude Testing of the Aerojet-General Corporation AJ10-137 Rocket Engine - Mission Duty Cycles (Report V, Phase I Development Test)." AEDC-TDR-64-158 (AD352700), August 1964. [redacted]

3. Test Facilities Handbook (5th Edition). "Rocket Test Facility, Vol. 2." Arnold Engineering Development Center, July 1963.

4. Robinson, C. E. and Runyan, R. B. "Thrust Vector Determination for the Apollo Service Propulsion Engine Using a Six-Component Force Balance." AEDC-TR-65-250, December 1965.

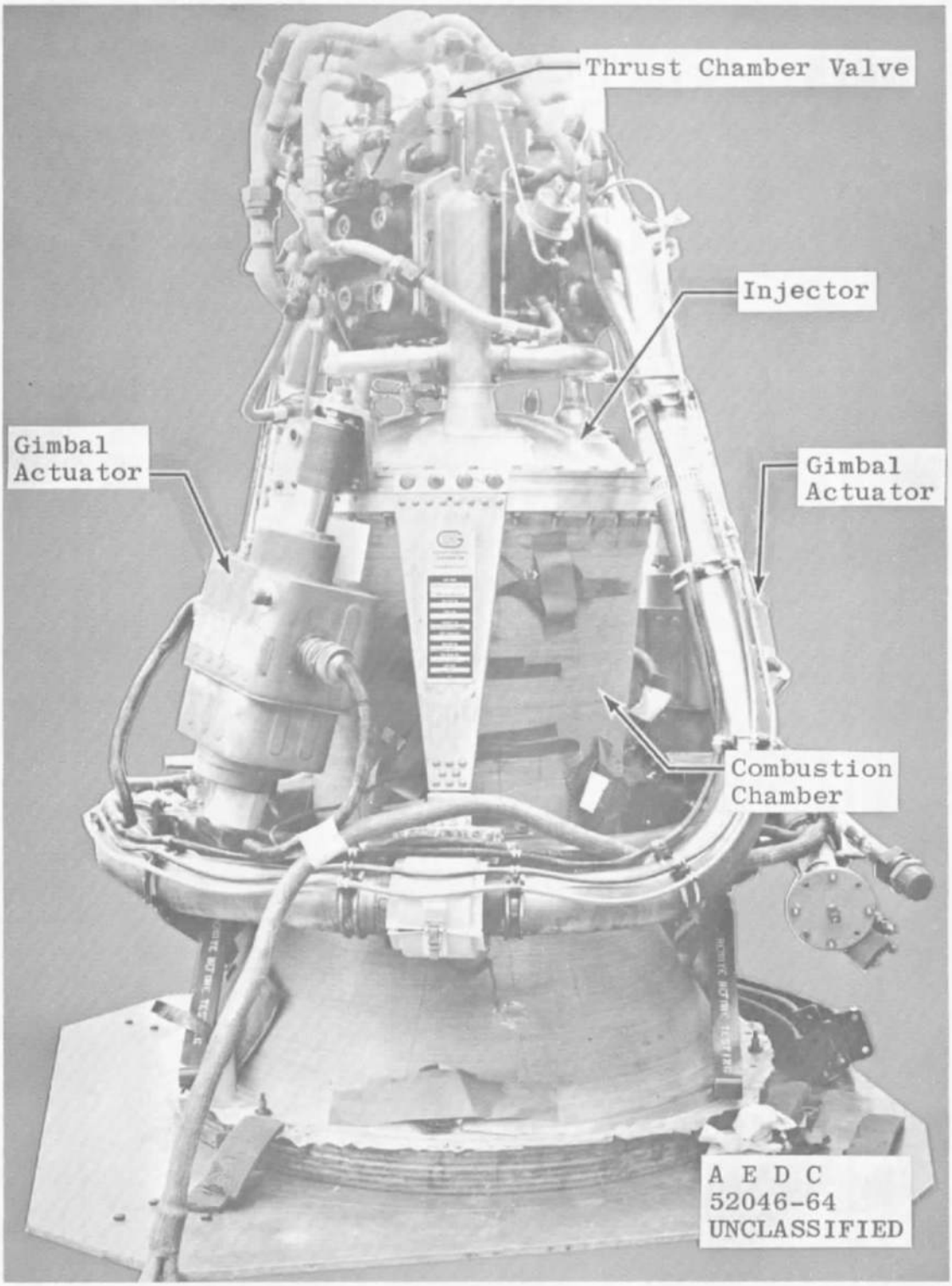

a. Engine S/N 9 as Received

Fig. 1 AJ10-137 Rocket Engine W/O Nozzle Extension

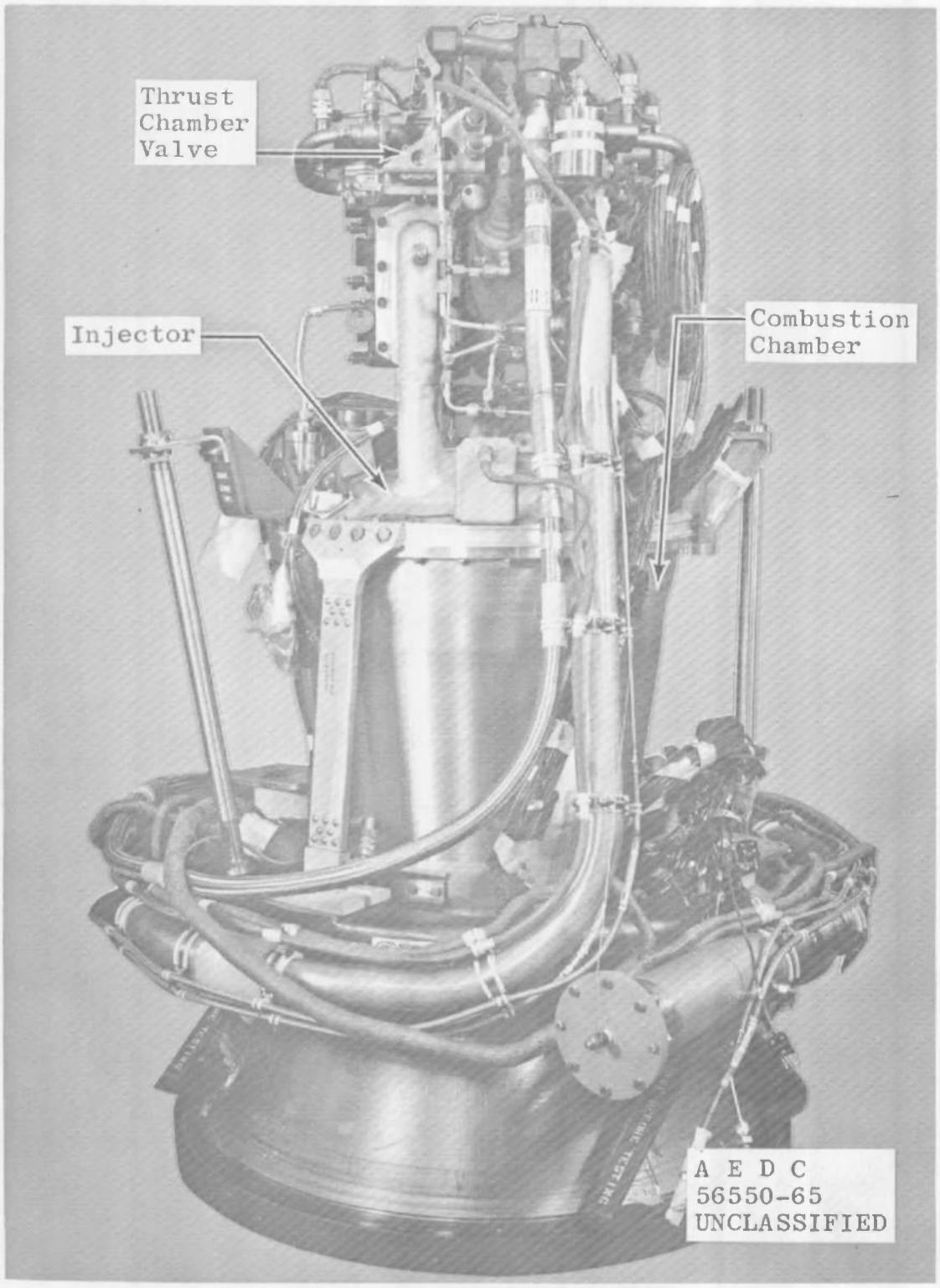

b. Engine S/N 11 as Received

Fig. 1 Concluded

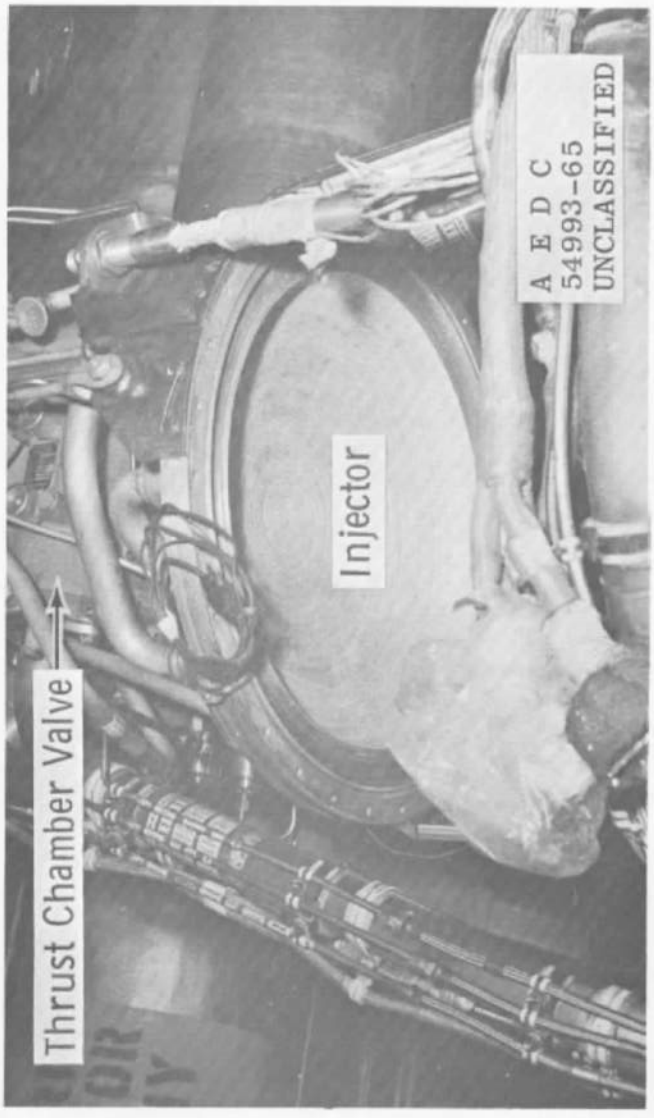

a. Non-Baffled Prototype

Fig. 2 Injector Configuration

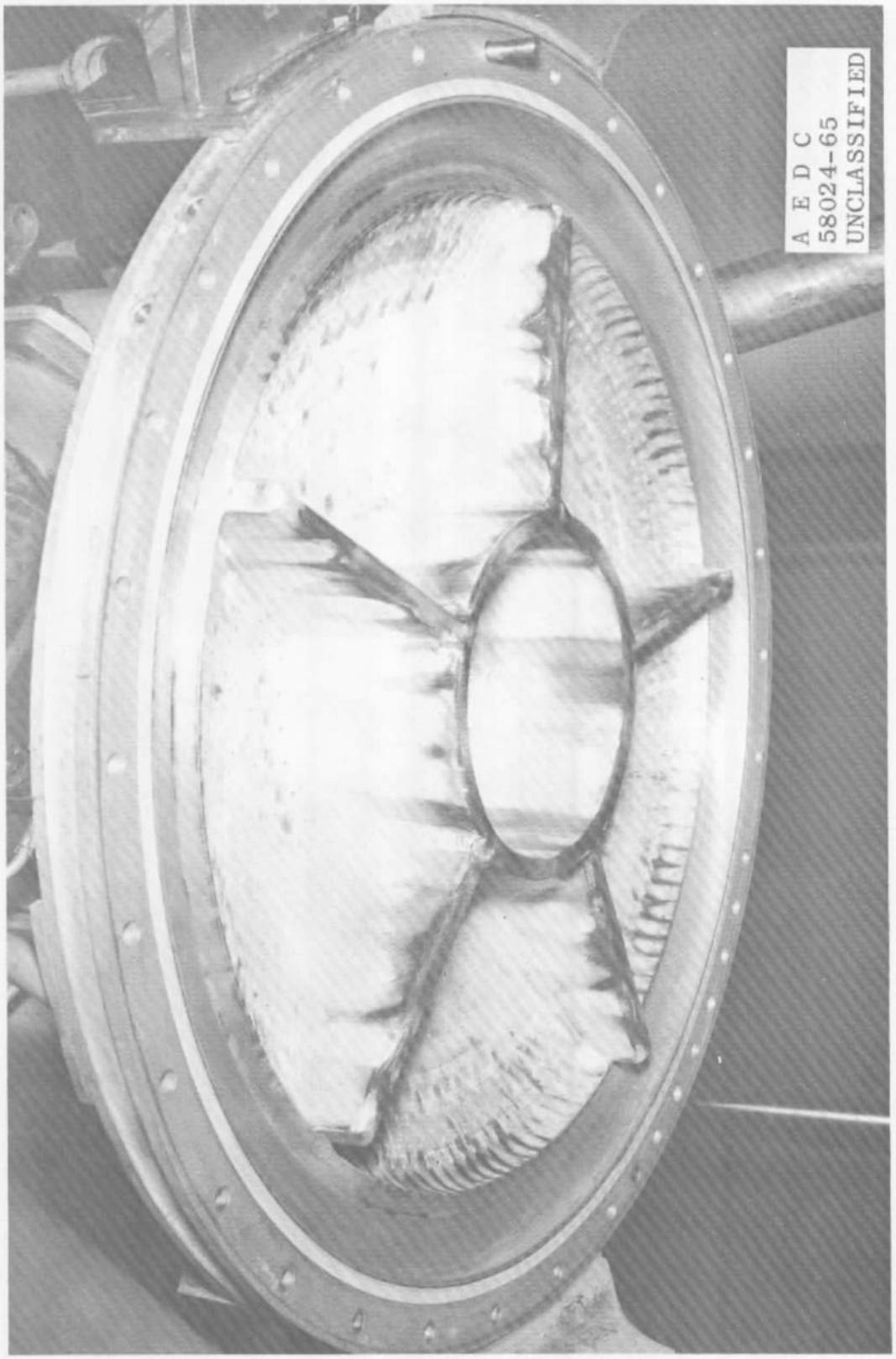

b. Baffled

Fig. 2 Concluded

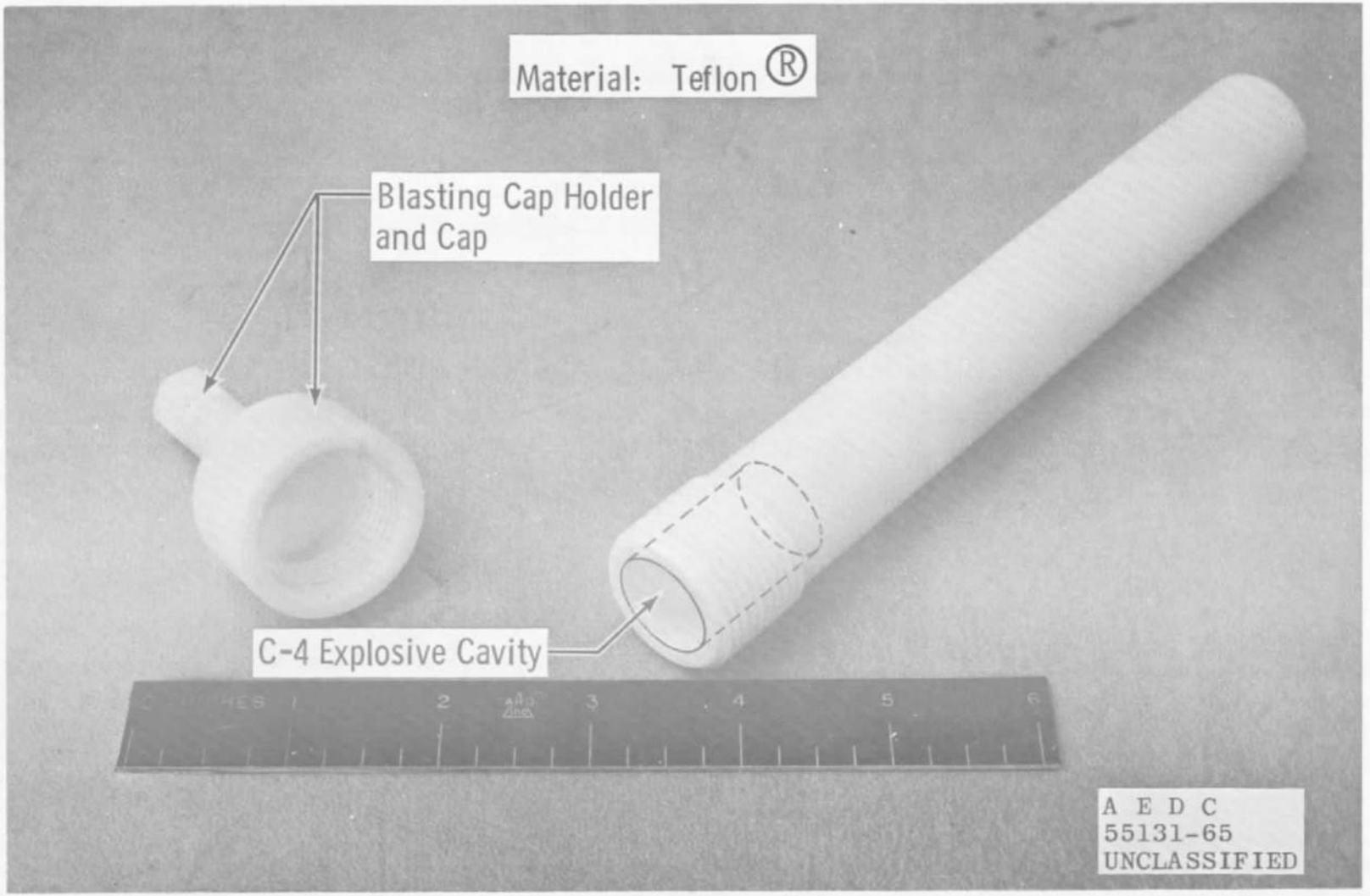

a. Holder Disassembled

Fig. 3 Pulse Charge Container

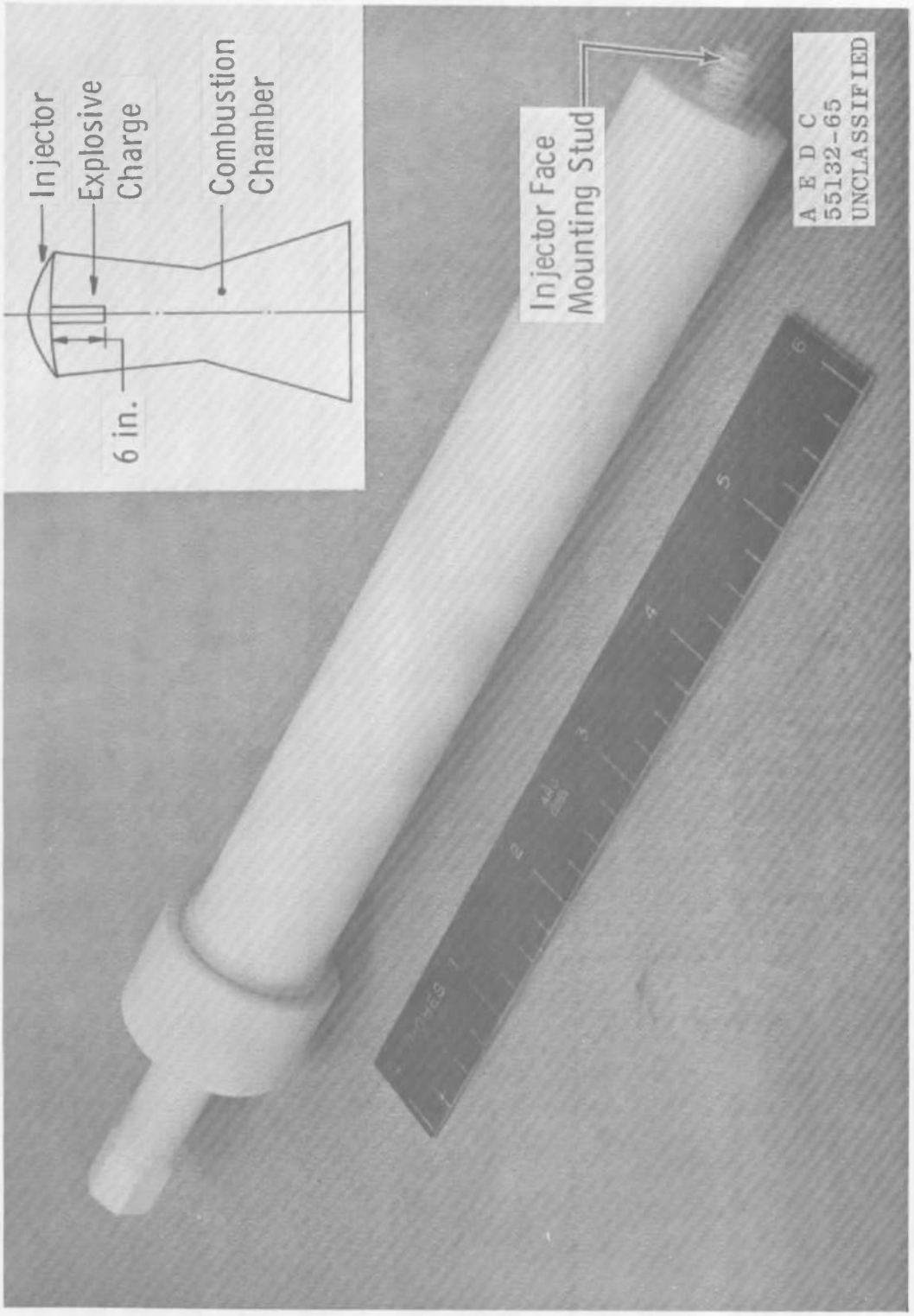

b. Holder Assembled

Fig. 3 Concluded

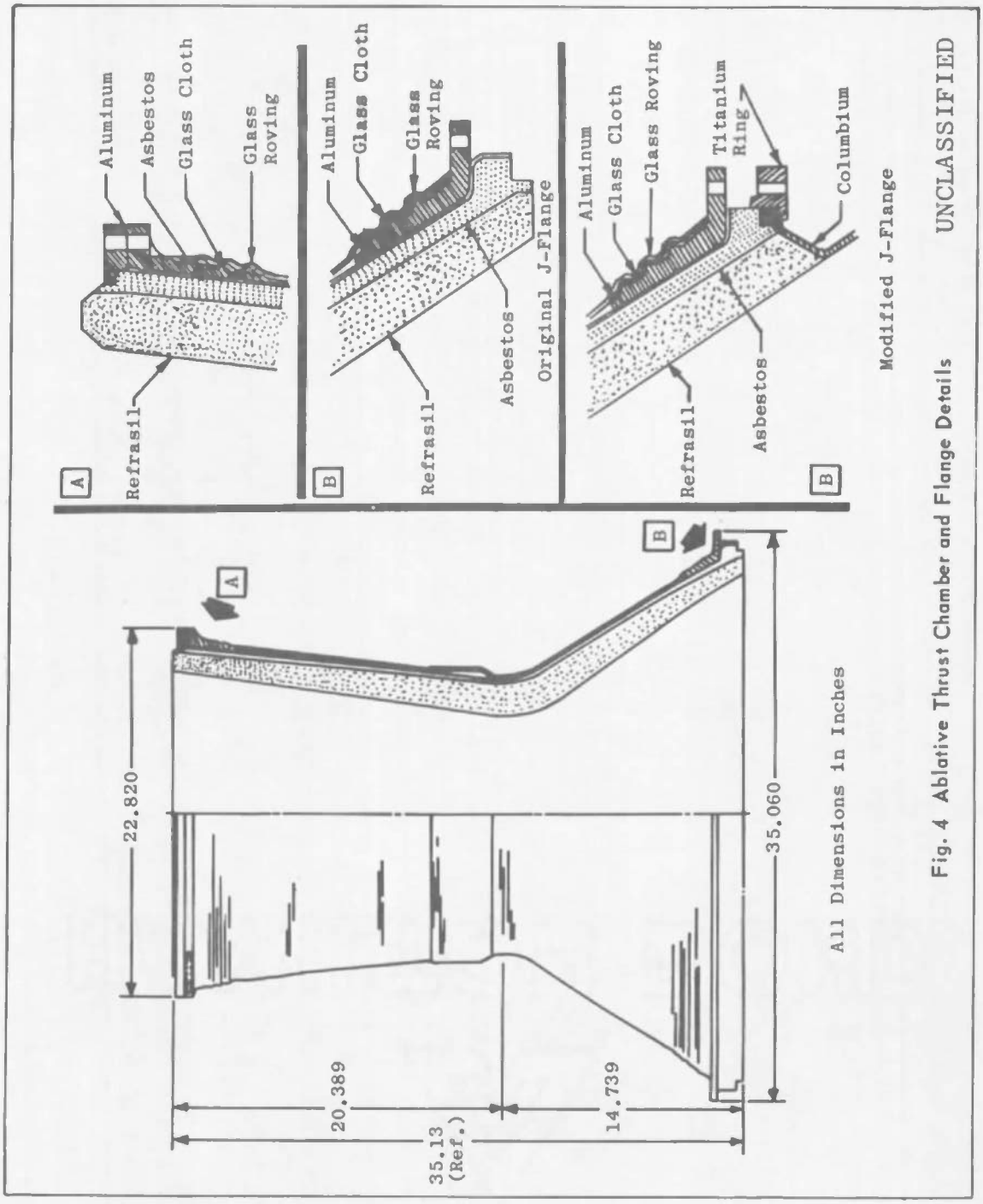

Fig. 4 Ablative Thrust Chamber and Flange Details

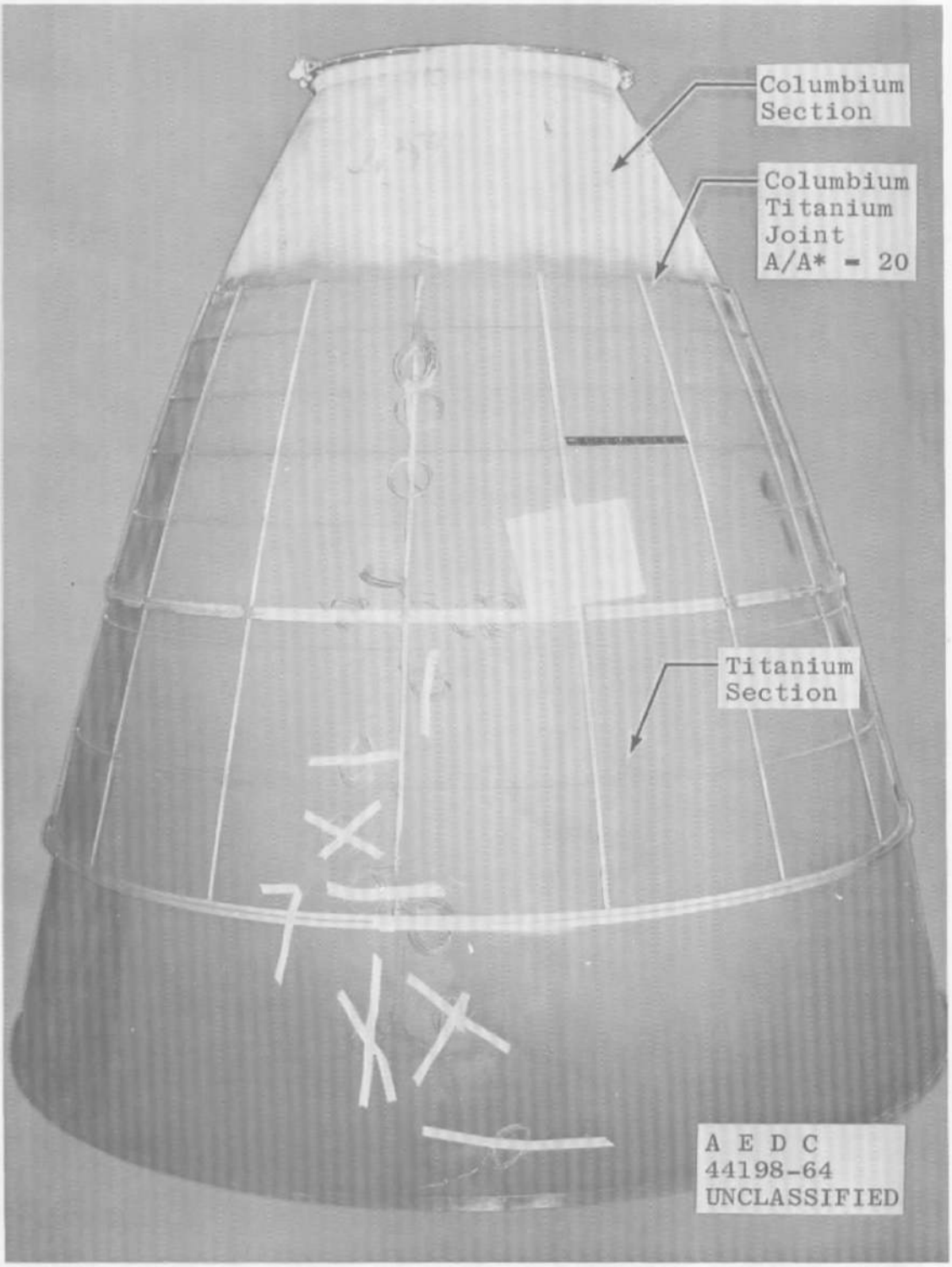

a. Extension Used with Engine S/N 9

Fig. 5 Exit Nozzle Extension

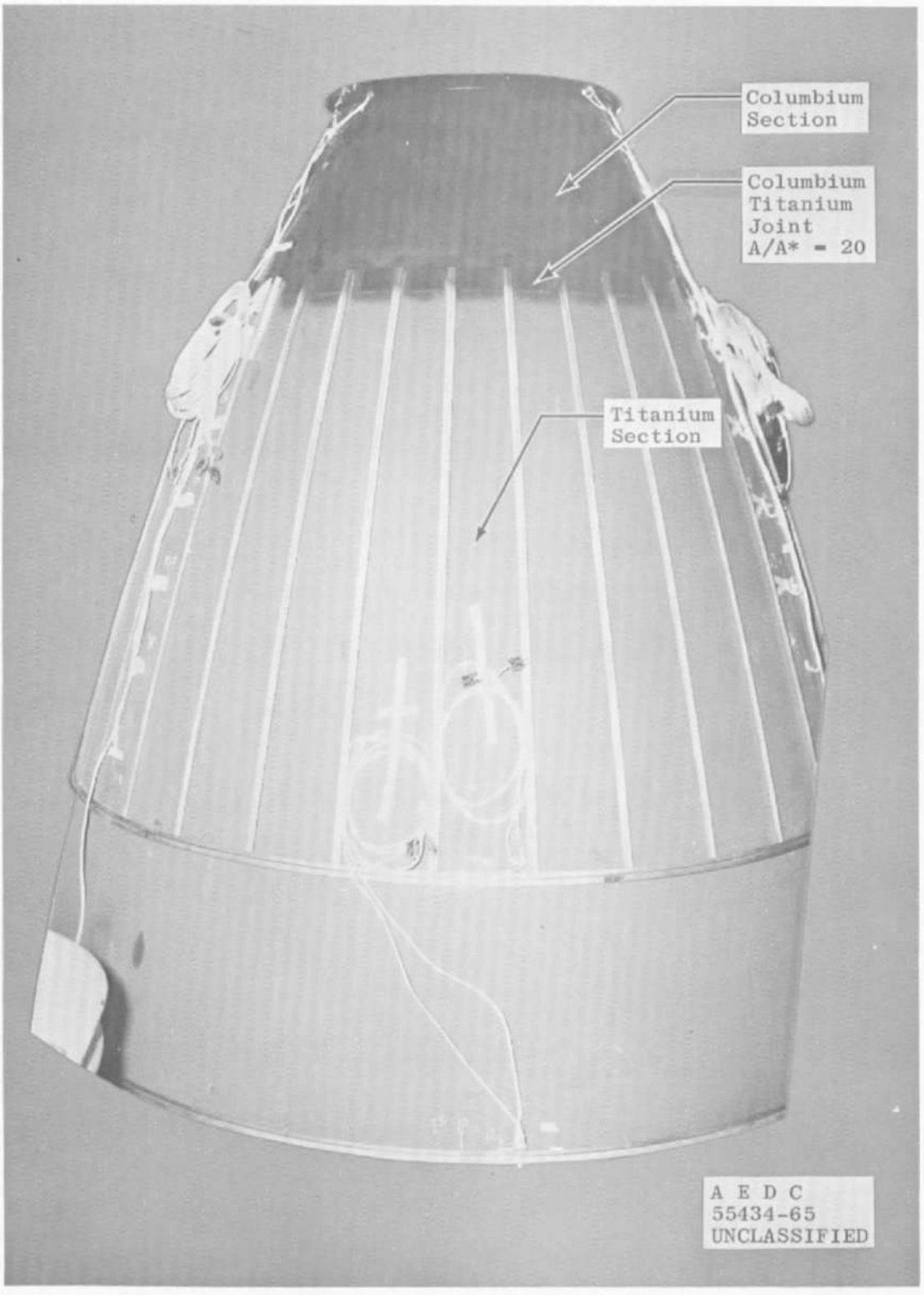

b. Extension Used with Engine S/N 9-1

Fig. 5 Continued

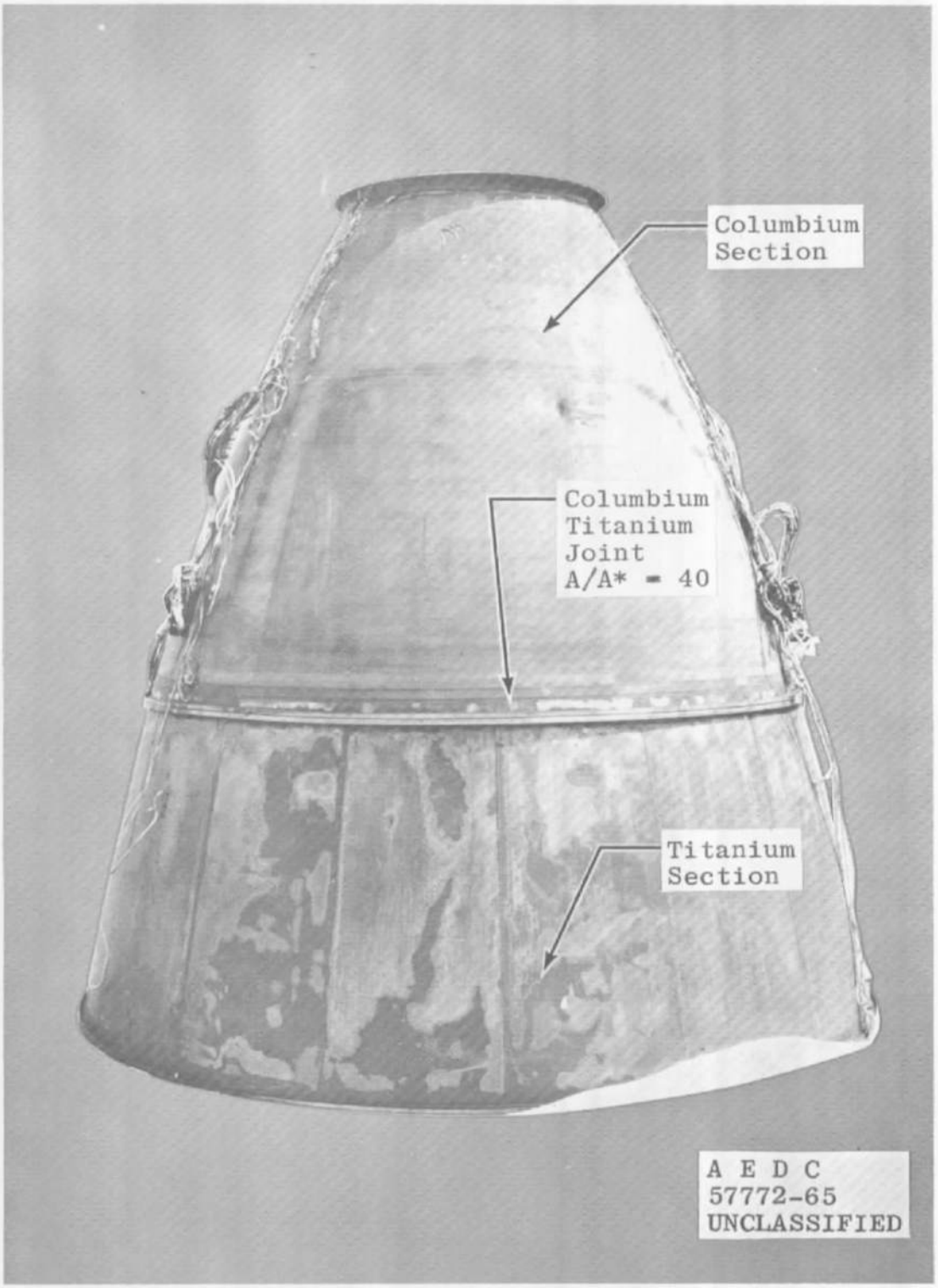

c. Extension Used with Engine S/N 11

Fig. 5 Concluded

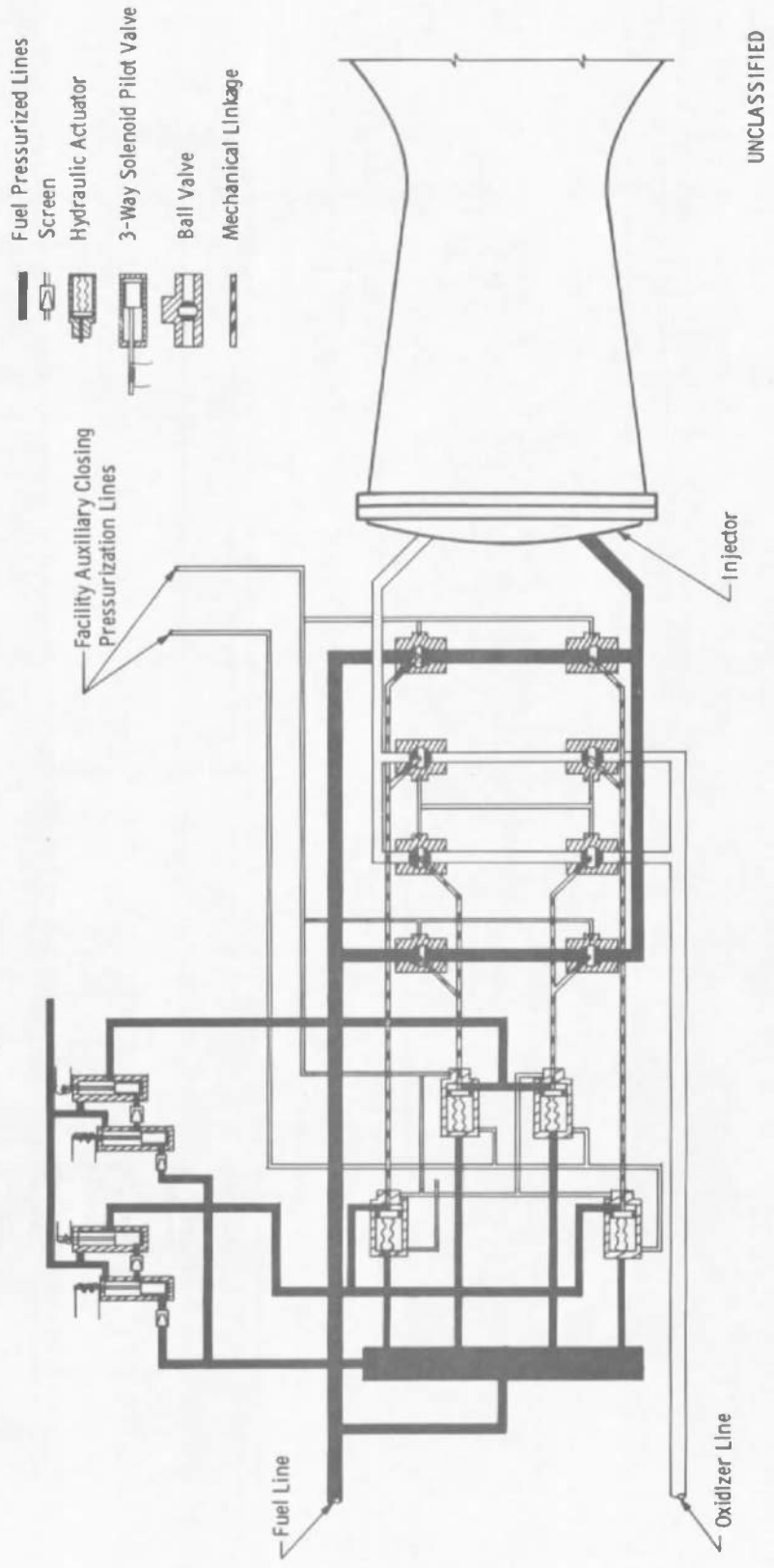

Fig. 6 Apollo Thrust Chamber Valve

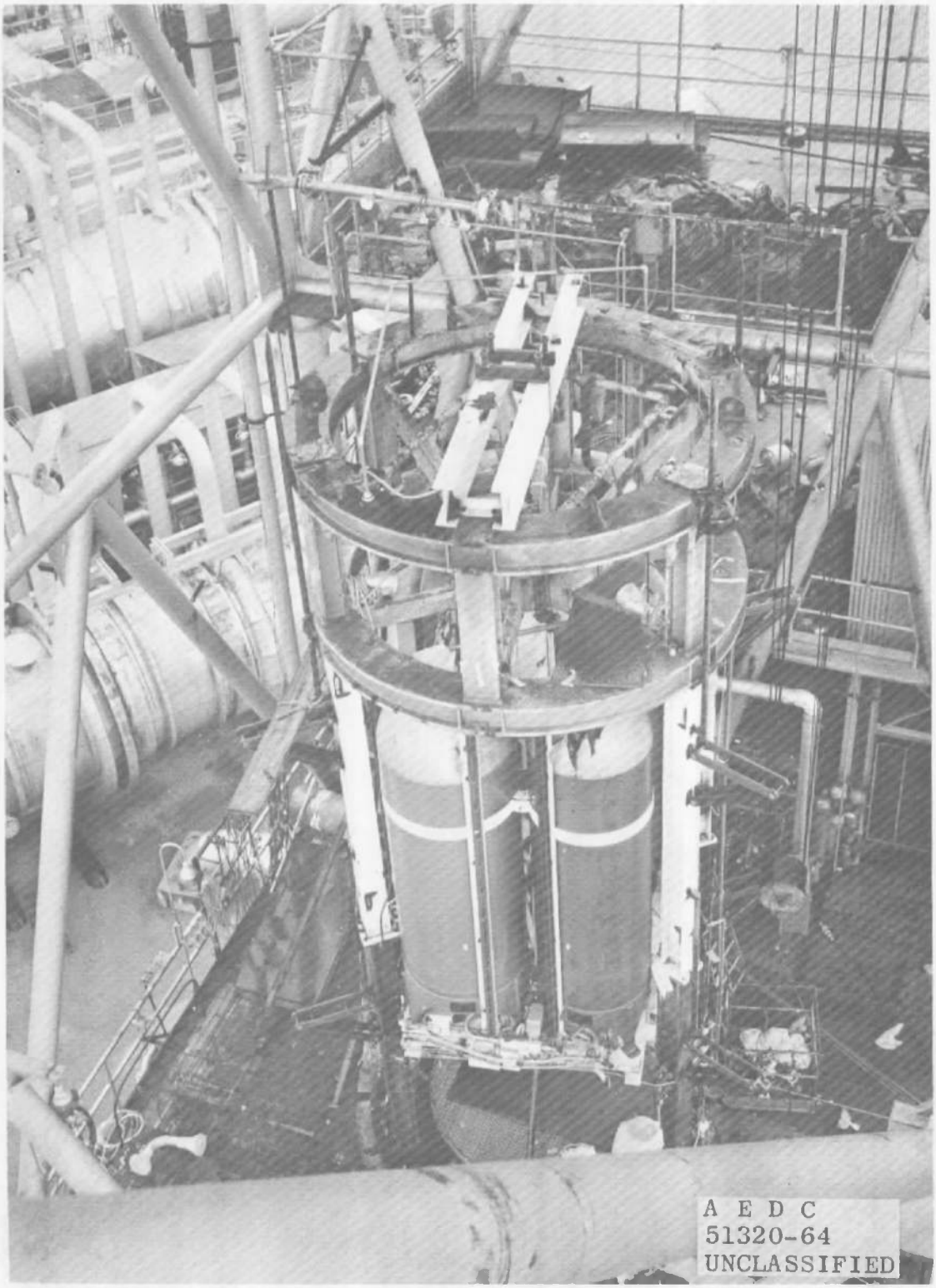

a. Cell Installation

Fig. 7 F-3 Fixture

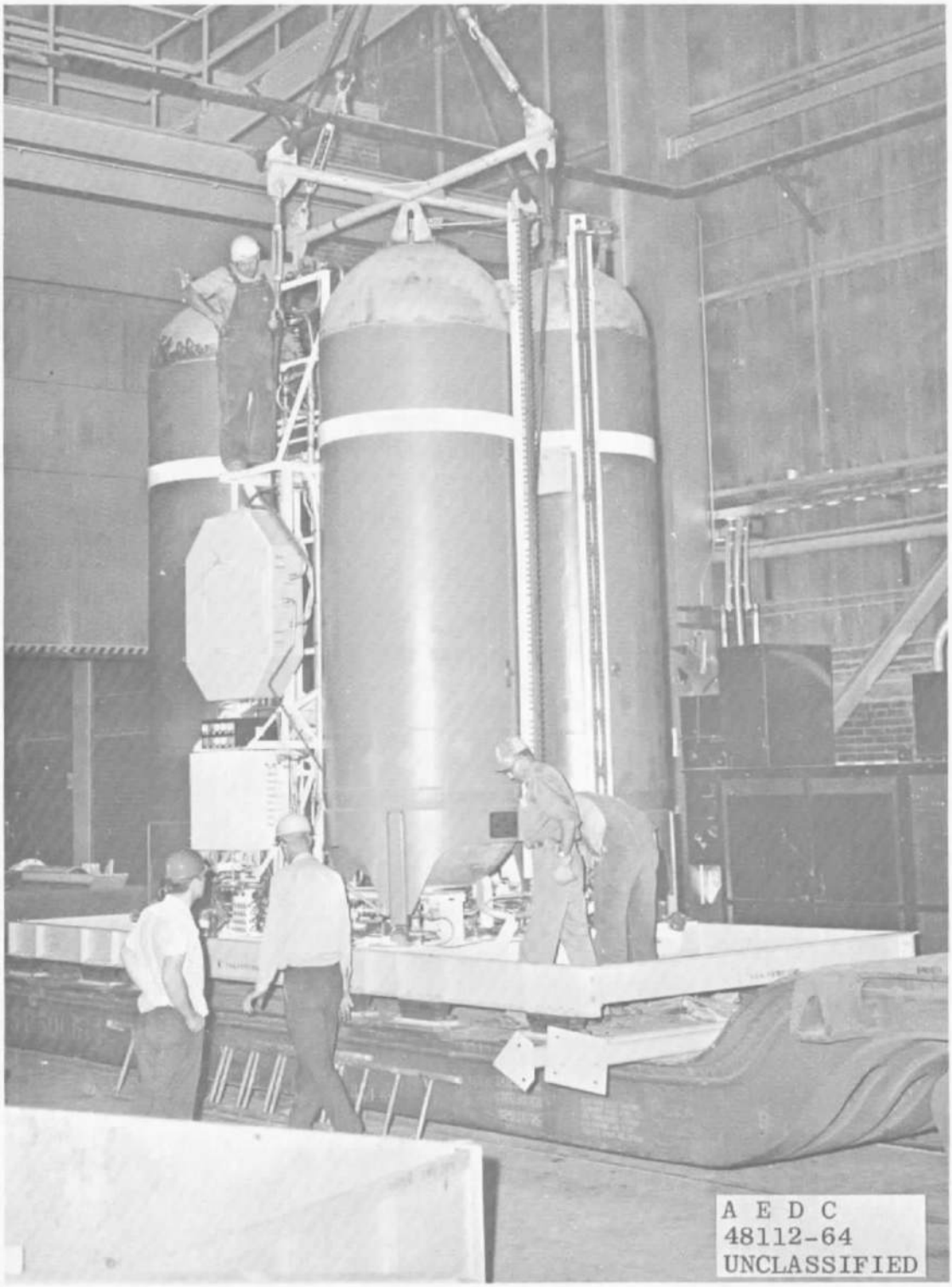

b. F-3 Fixture as Received

Fig. 7 Concluded

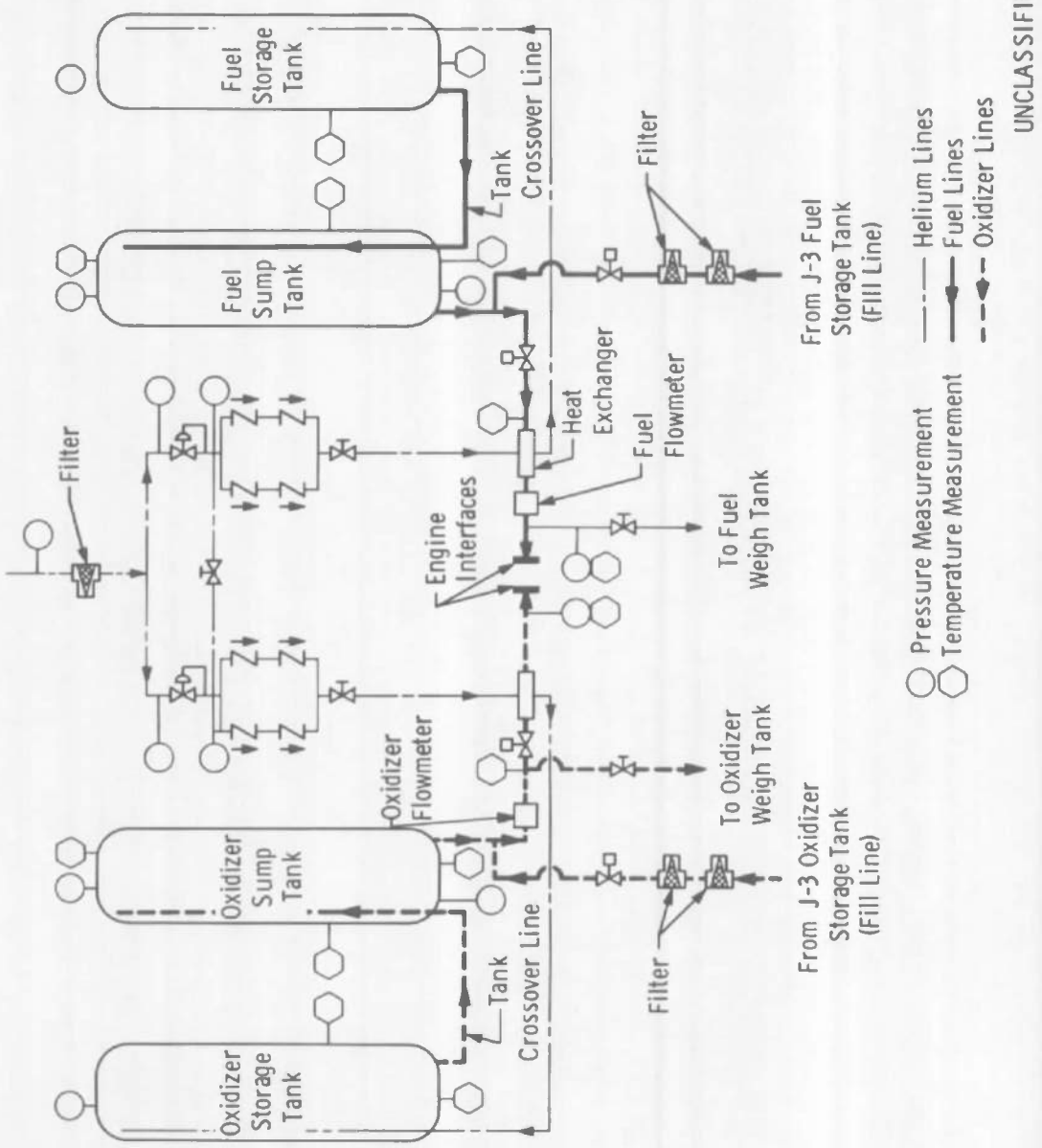

Fig. 8 NAA F-3 Fixture System Schematic

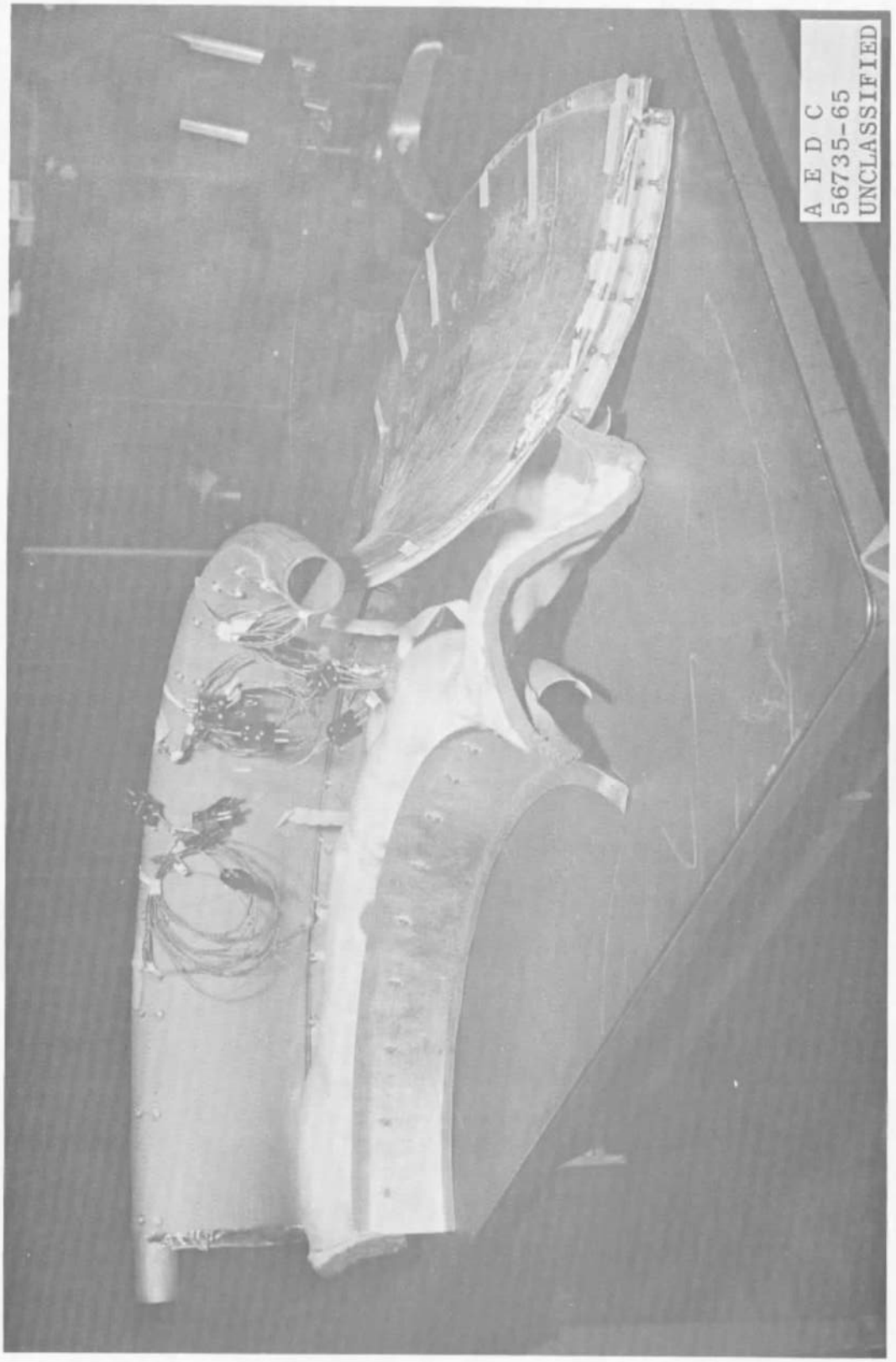

a. As Received

Fig. 9 NAA Heat Shield Segment

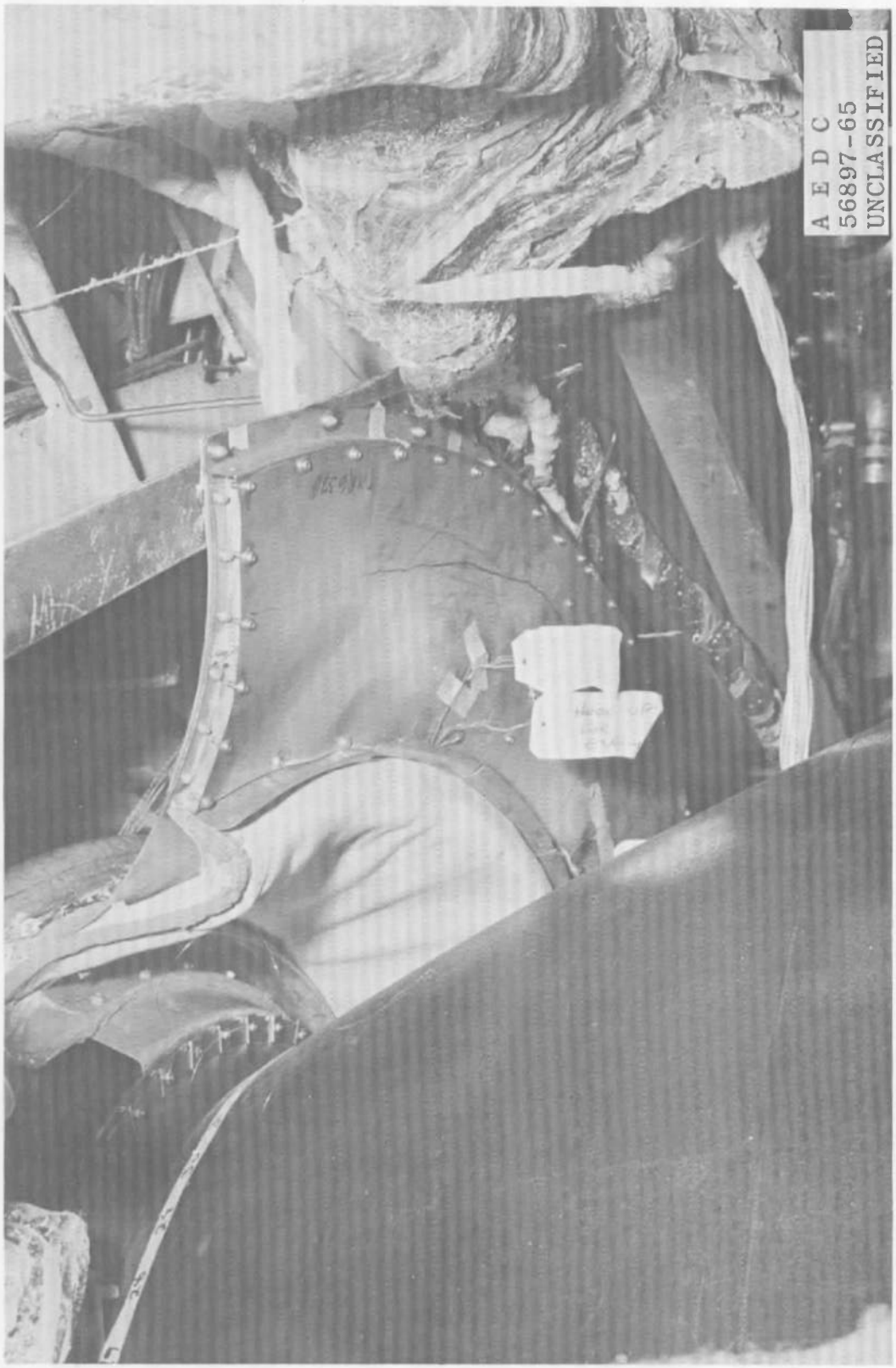

b. Installed

Fig. 9 Concluded

a. J-3 Complex

Fig. 10 Propulsion Engine Test Cell (J-3)

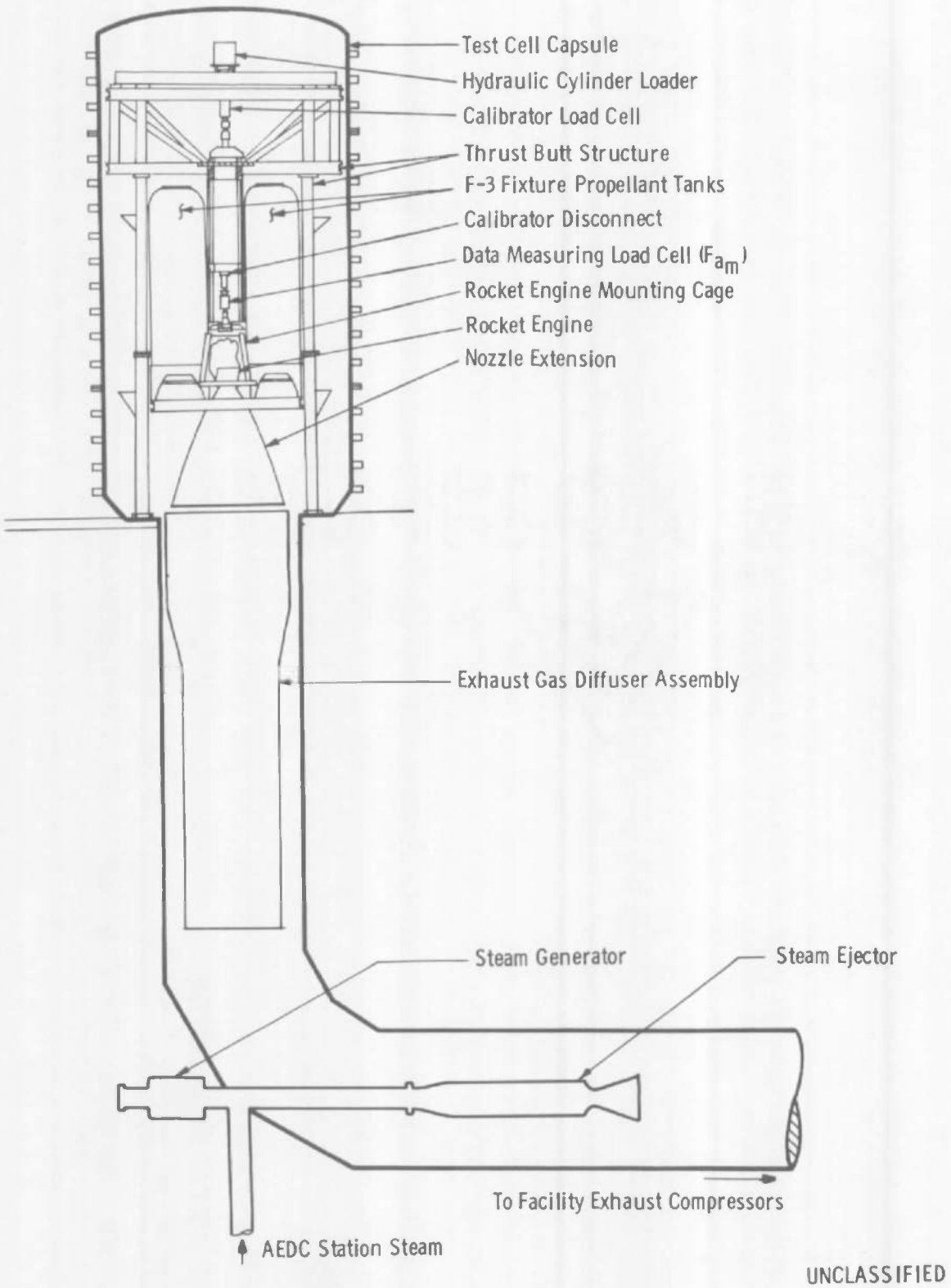

b. Side View, Test Article Installation

Fig. 10 Concluded

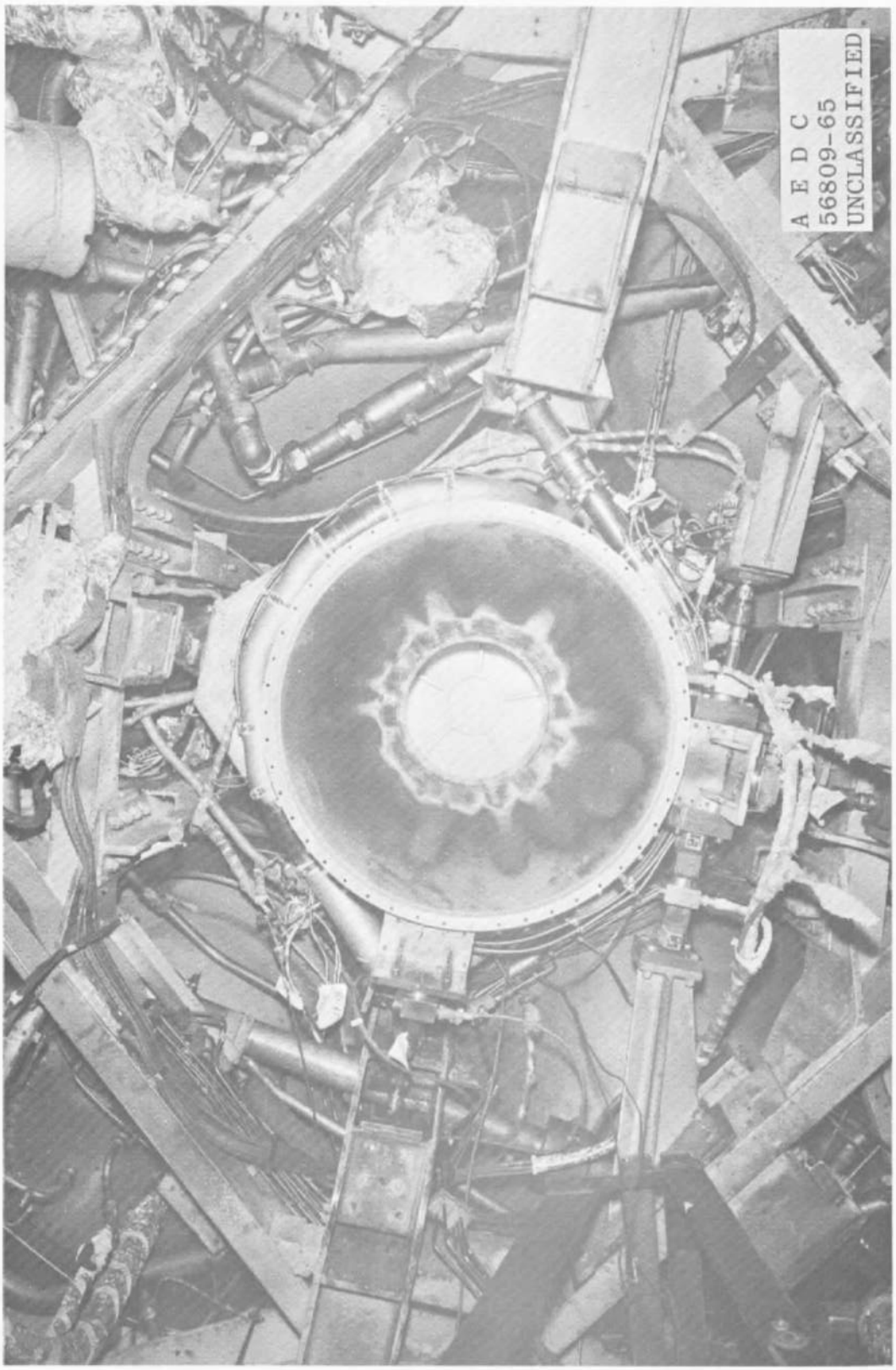

a. Engine and Thrust Frame, Looking Forward

Fig. 11 Six-Component Thrust Force Balance

UNCLASSIFIED

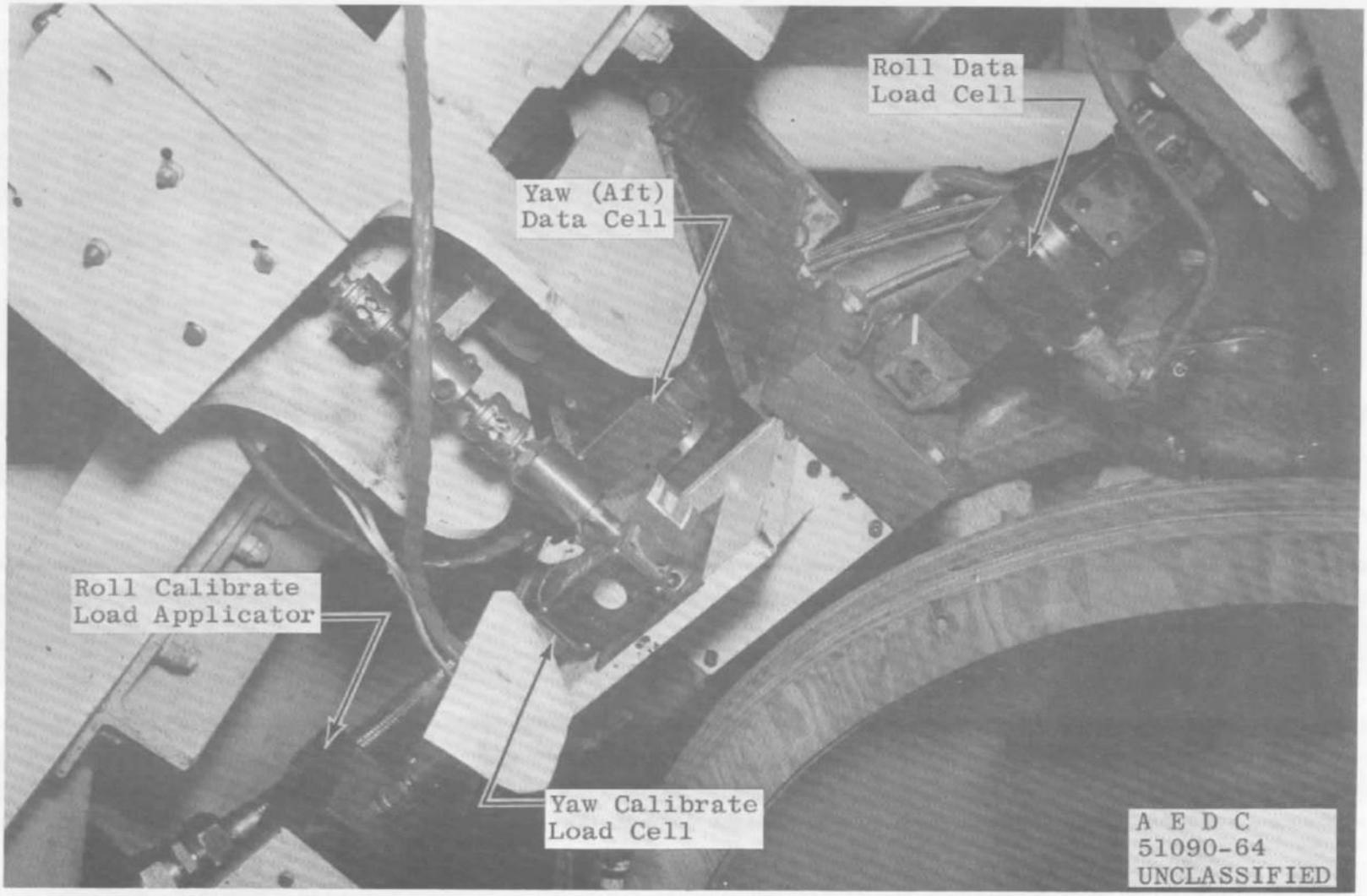

b. Side Load Trains

Fig. 11 Continued

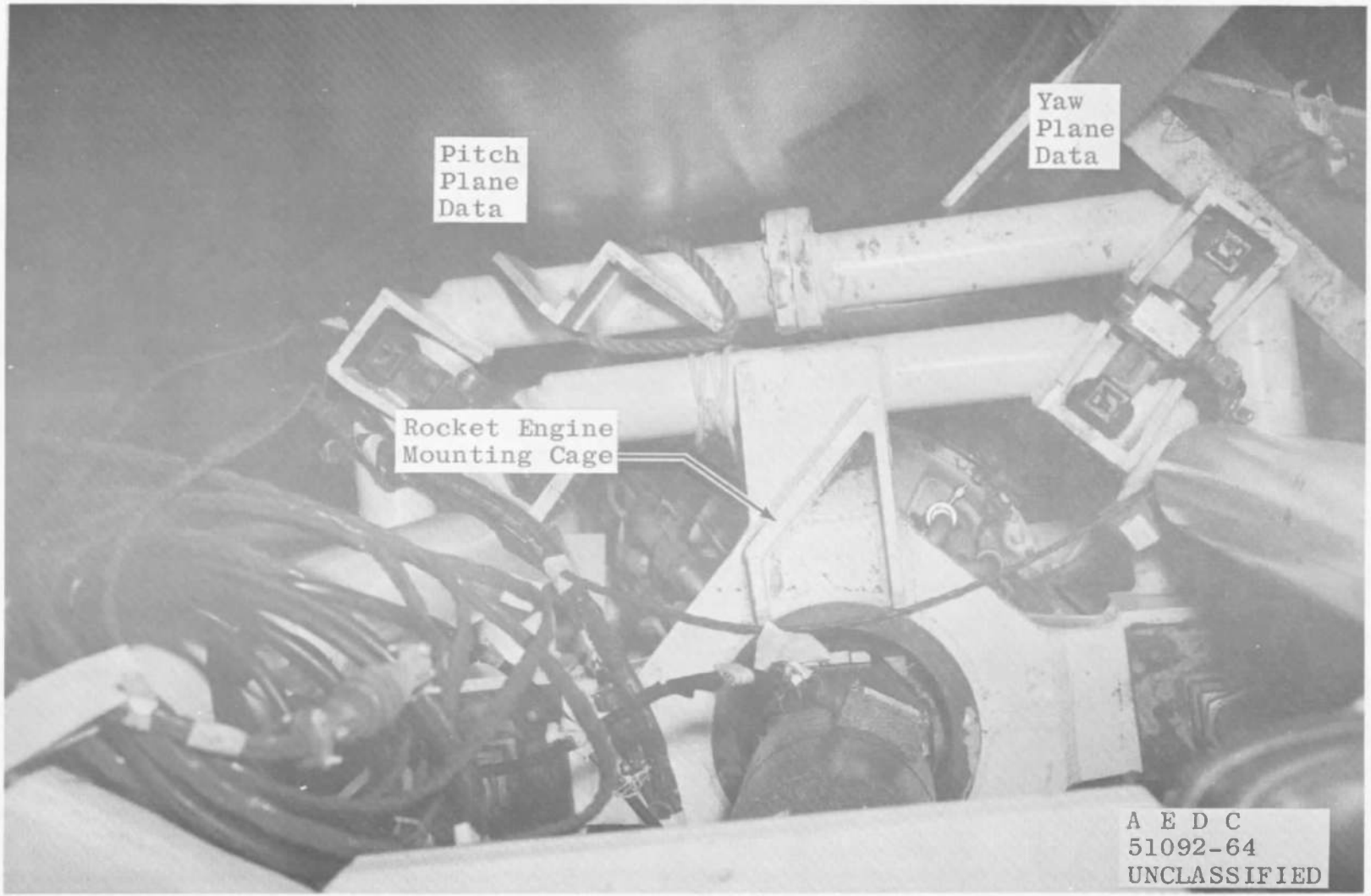

c. Forward Side Load Trains

Fig. 11 Continued

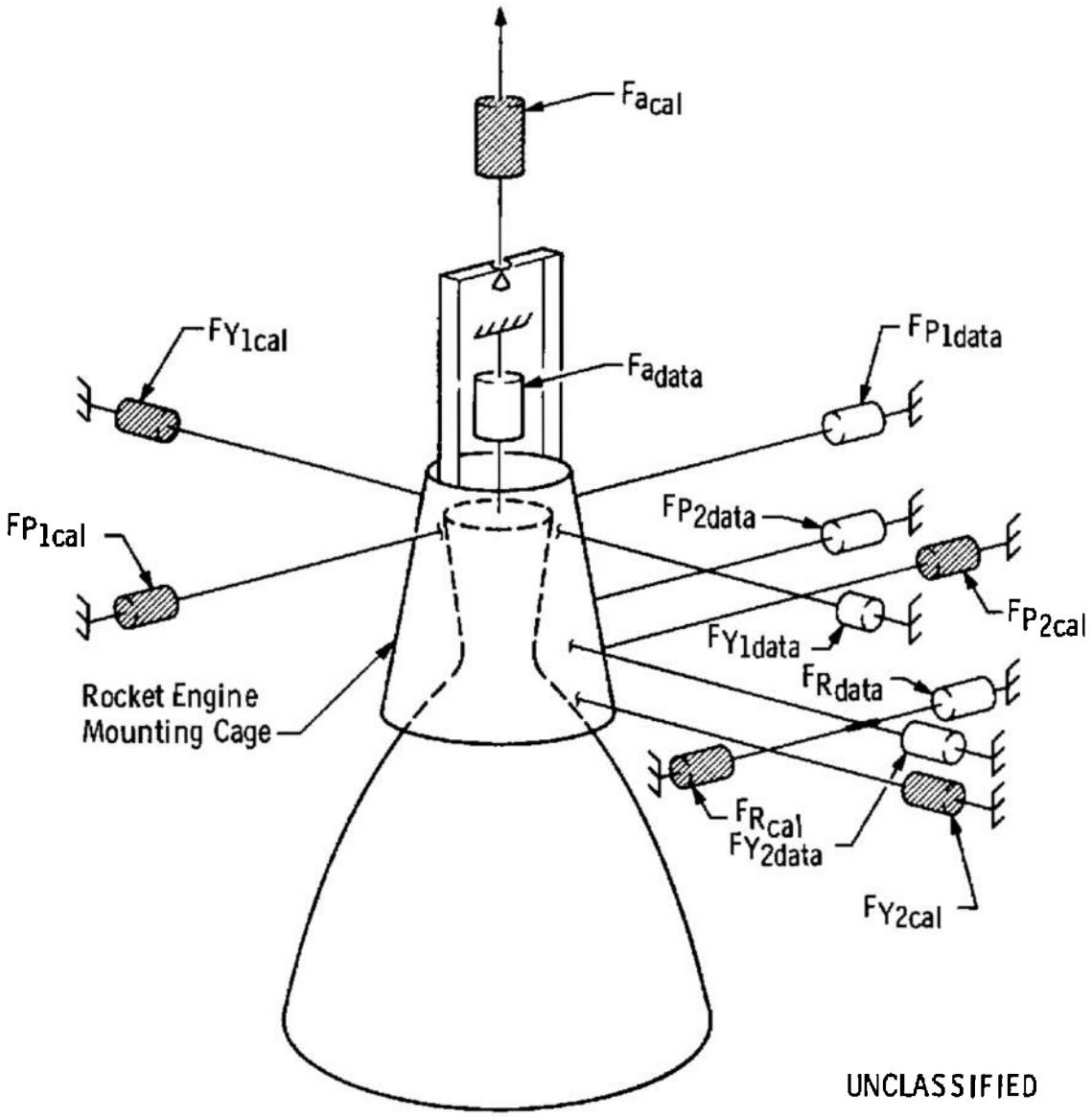

d. Schematic of Six-Component Thrust System

Fig. 11 Continued

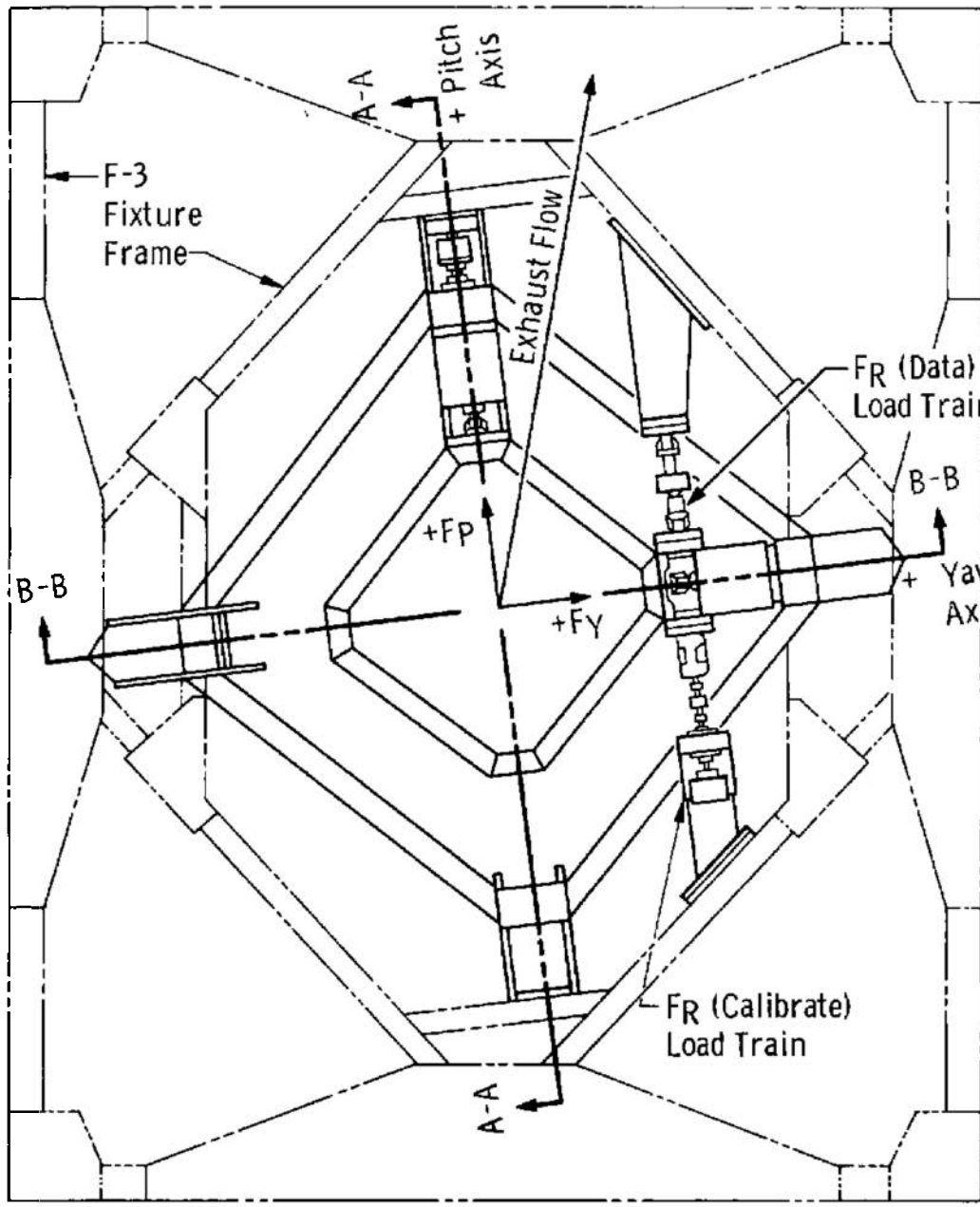

e. Plan View of Thrust System

Fig. 11 Continued

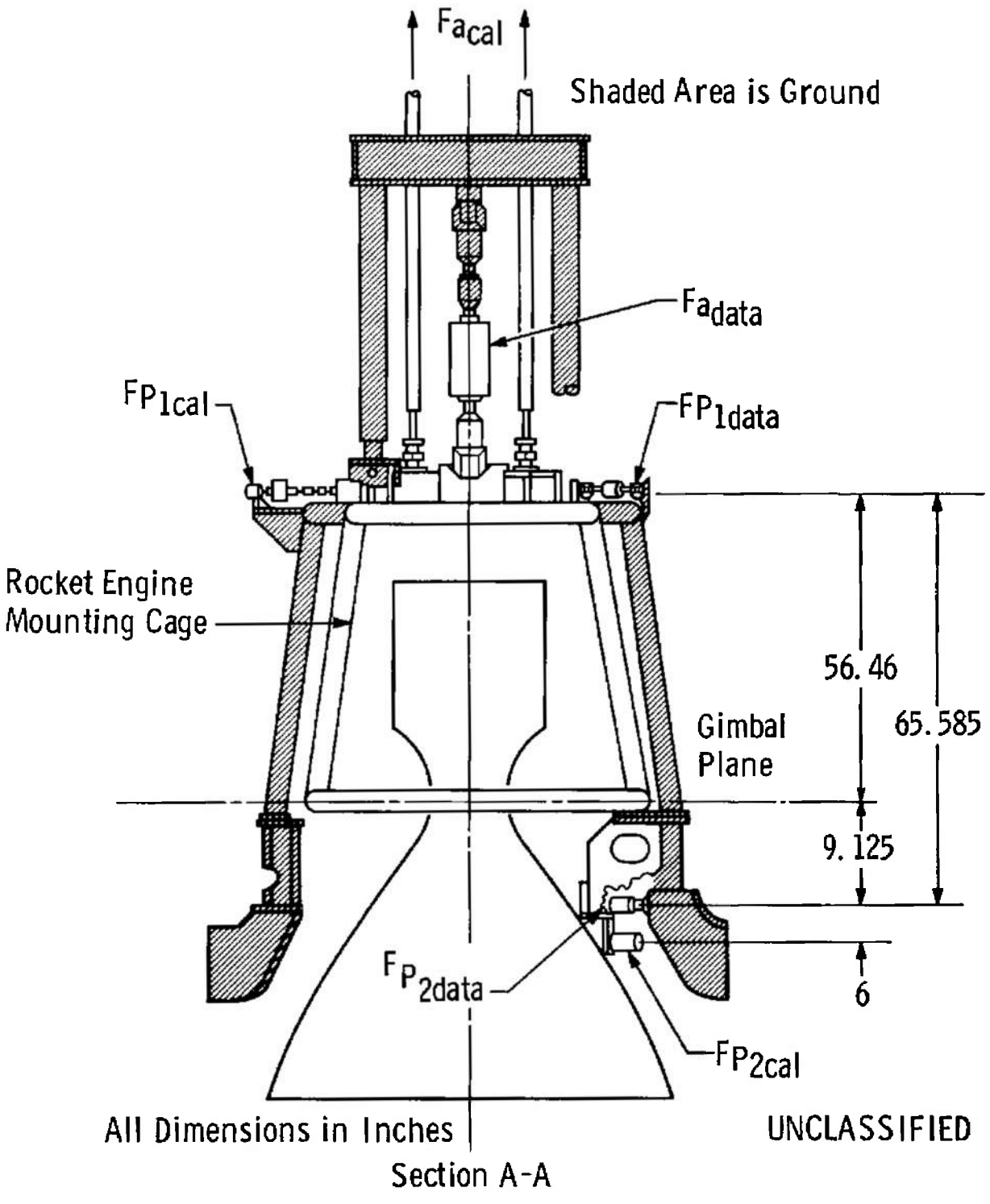

f. Pitch Plane Load Cells

Fig. 11 Continued

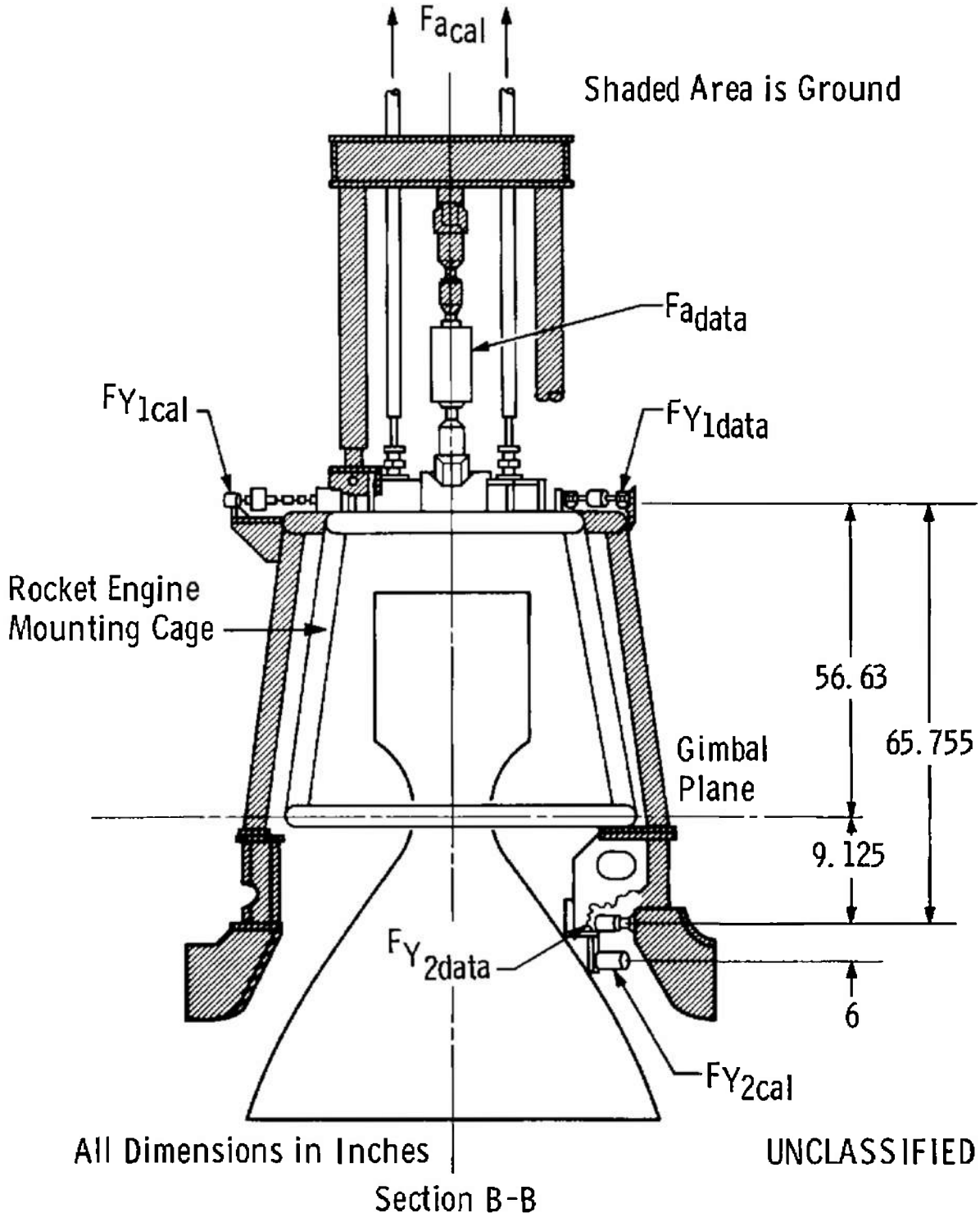

g. Yaw Plane Load Cells

Fig. 11 Concluded

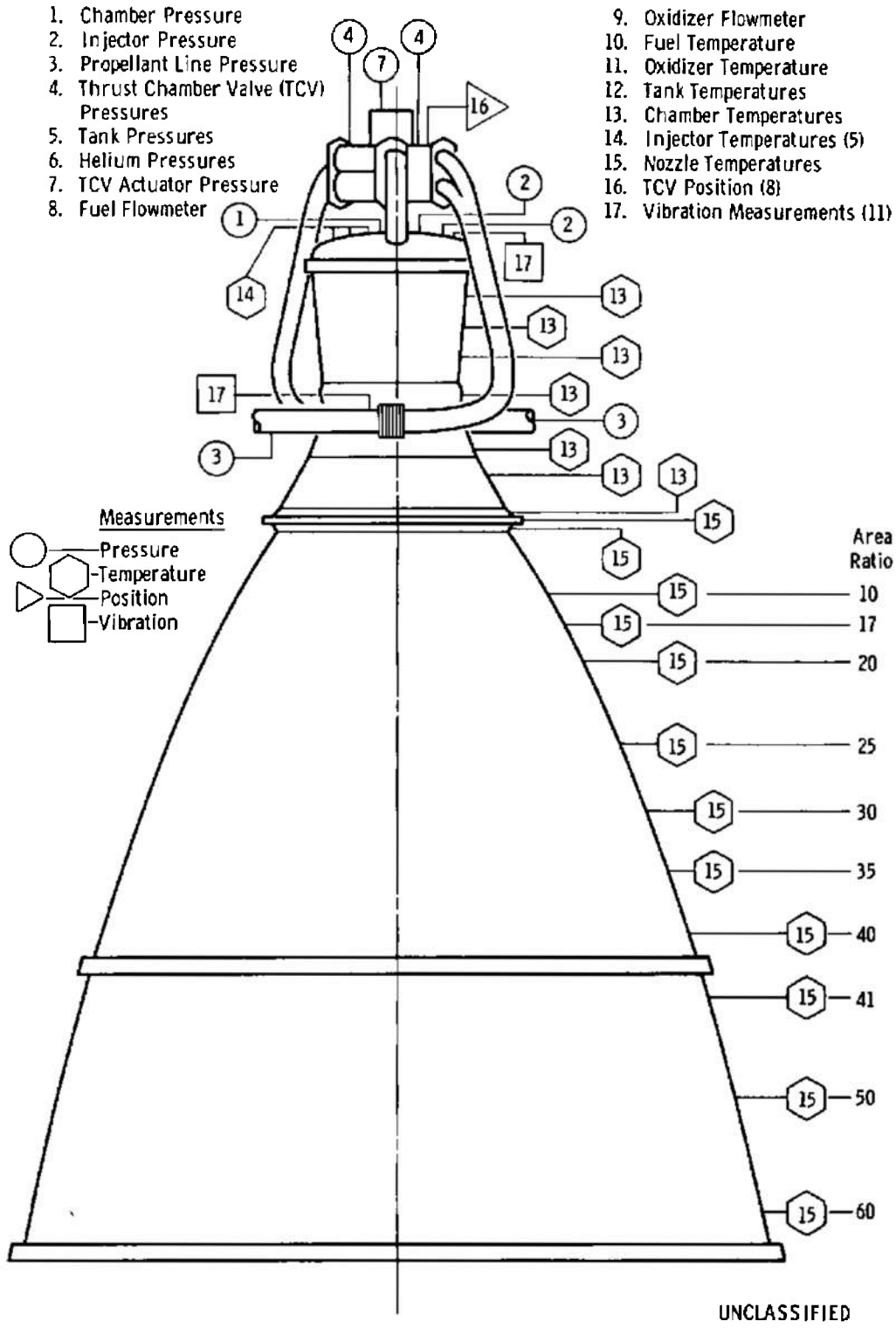

Fig. 12 Engine and Nozzle Extension Instrumentation Locations

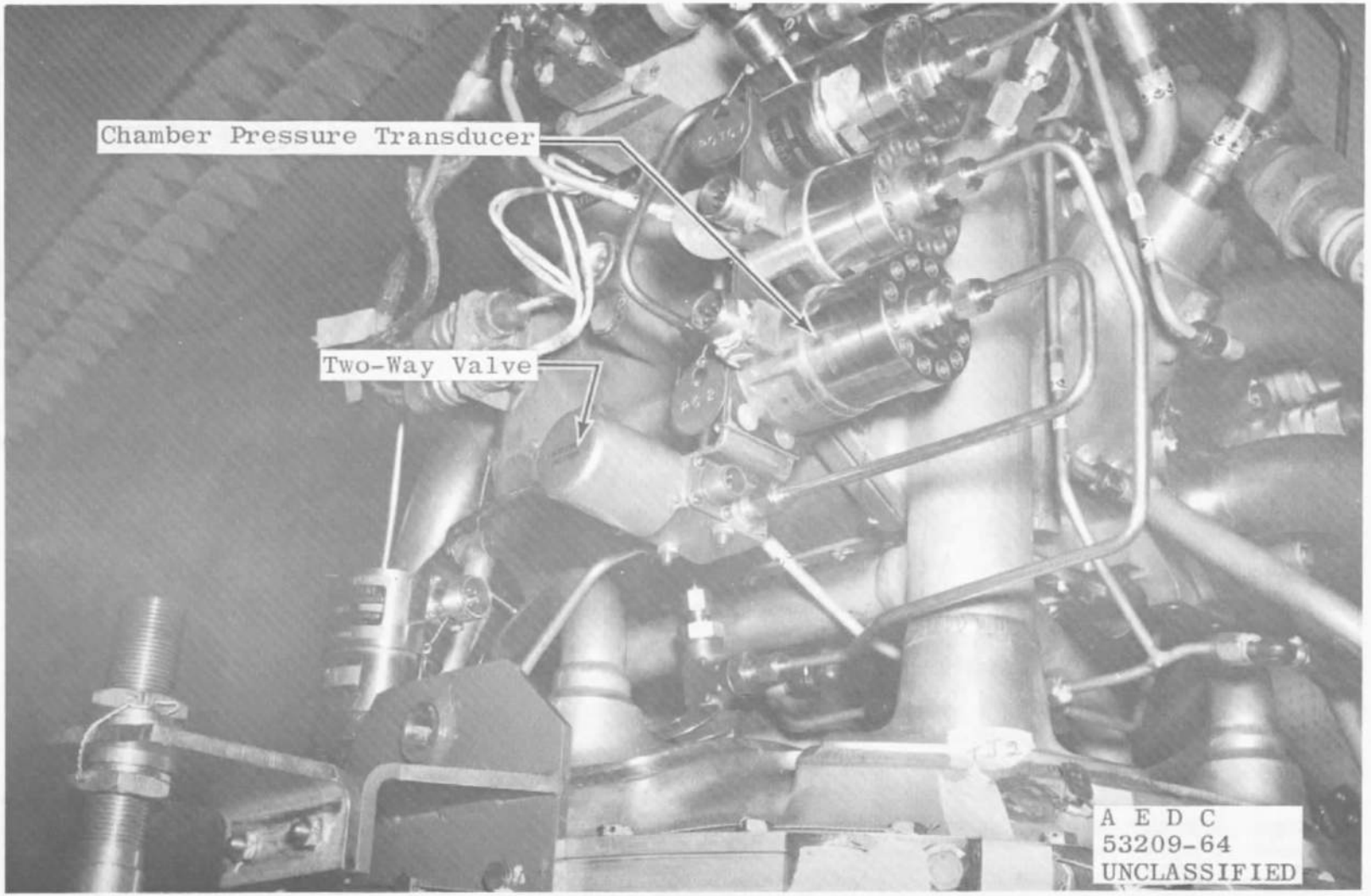

a. Chamber Pressure Transducer (In-Place Calibrated)

Fig. 13 Engine Instrumentation

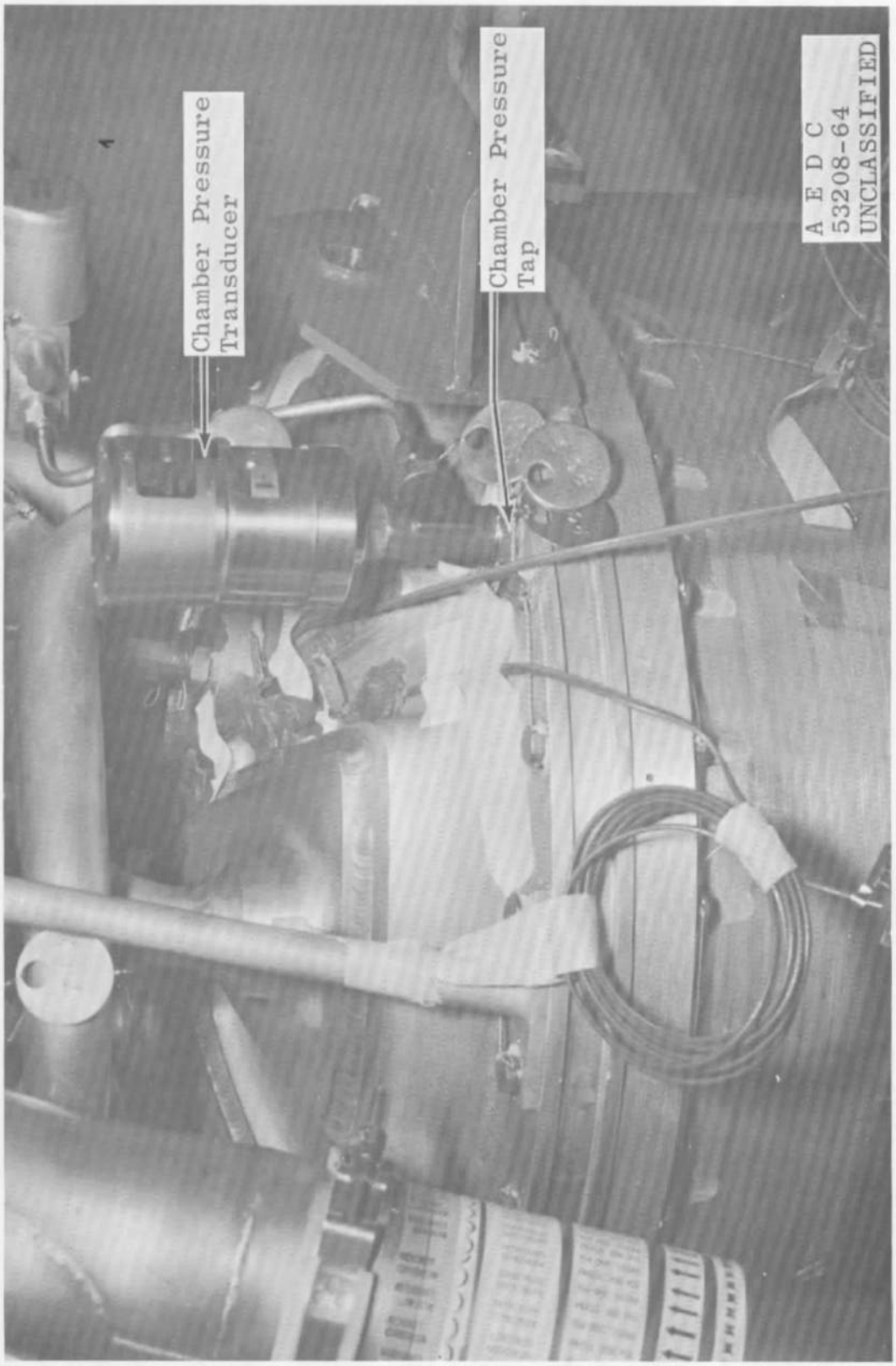

b. Chamber Pressure Transducer (Close-Coupled)

Fig. 13 Concluded

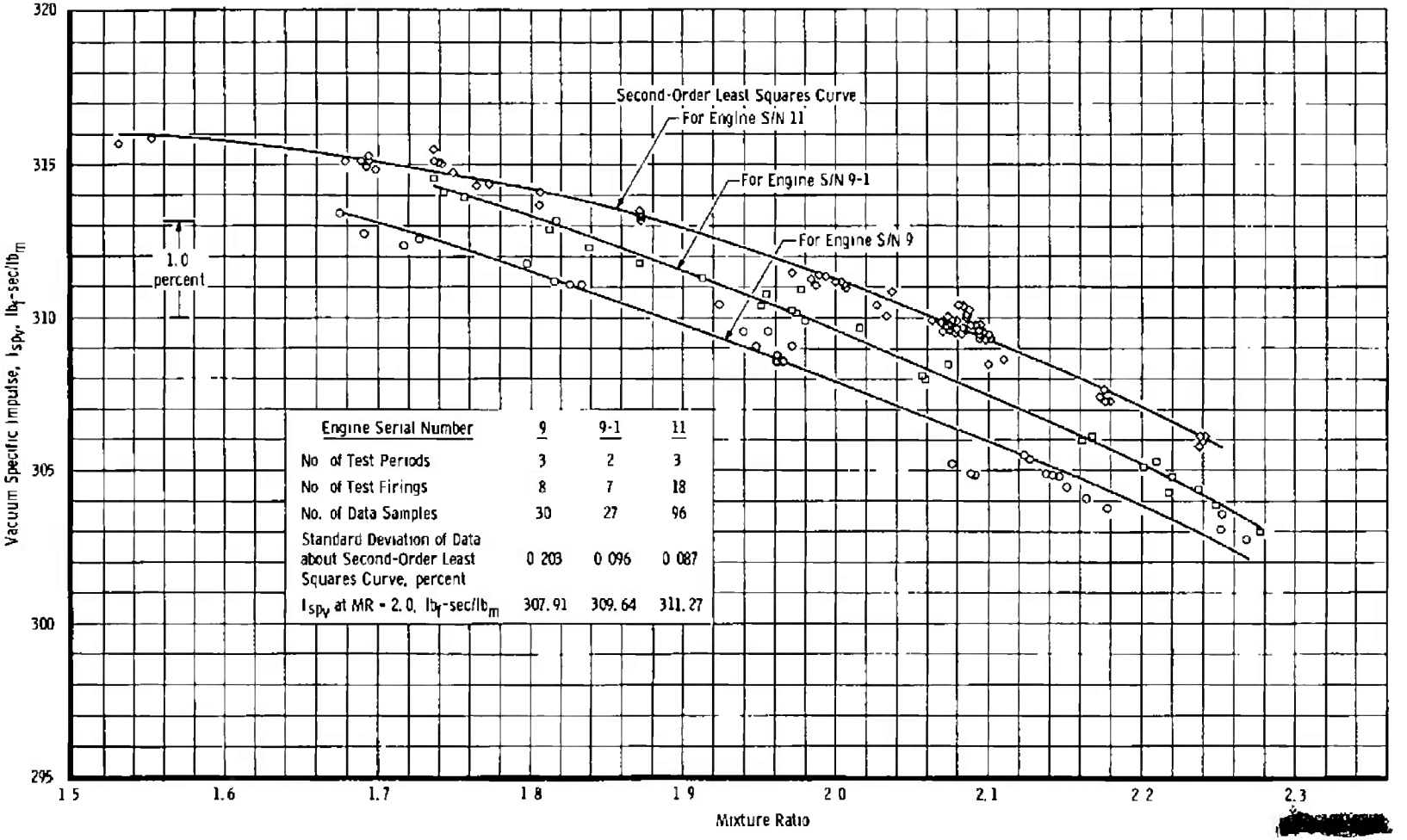

Engine Serial Number	9	9-1	11
No. of Test Periods	3	2	3
No. of Test Firings	8	7	18
No. of Data Samples	30	27	96
Standard Deviation of Data about Second-Order Least Squares Curve, percent	0.203	0.096	0.087
I_{sp_V} at MR = 2.0, lb_f-sec/lb_m	307.91	309.64	311.27

Fig. 14 Engine Performance at Design Chamber Pressure

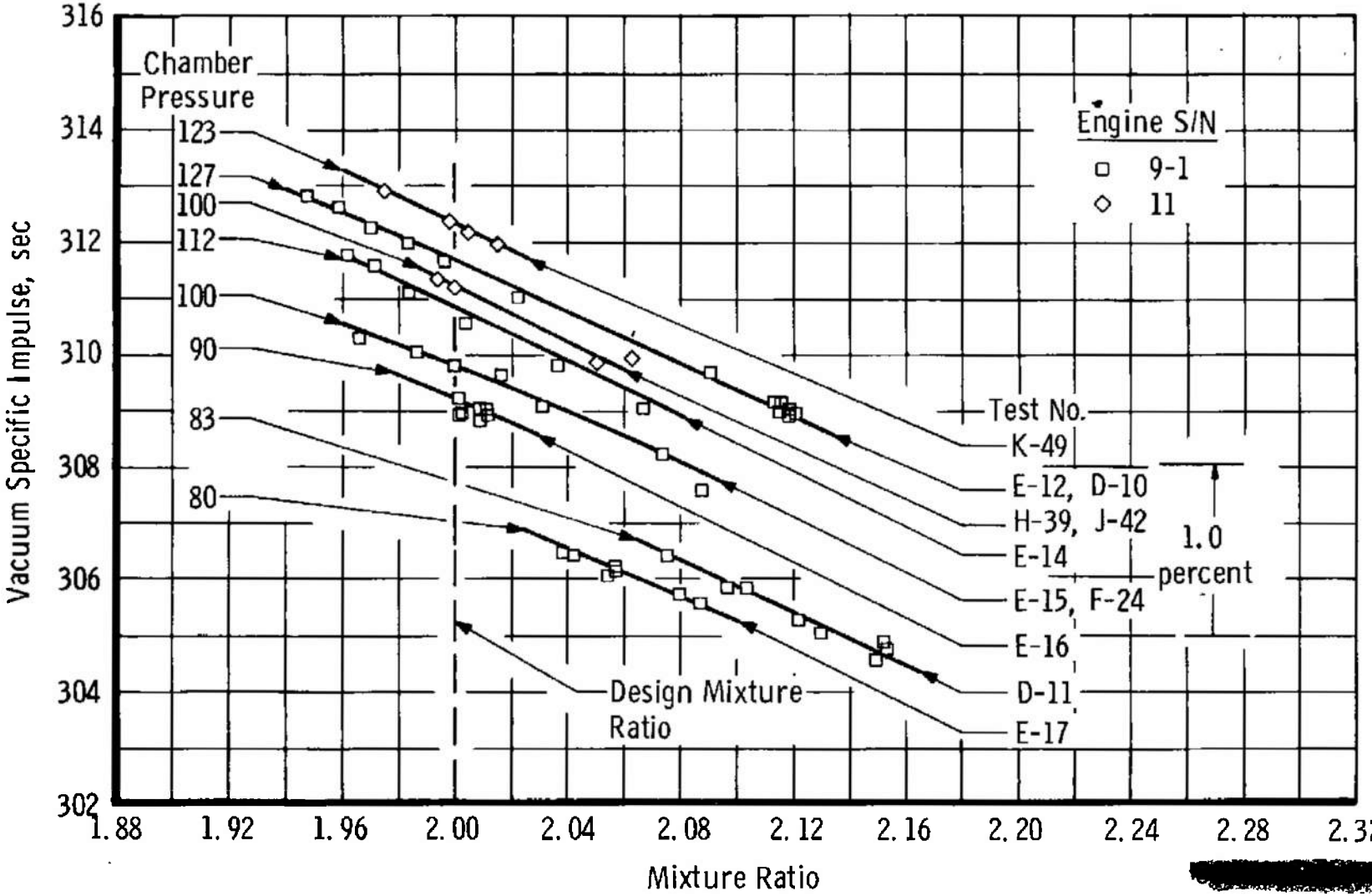

Fig. 15 Variation of Vacuum Specific Impulse with Mixture Ratio at Various Chamber Pressures

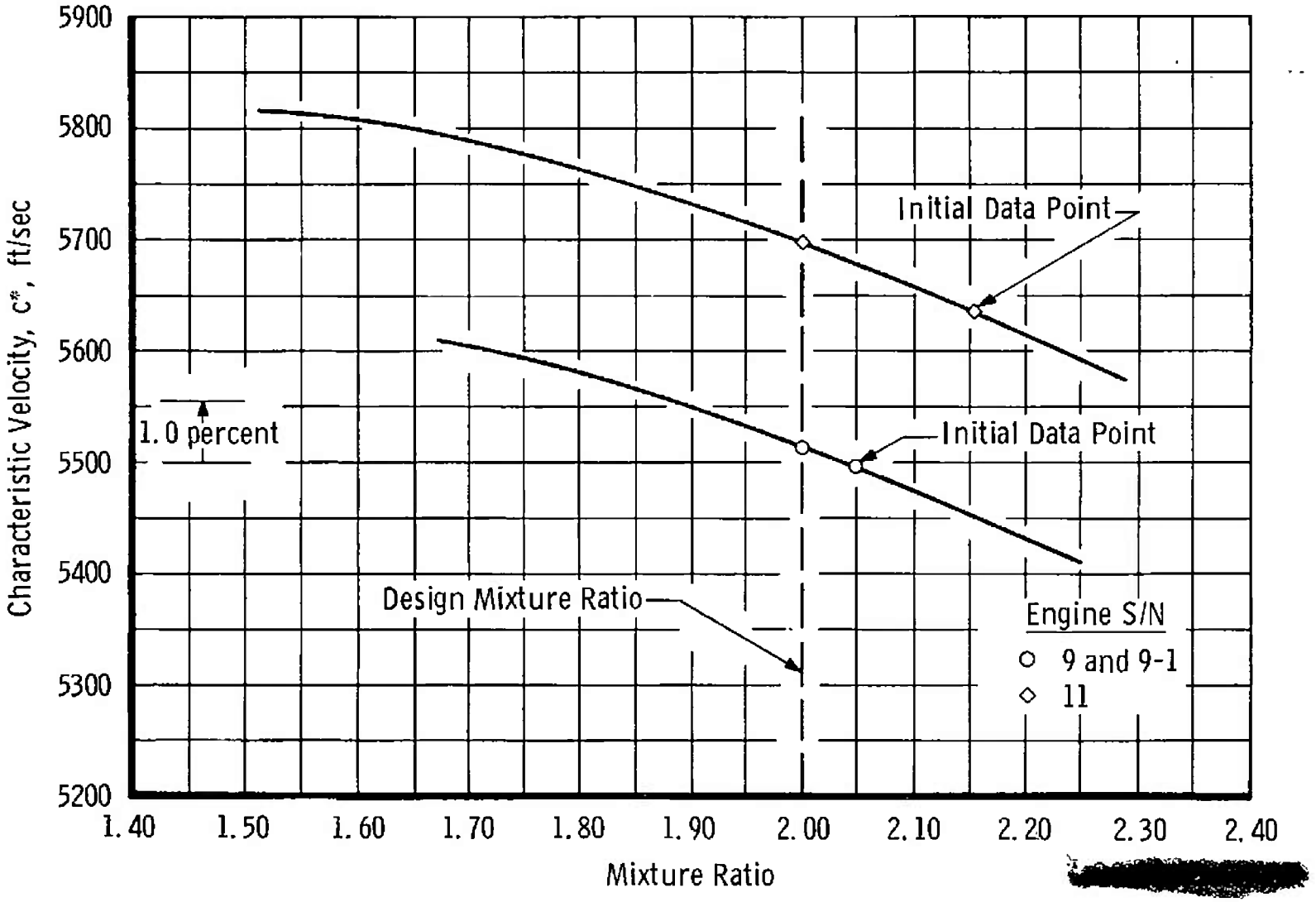

Fig. 16 Characteristic Velocity versus Mixture Ratio Relation at Design Chamber Pressure

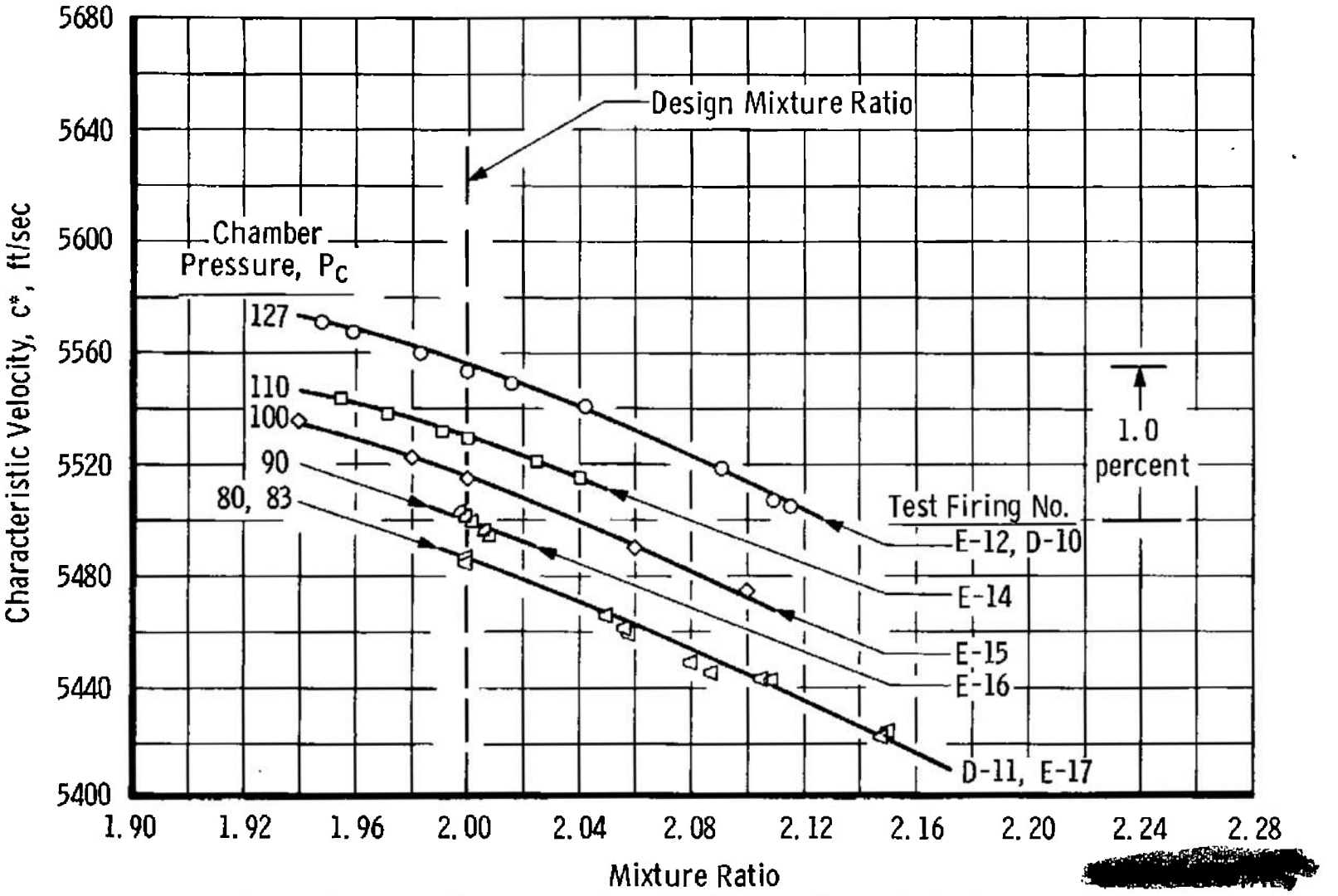

Fig. 17 Characteristic Velocity versus Mixture Ratio Relation at Various Chamber Pressures

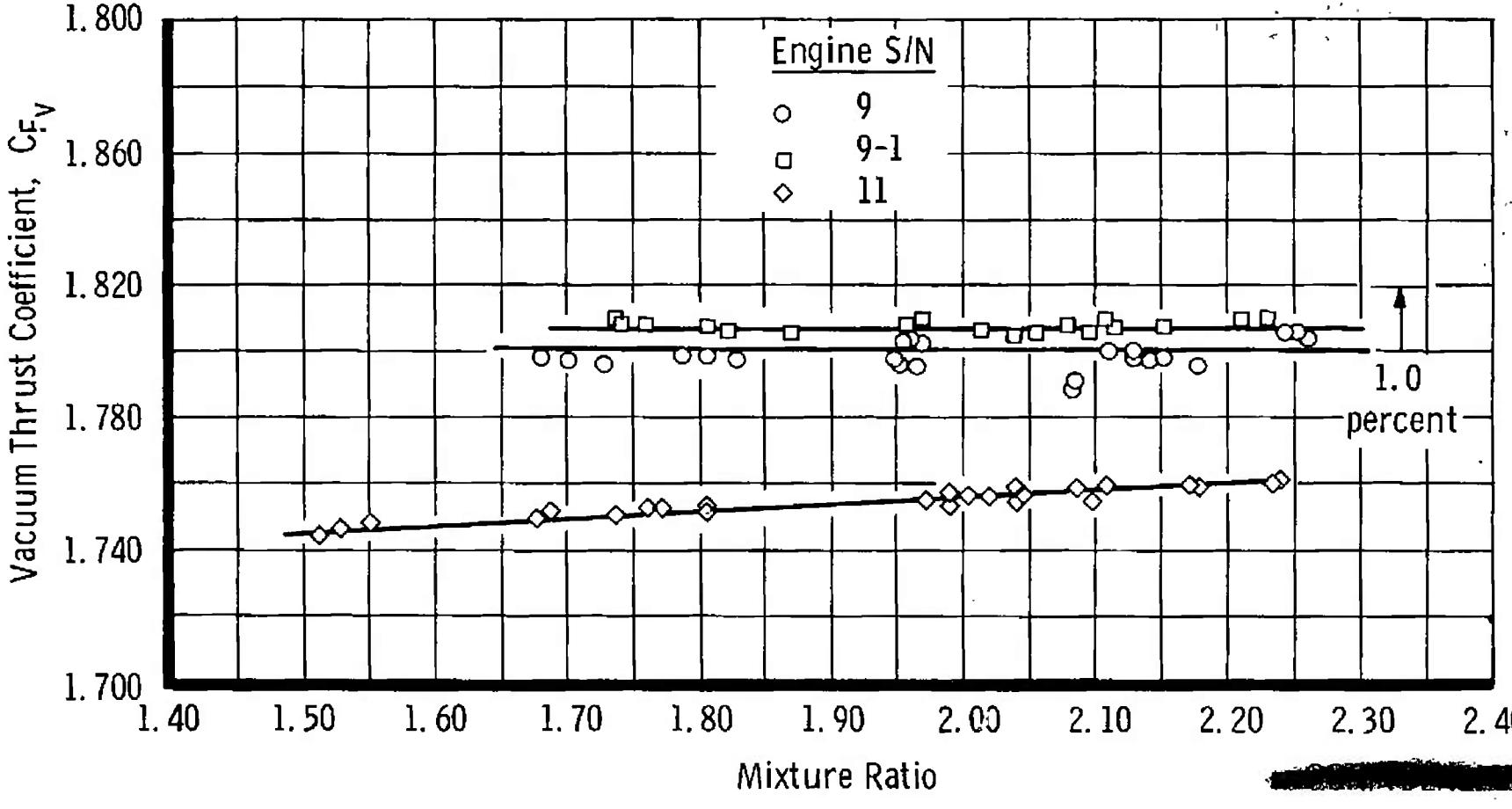

Fig. 18 Variation of Vacuum Thrust Coefficient with Mixture Ratio

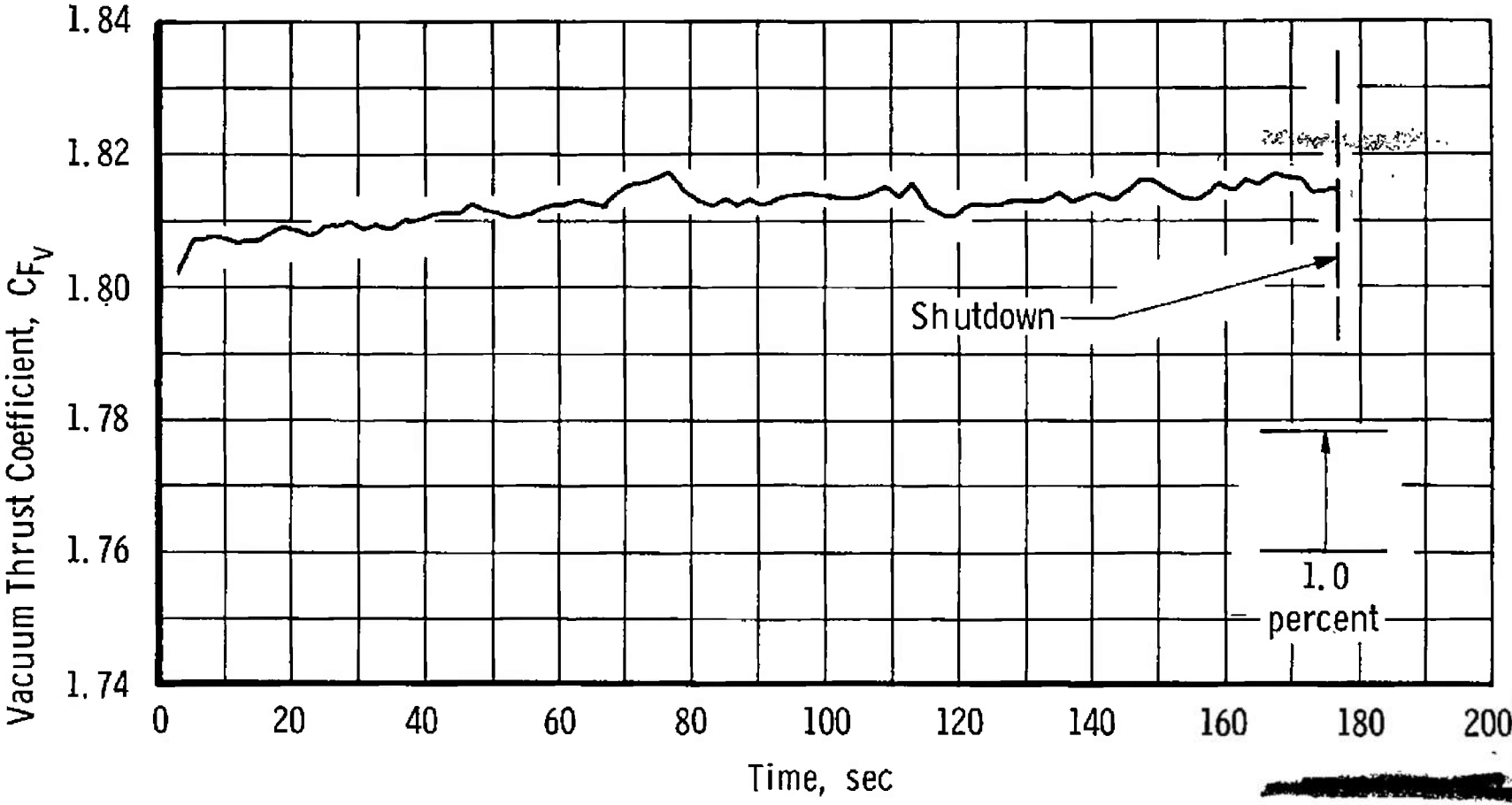

Fig. 19 Variation of Vacuum Thrust Coefficient during 180-sec Test (Test F-24)

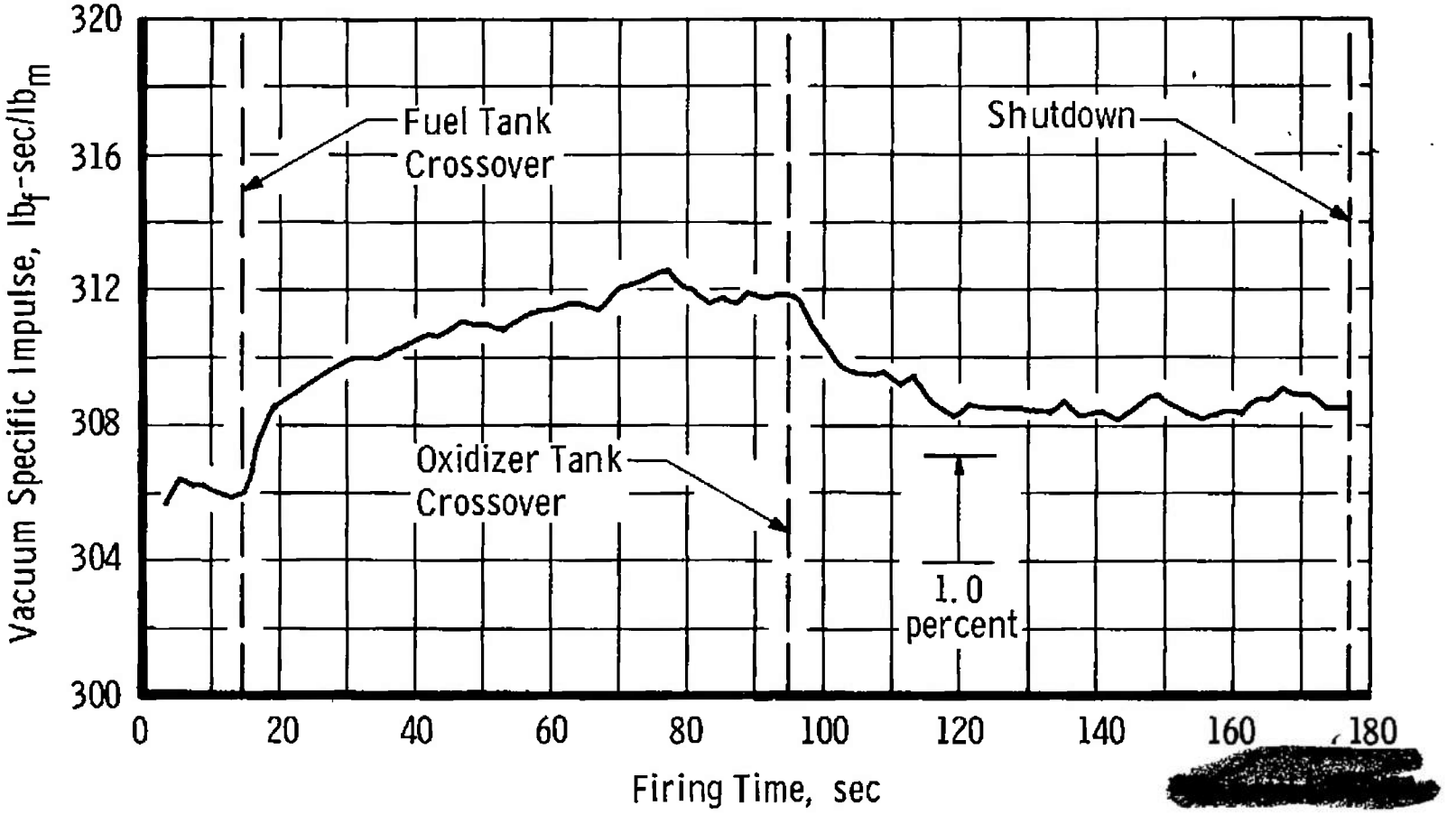

a. Vacuum Specific Impulse

Fig. 20 Effect of Propellant Tank Crossover on Engine Performance (Test F-24)

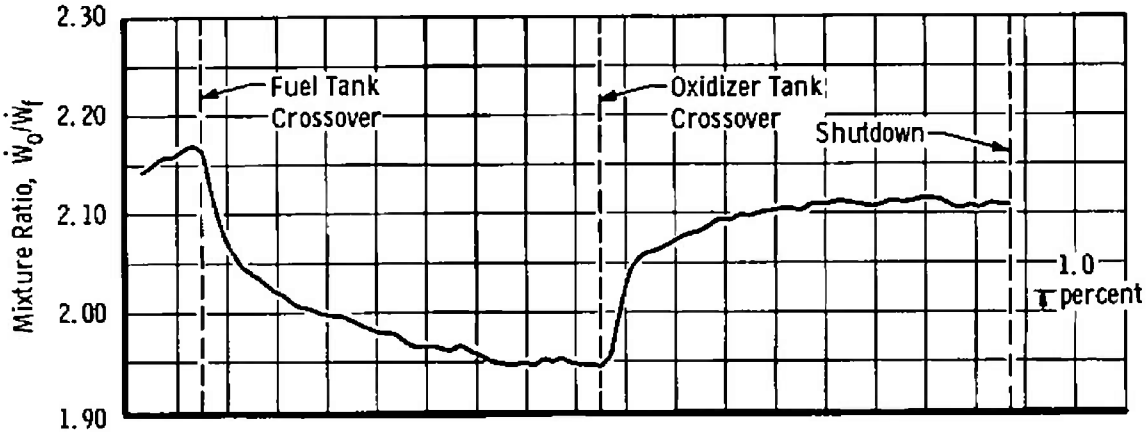

b. Mixture Ratio

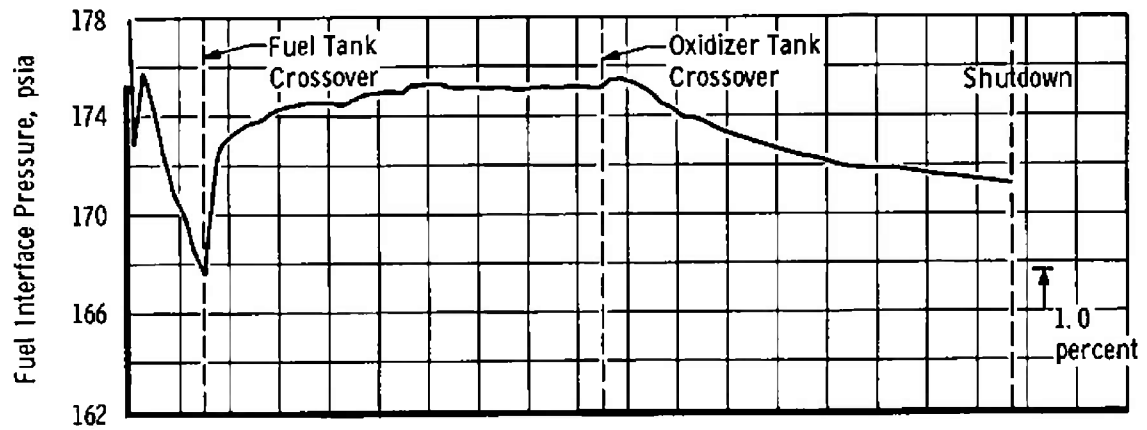

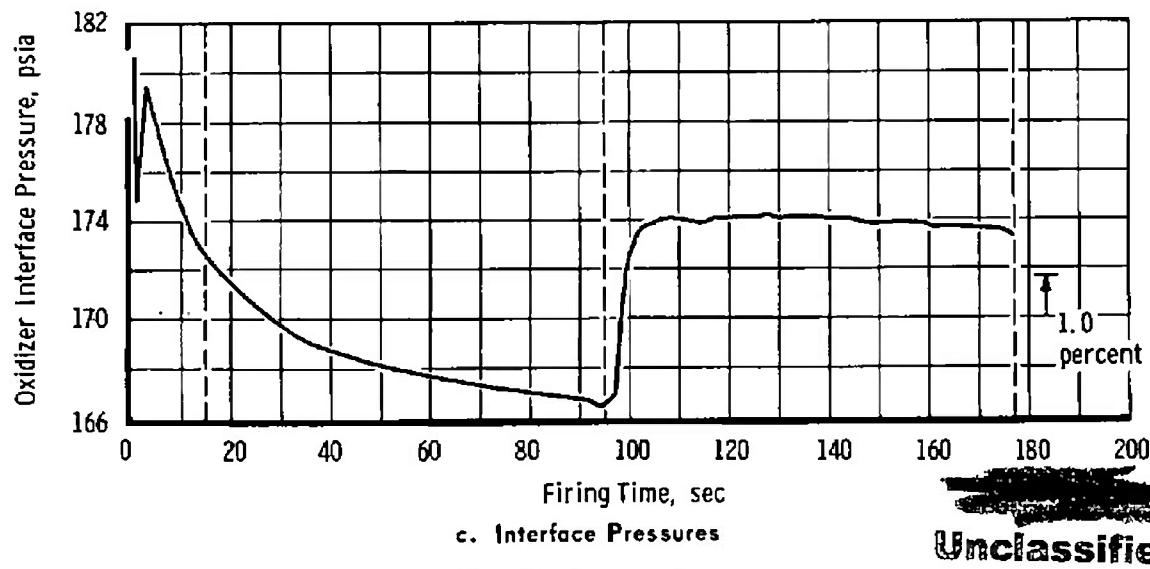

c. Interface Pressures

Fig. 20 Continued

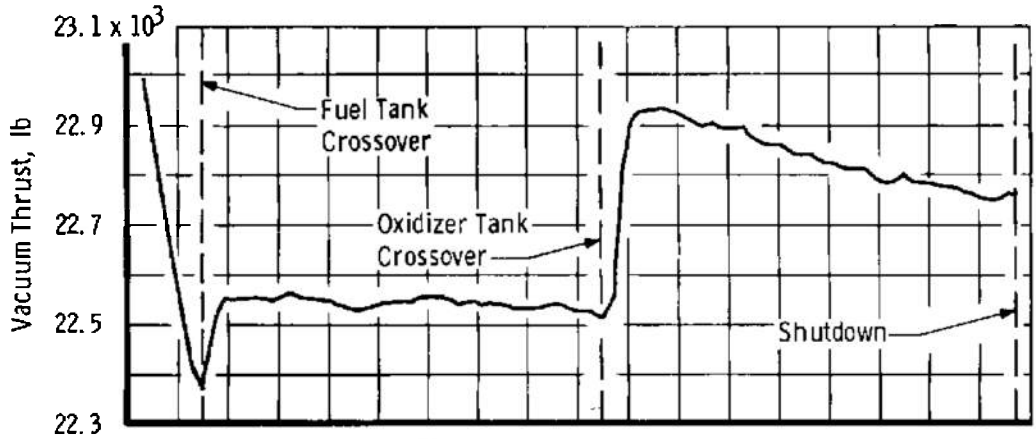

d. Vacuum Thrust

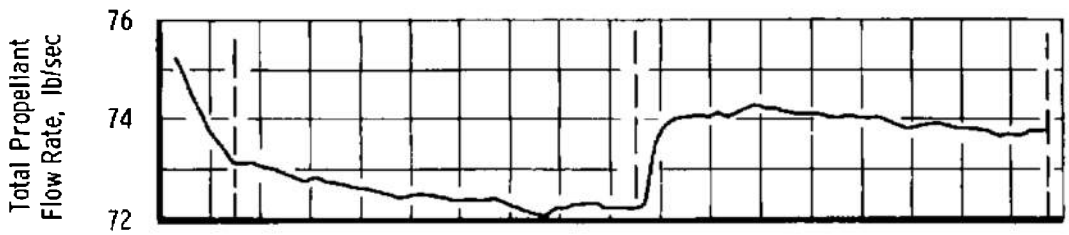

e. Total Propellant Flow Rate

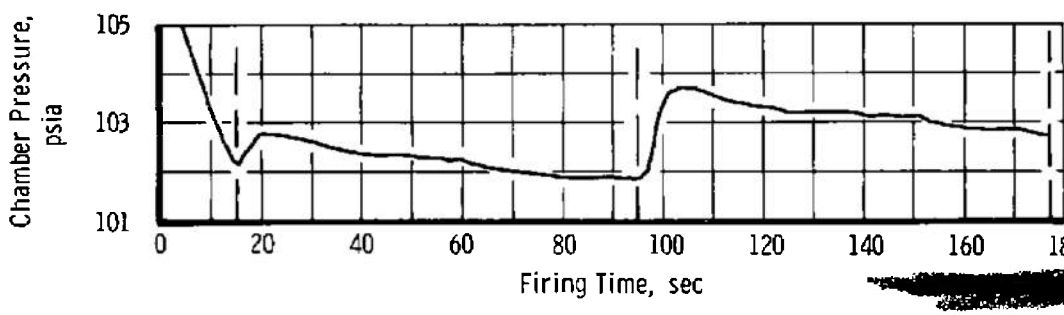

f. Chamber Pressure

Fig. 20 Concluded

[redacted] Unclassified

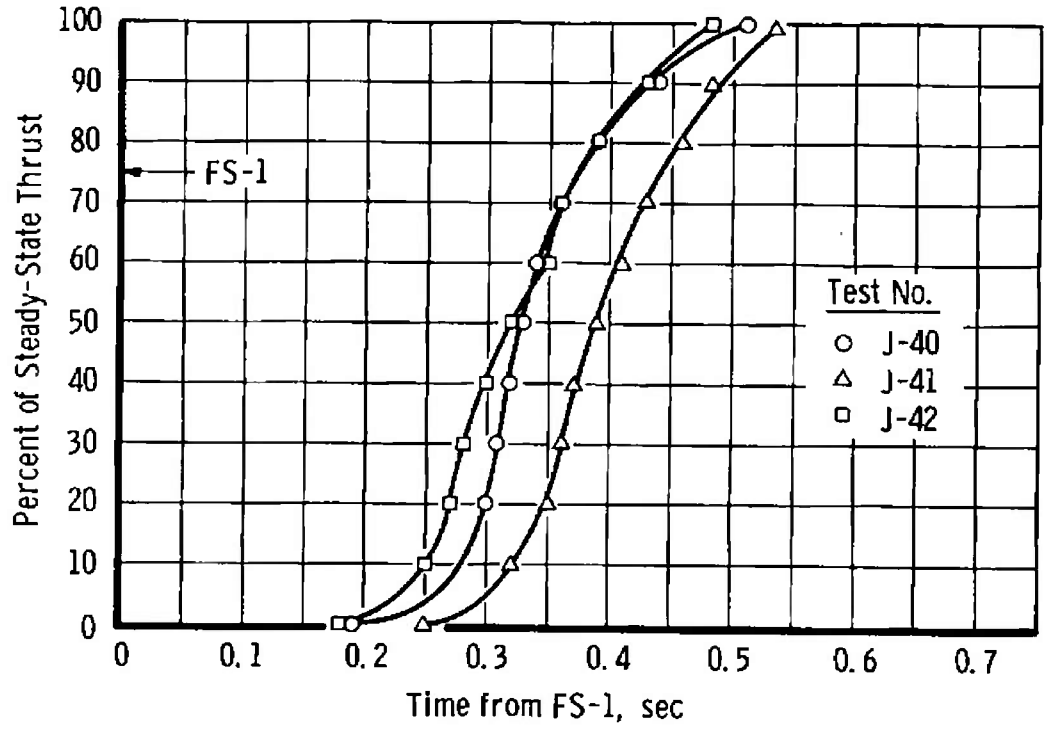

a. Ignition Thrust Buildup

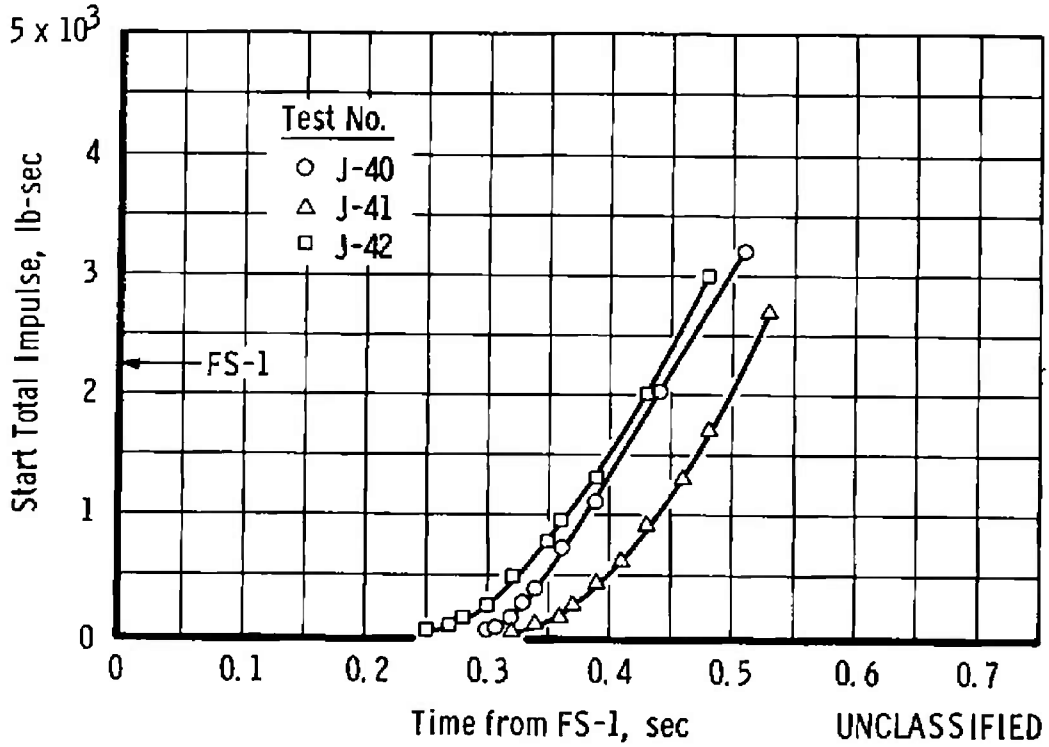

b. Ignition Transient Impulse

Fig. 21 Ignition Transient Characteristics

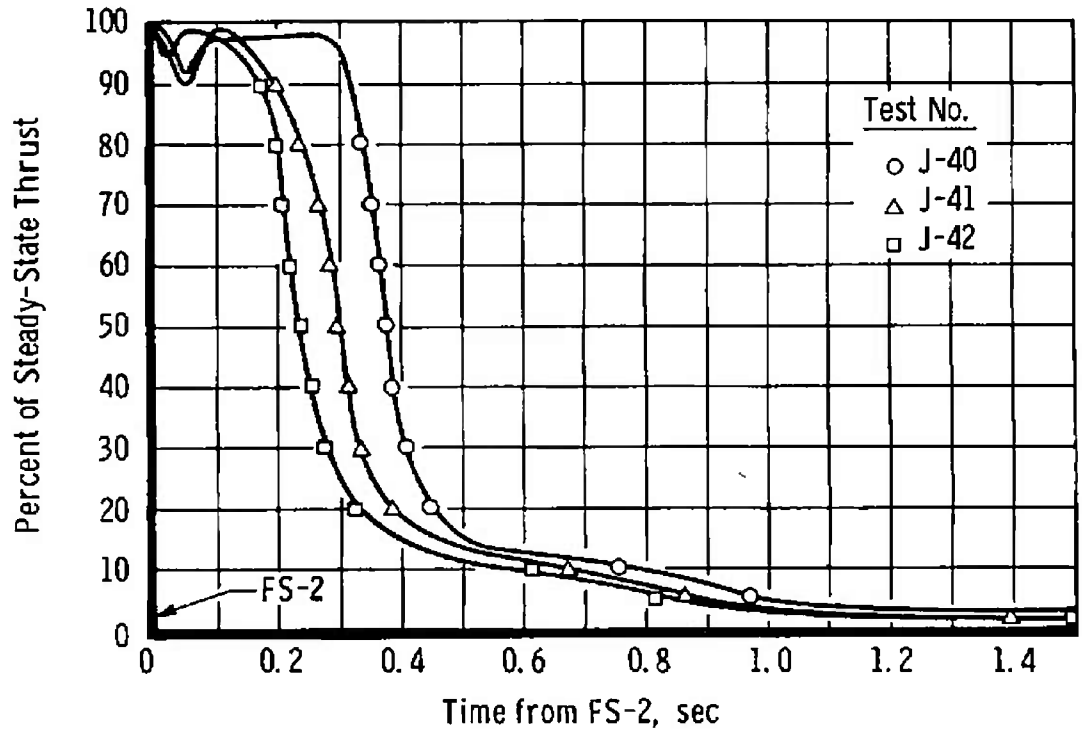

a. Shutdown Thrust Tailoff

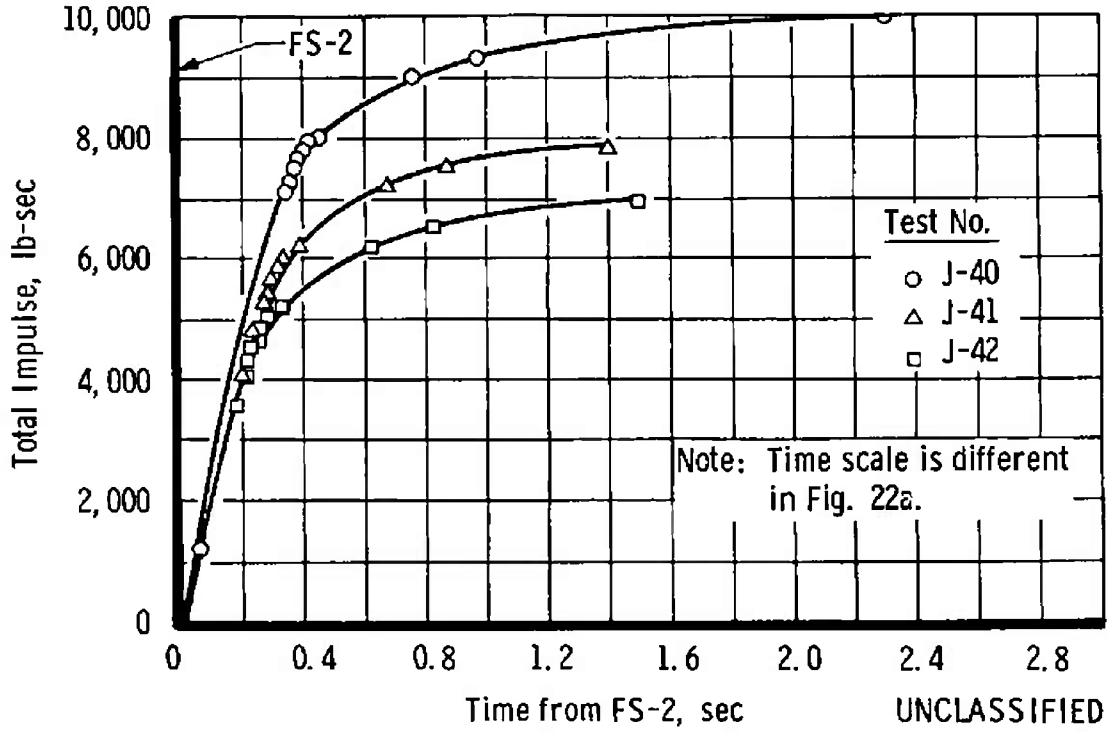

b. Shutdown Transient Impulse

Fig. 22 Shutdown Transient Characteristics

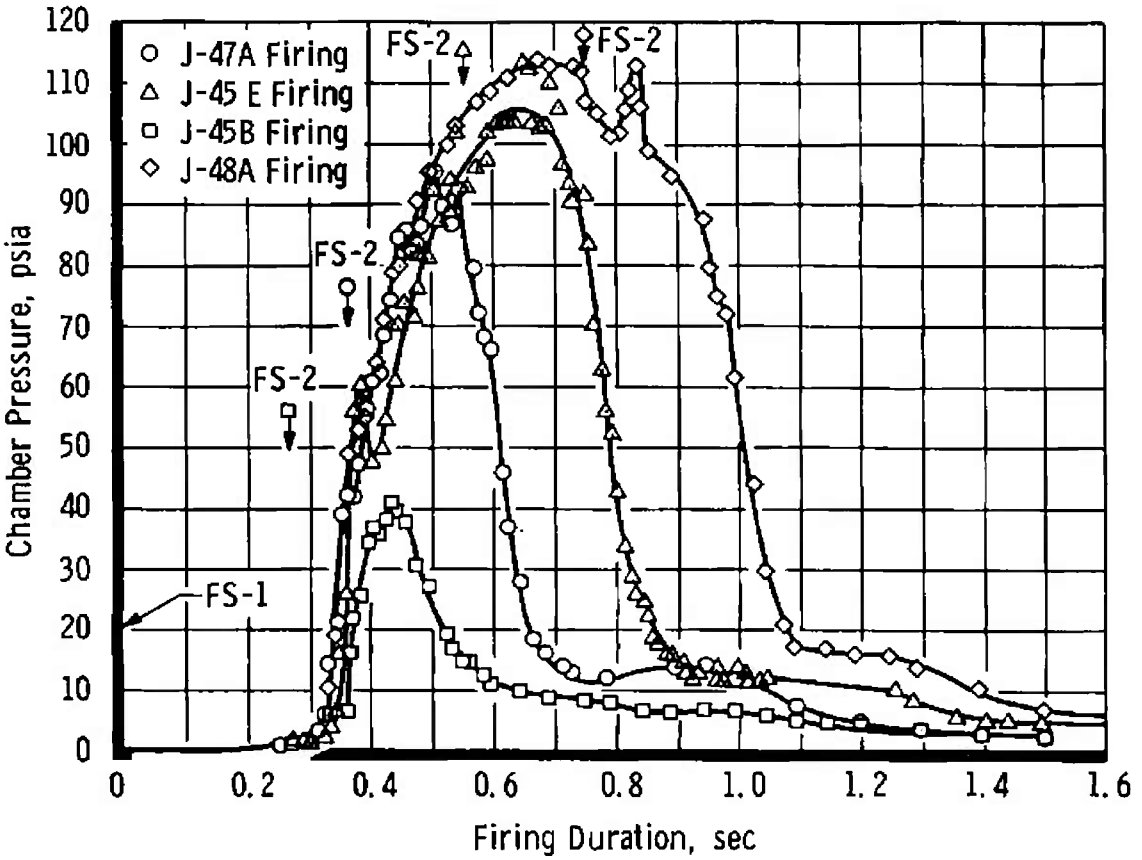

a. Chamber Pressure Transients

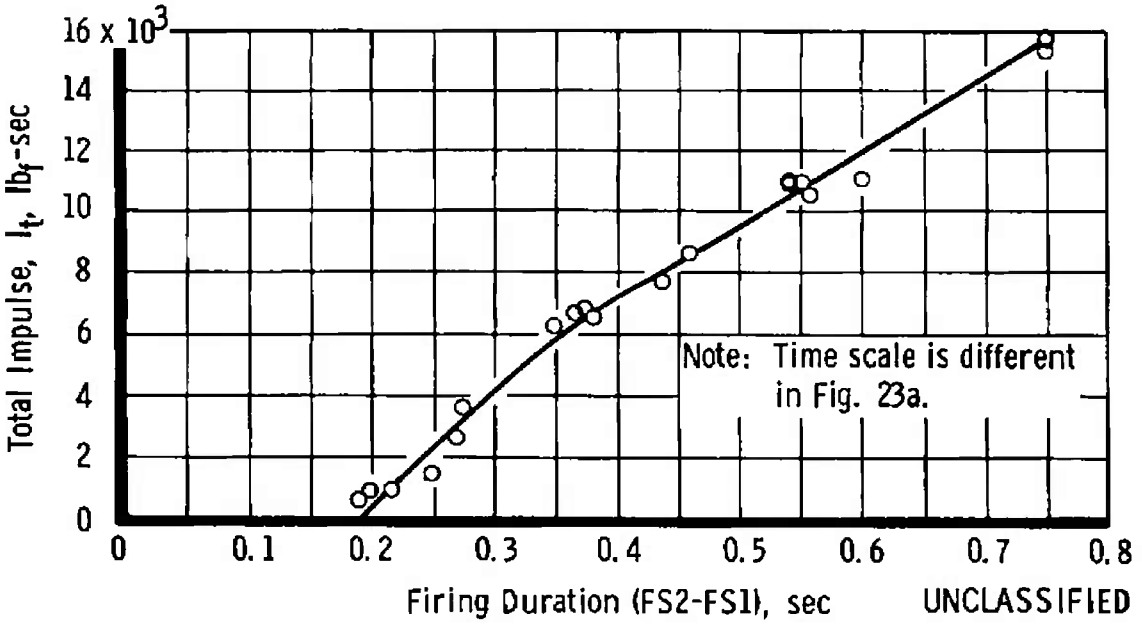

b. Integrated Total Impulse

Fig. 23 Minimum Impulse Bit Operation

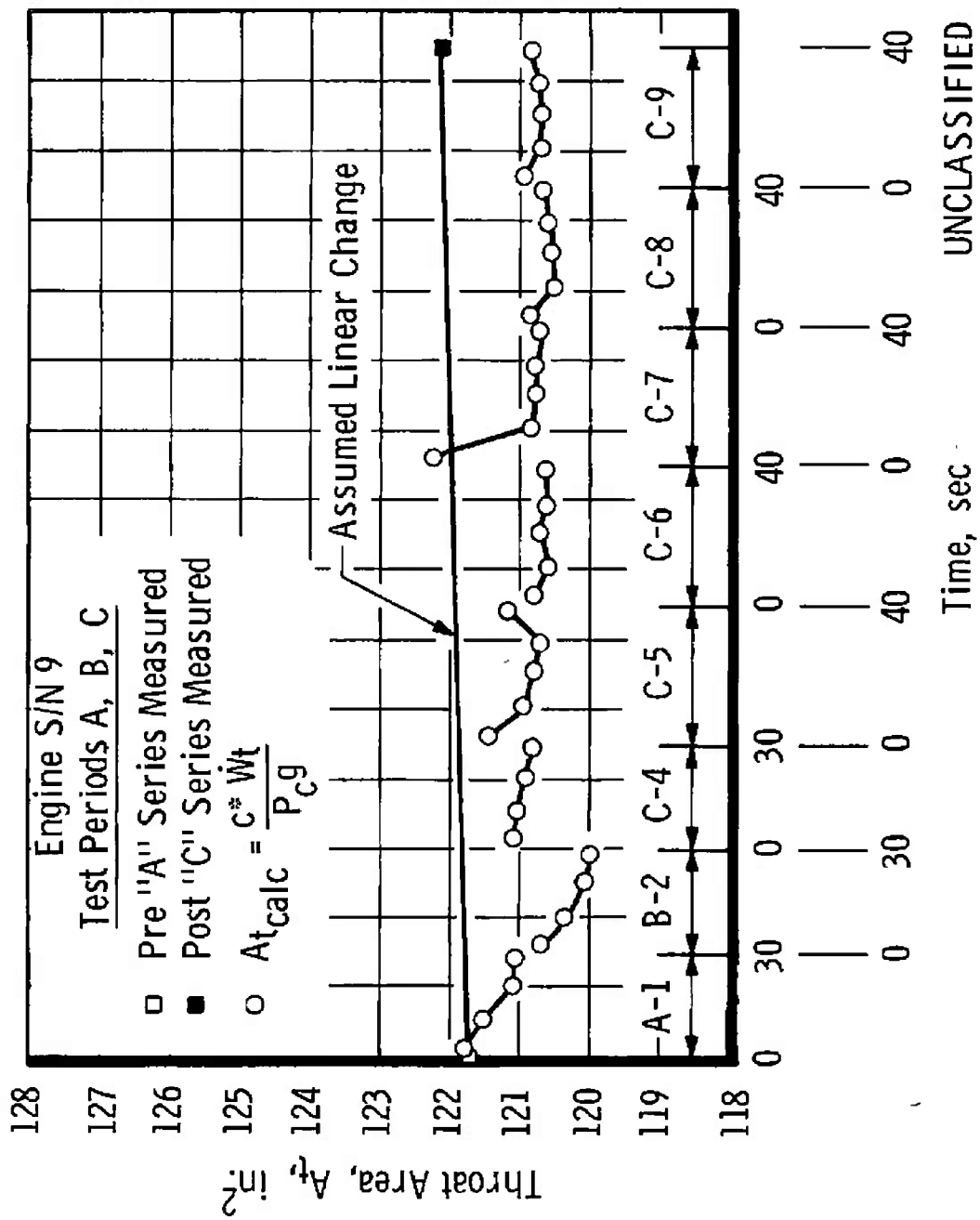

a. Engine S/N 9

Fig. 24 Comparison of Measured and Calculated Throat Areas

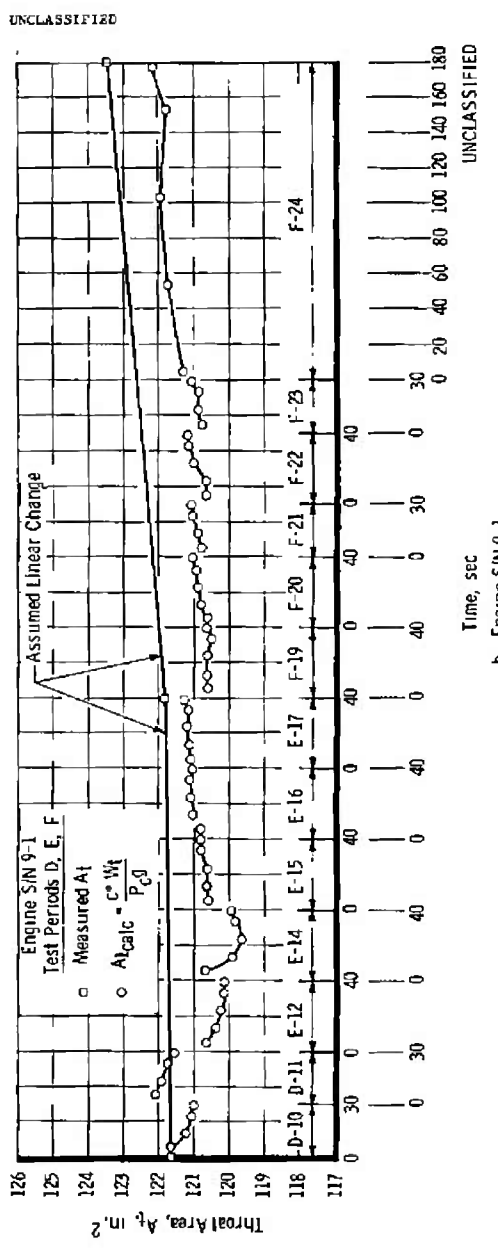

b. Engine S/N 9-1

Fig. 24 Continued

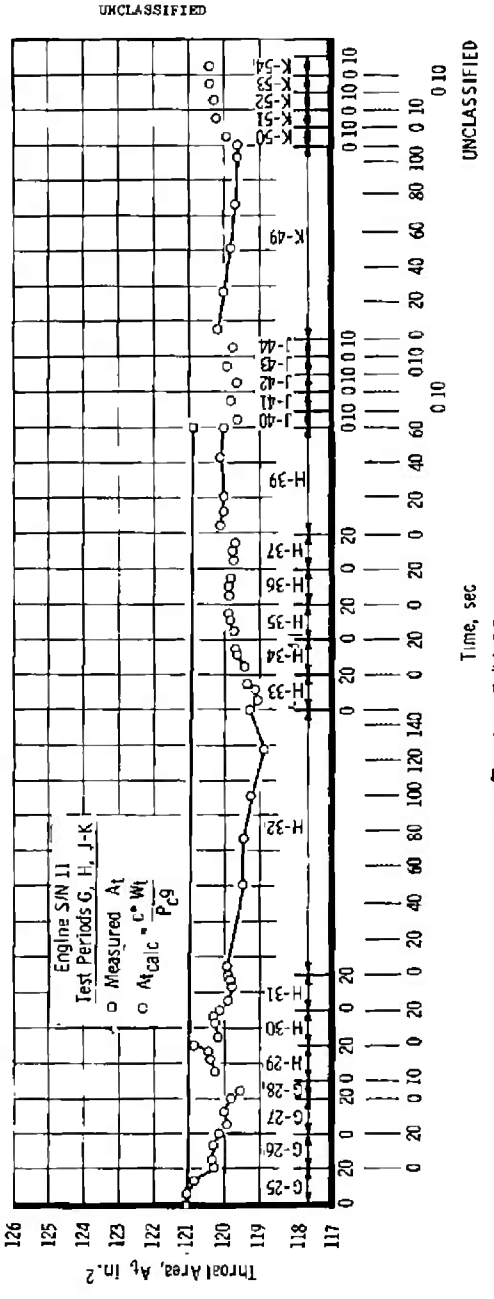

c. Engine S/N 11

Fig. 24 Concluded

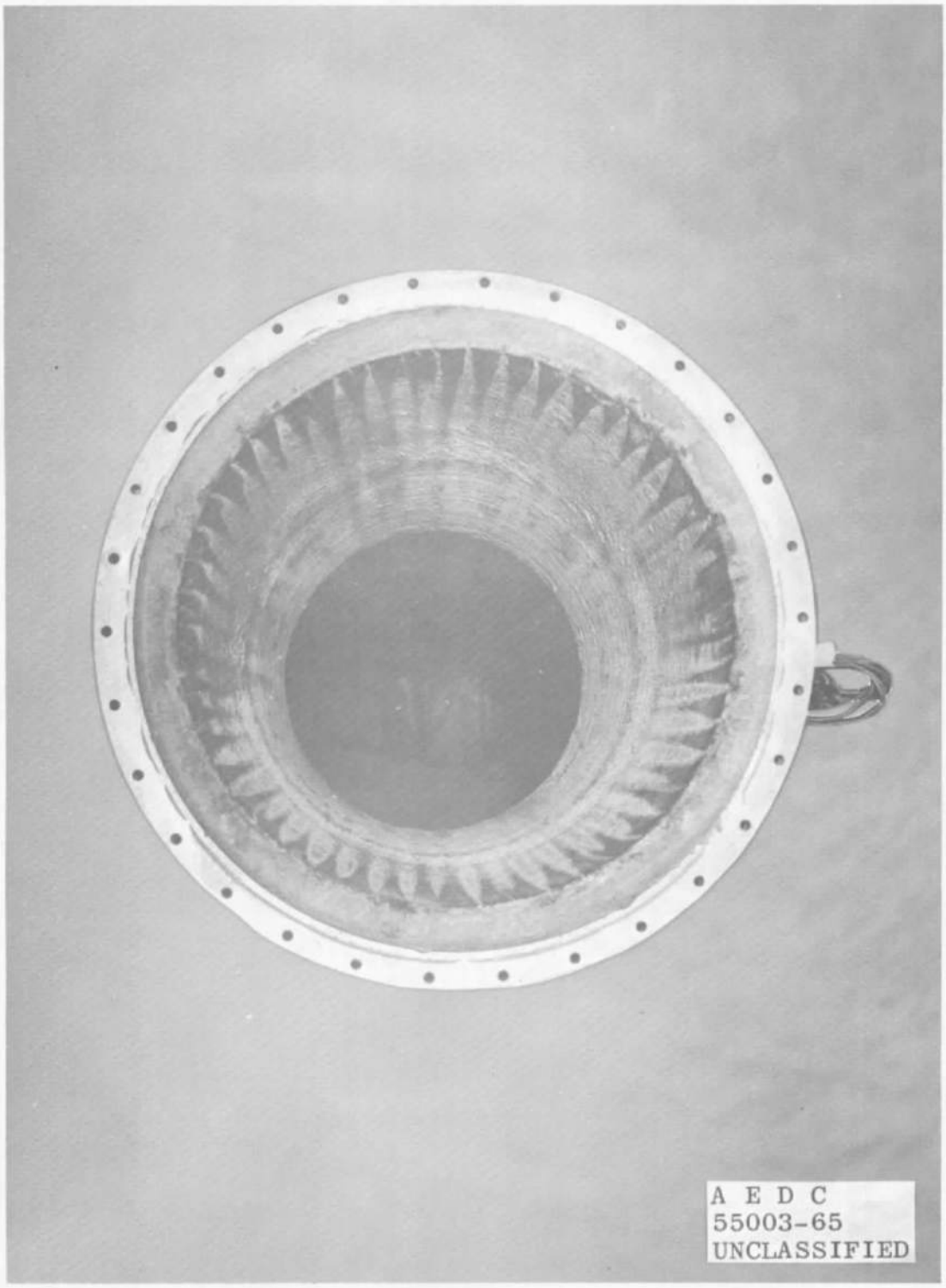

a. Engine S/N 9 (Looking Aft)

Fig. 25 Photograph of Combustion Chamber Post-Fire Ablation

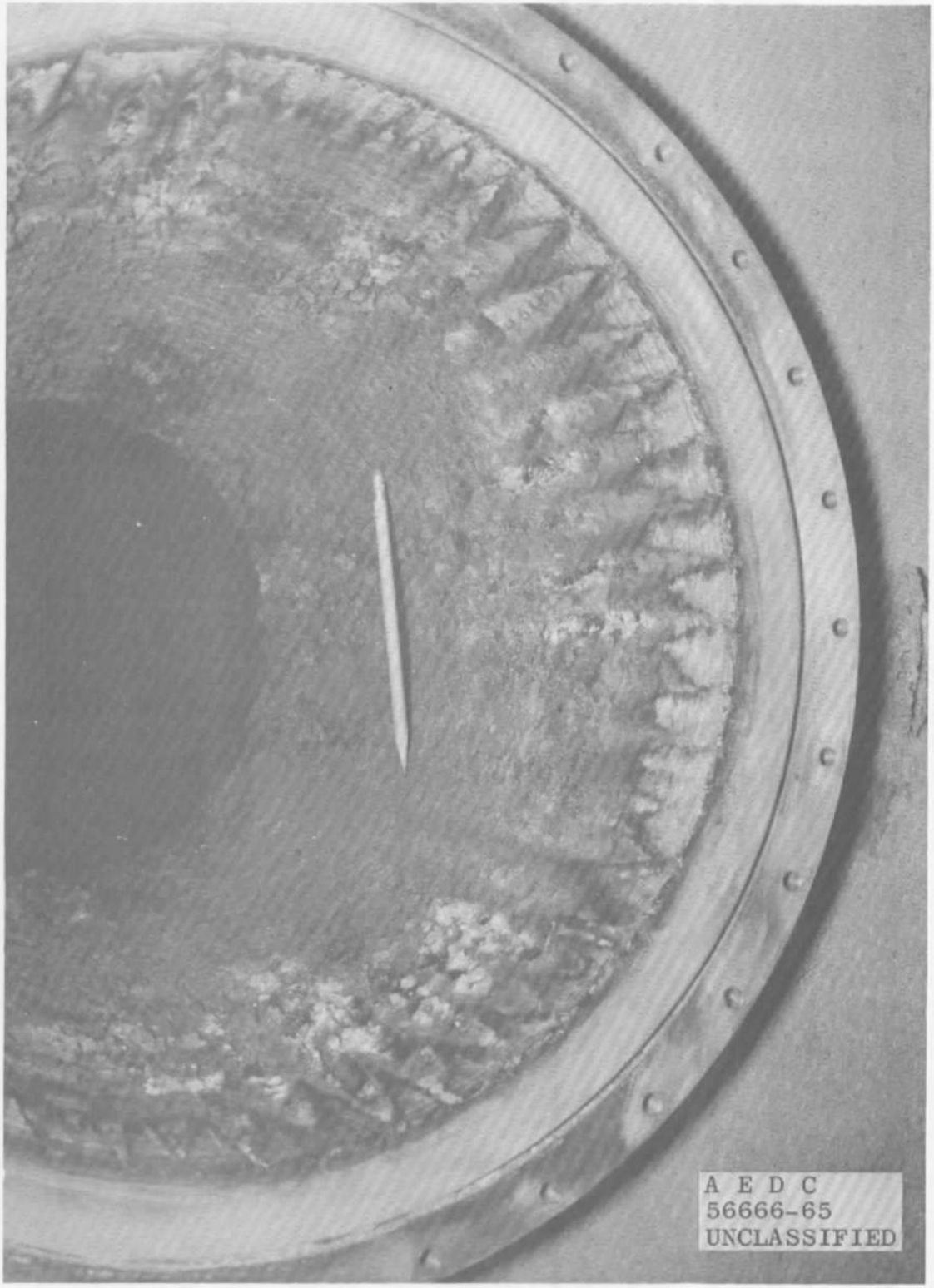

b. Engine S/N 9-1 (Looking Aft)

Fig. 25 Continued

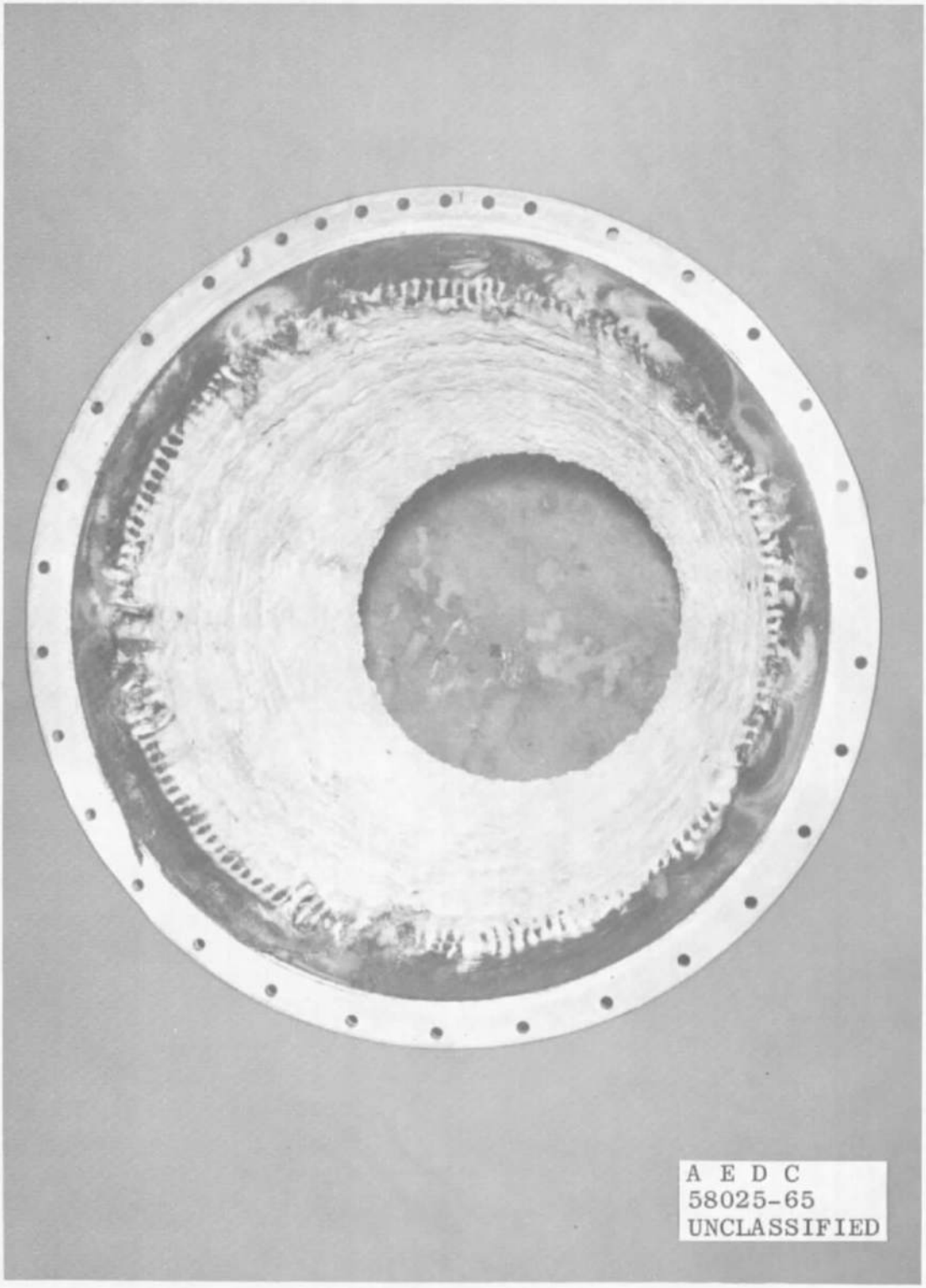

c. Engine S/N 11 (Looking Aft)

Fig. 25 Concluded

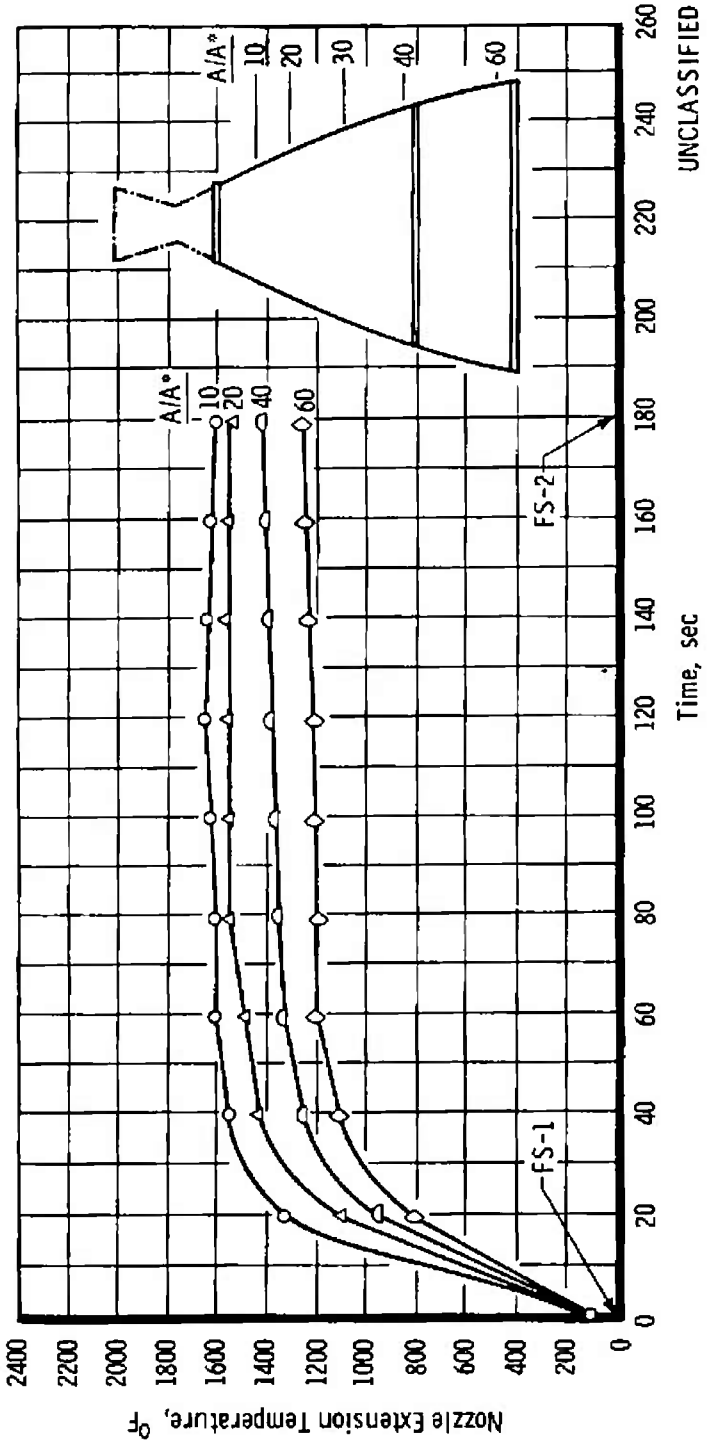

a. Test F-24

Fig. 26 Nozzle Extension Temperatures

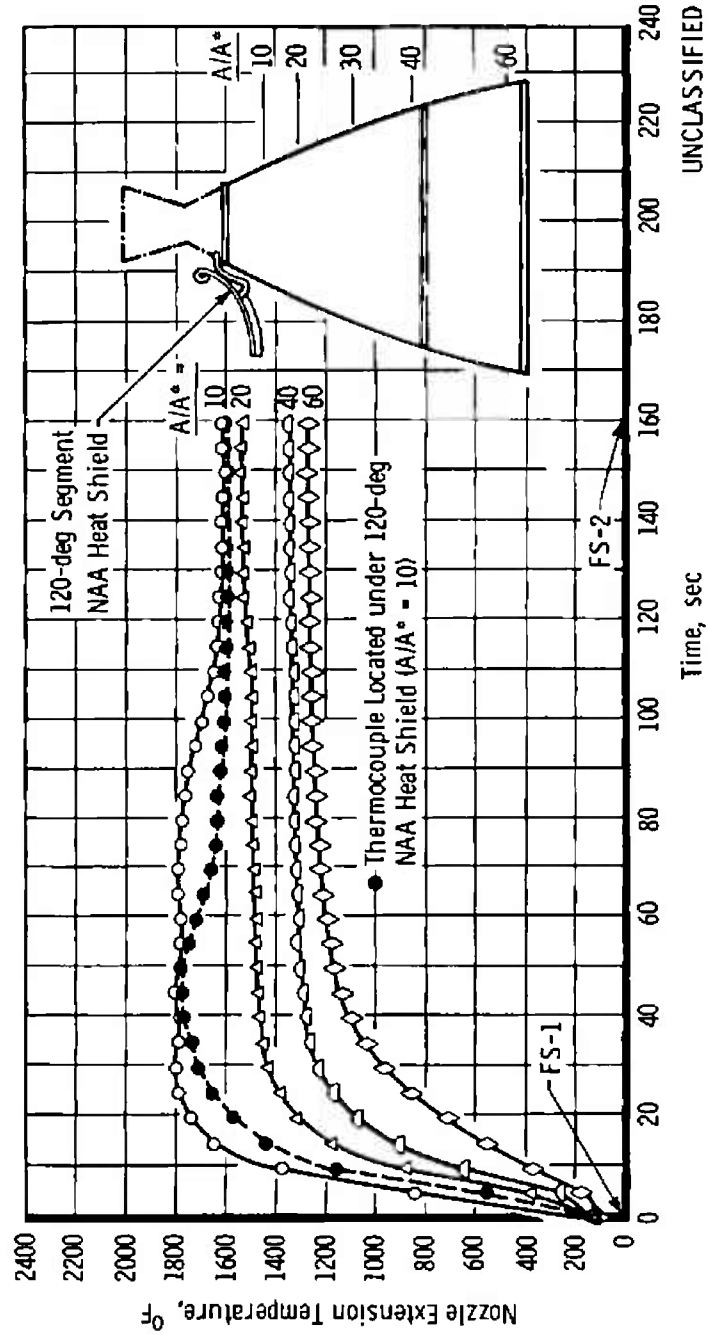

b. Test H-32
Fig. 26 Continued

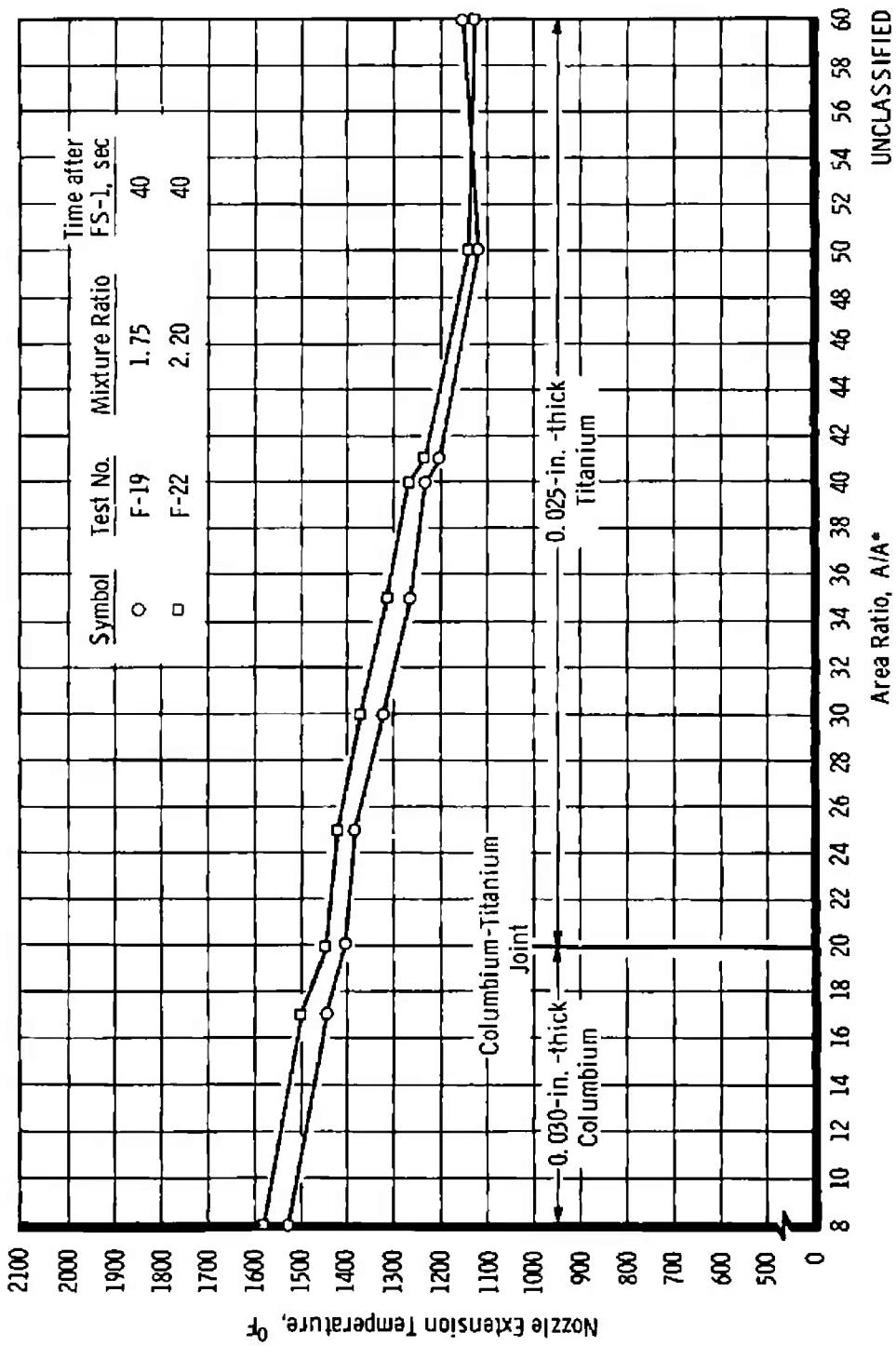

c. Mixture Ratio Survey, Nozzle S/N 039, Engine S/N 9-1

Fig. 26 Continued

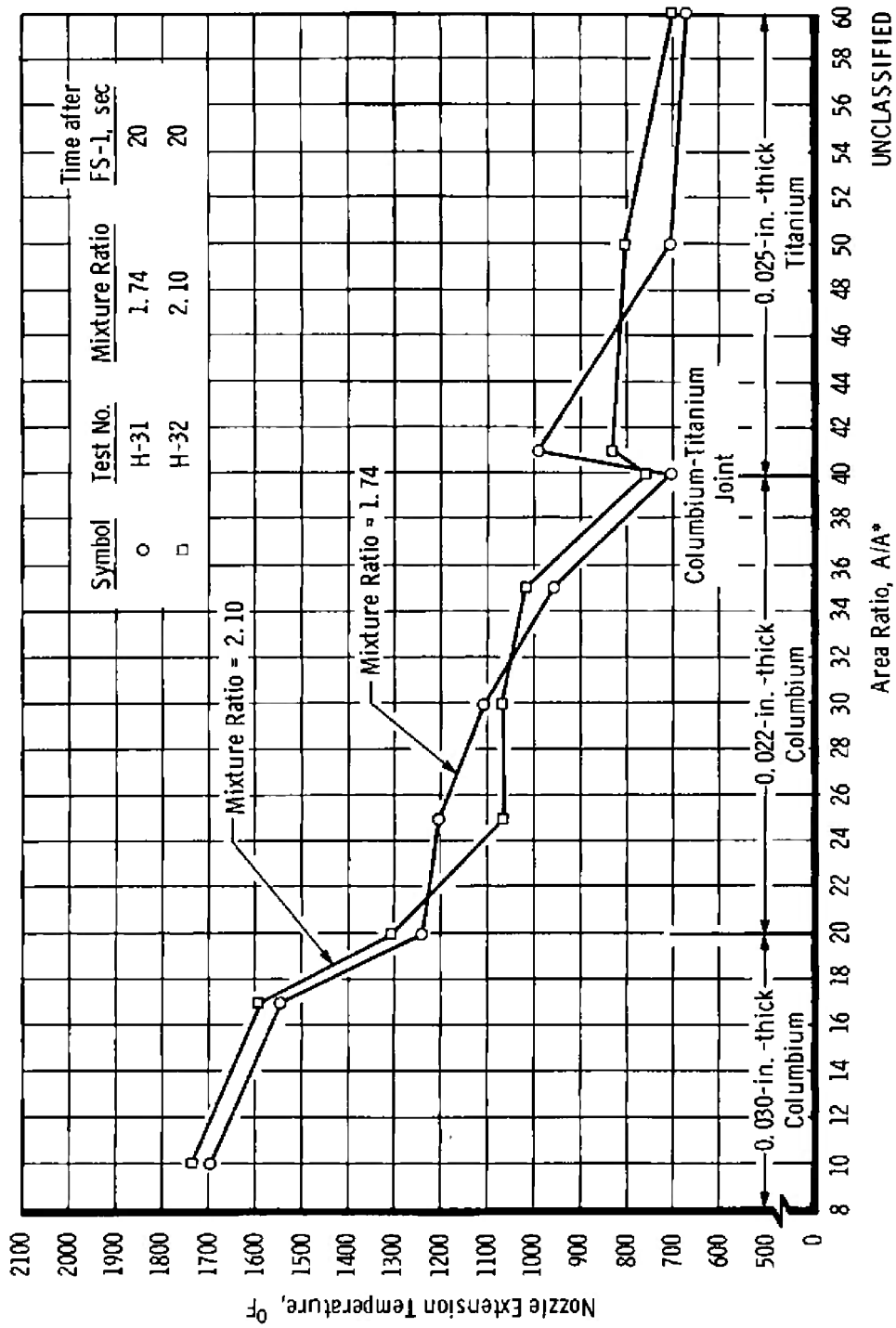

d. Mixture Ratio Survey, Nozzle S/N 026, Engine S/N 11

Fig. 26 Continued

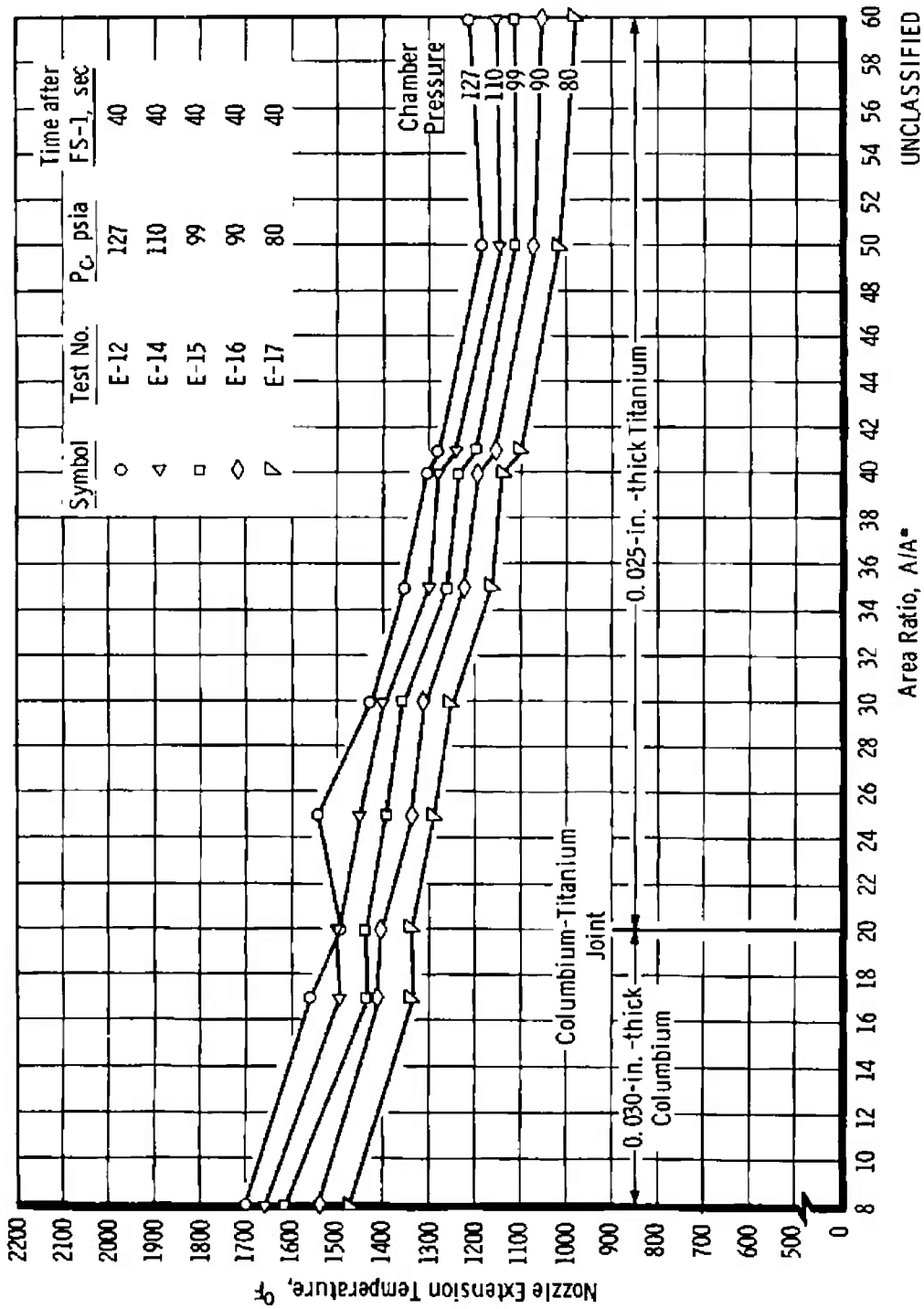

e. Chamber Pressure Survey, Nozzle S/N 039, Engine 9-1

Fig. 26 Continued

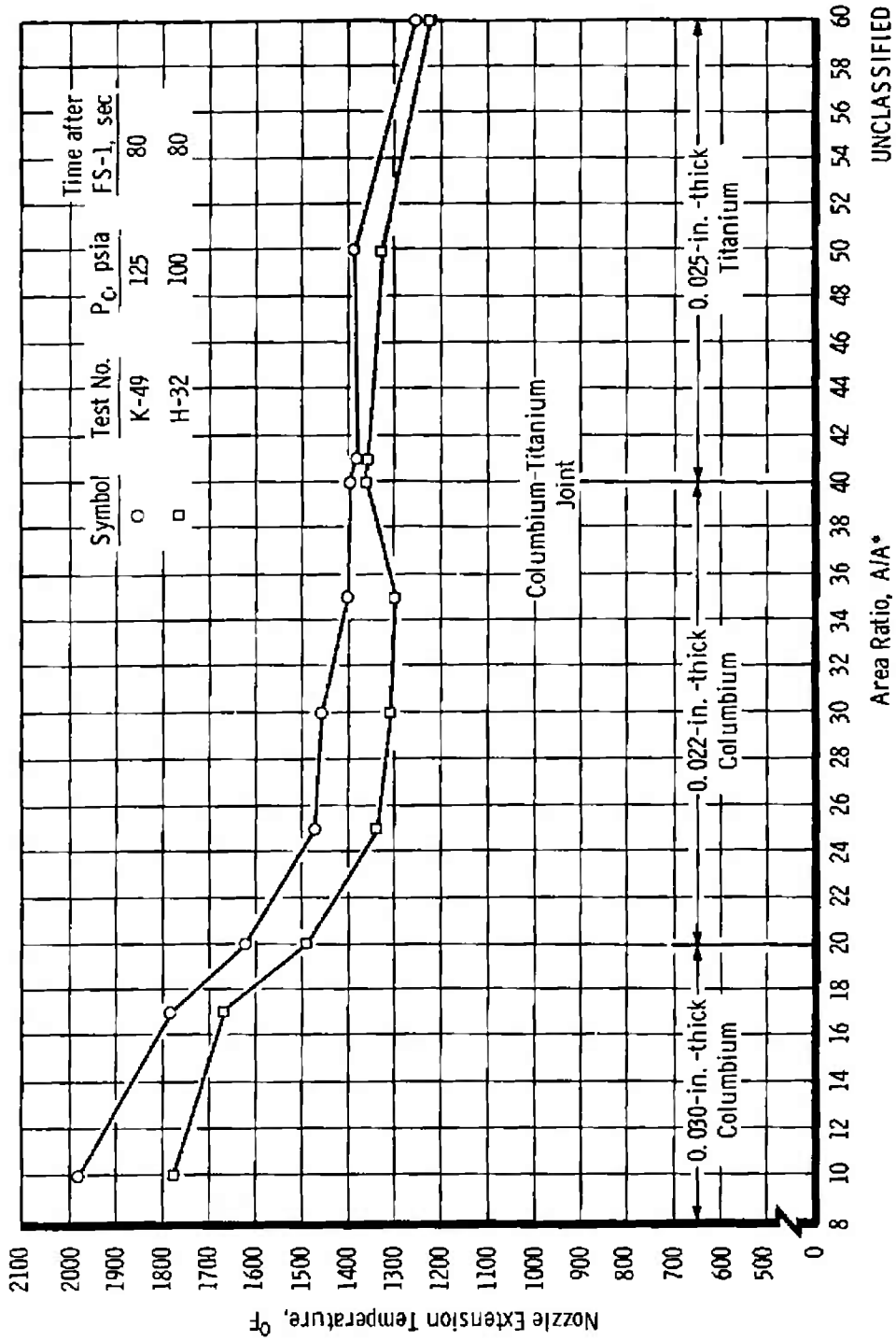

f. Chamber Pressure Survey, Nozzle S/N 026, Engine S/N 11

Fig. 26 Continued

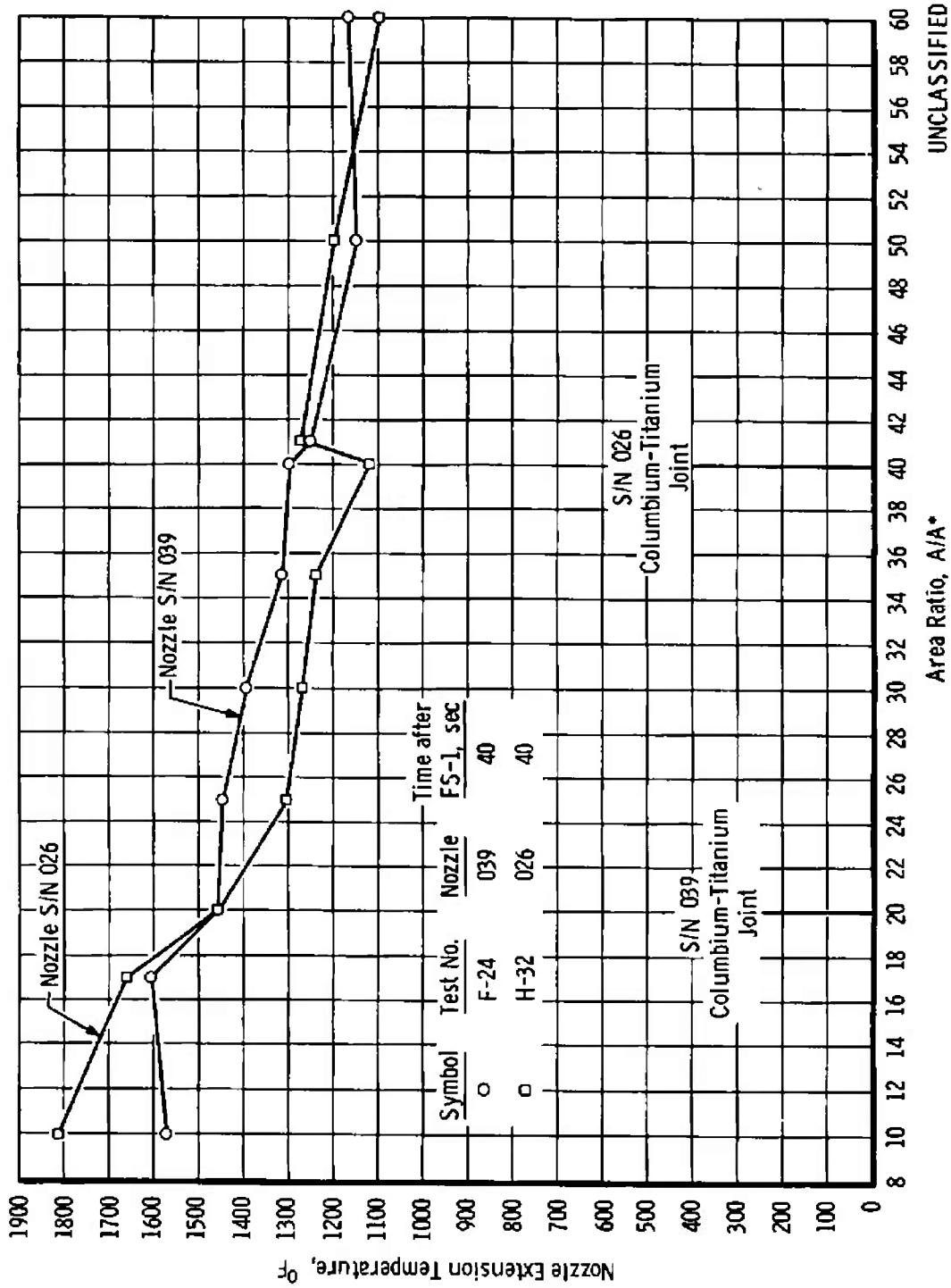

g. Comparison of Nozzle Temperatures for Two Different Designs

Fig. 26 Concluded

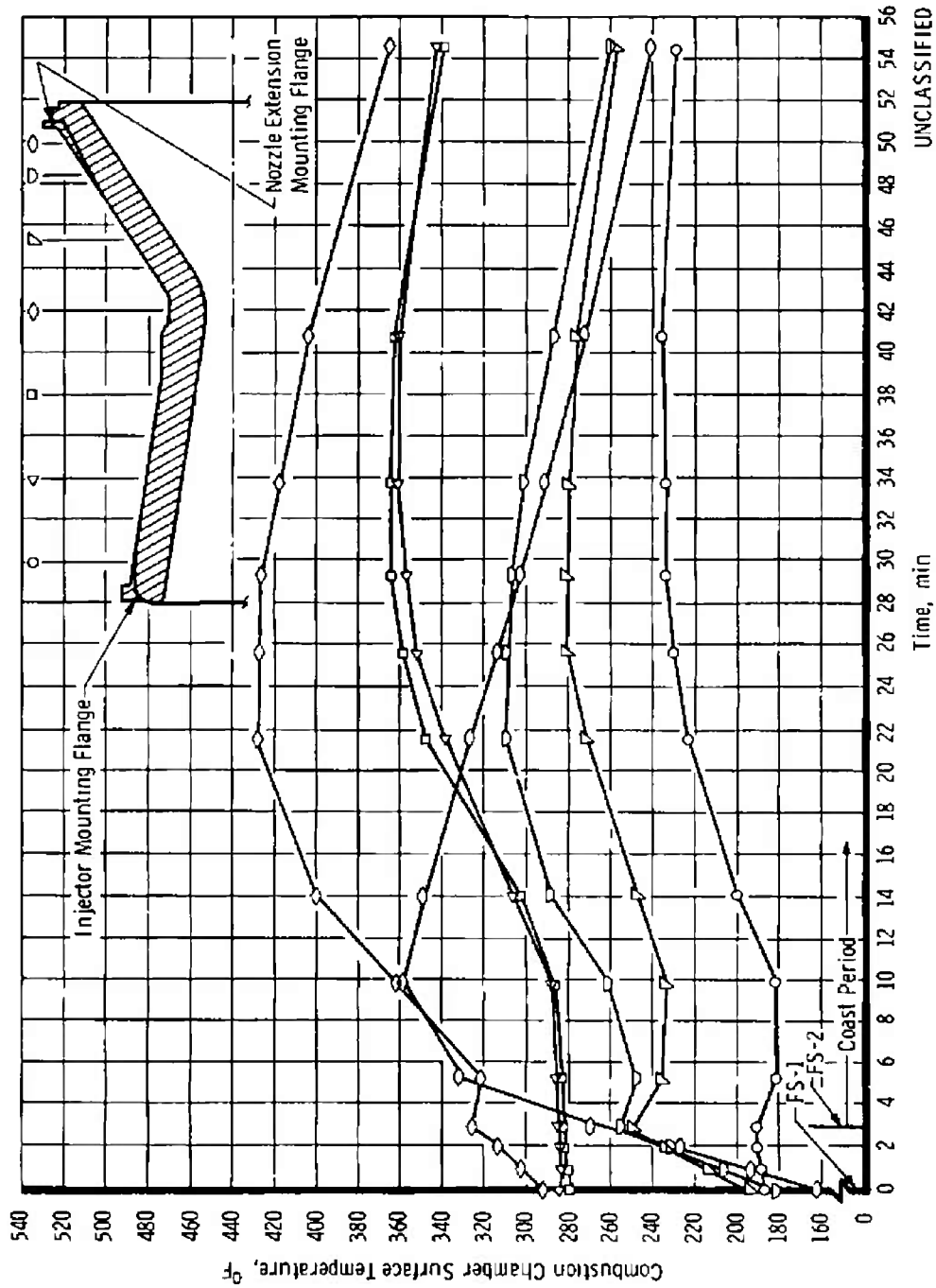

a. Test F-24

Fig. 27 Combustion Chamber Surface Temperatures versus Time

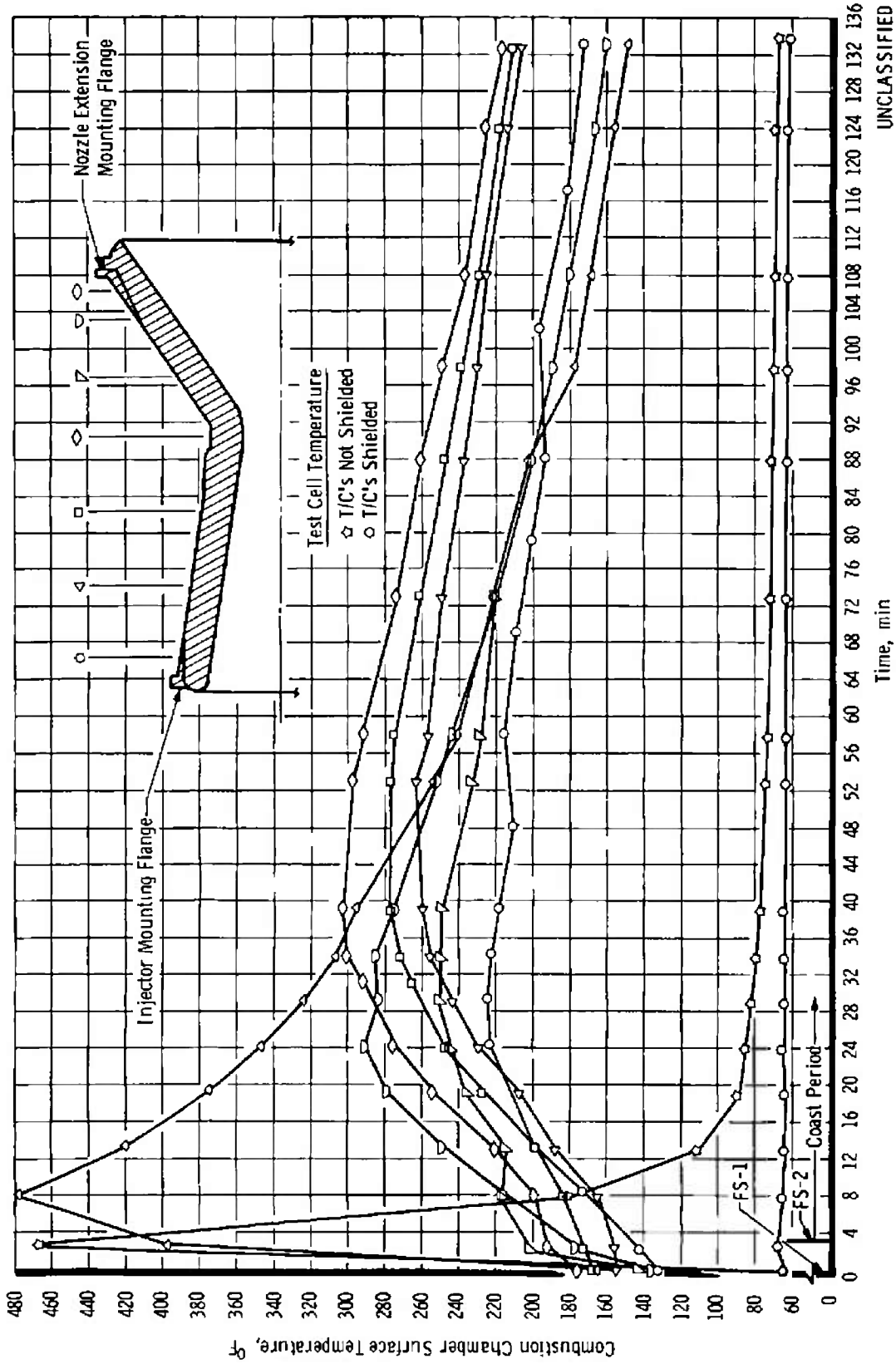

b. Test H-32

Fig. 27 Concluded

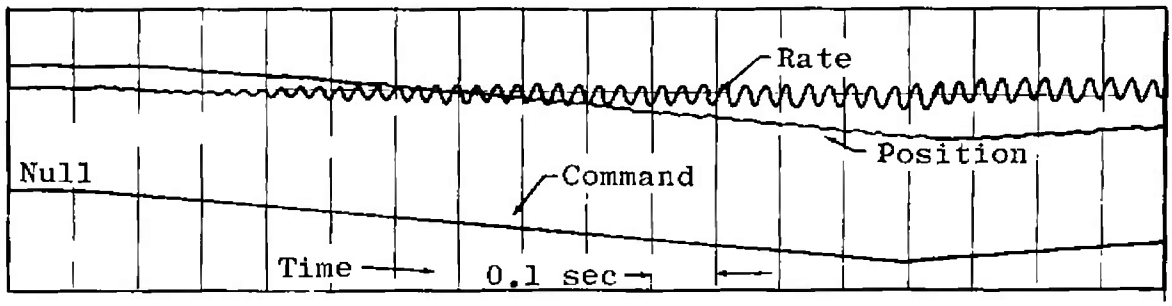

a. Ramp Command

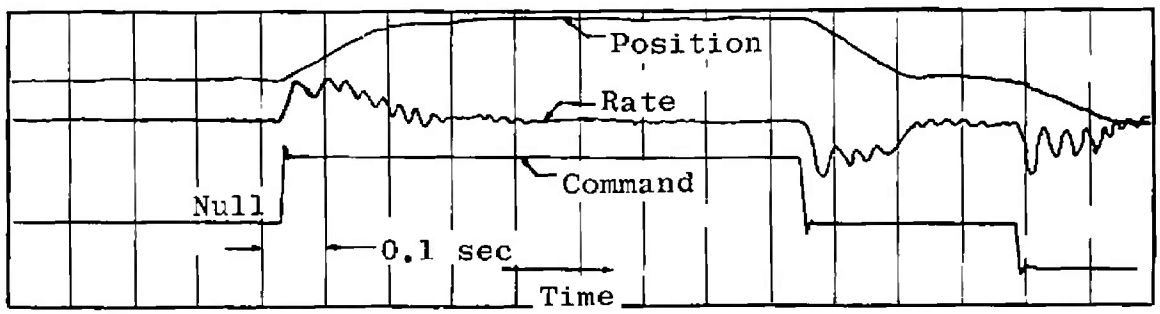

b. Step Command

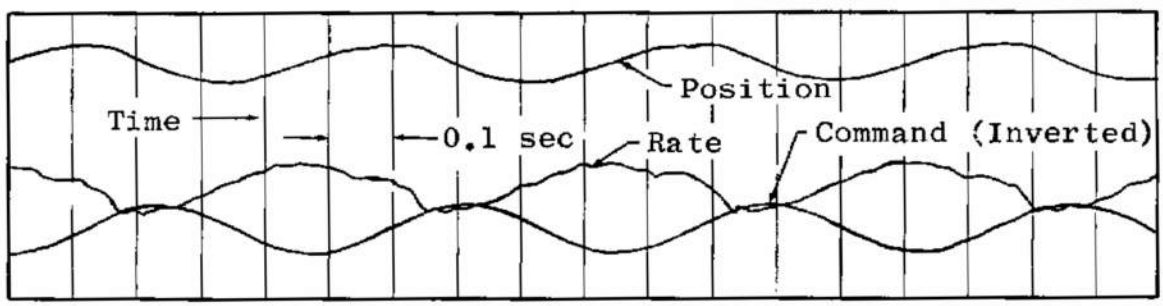

c. 2.0-cps Sine Function Command

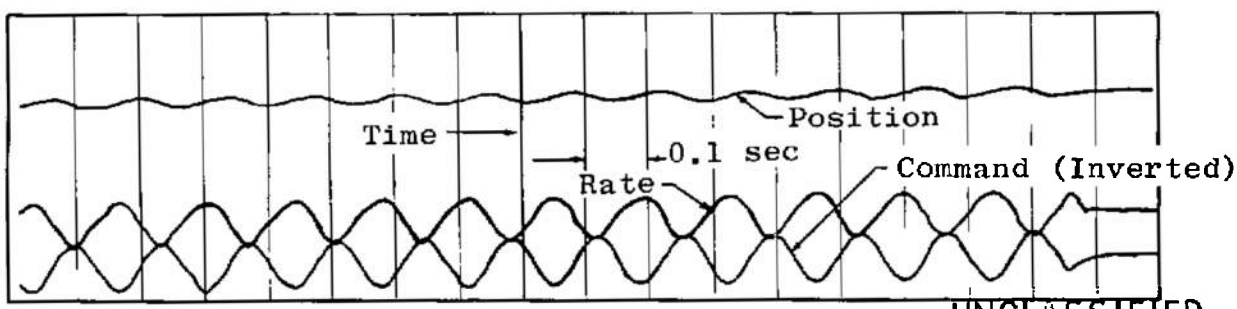

UNCLASSIFIED

d. 7.4-cps Sine Function Command

Fig. 28 Gimbal Operation Oscillograms

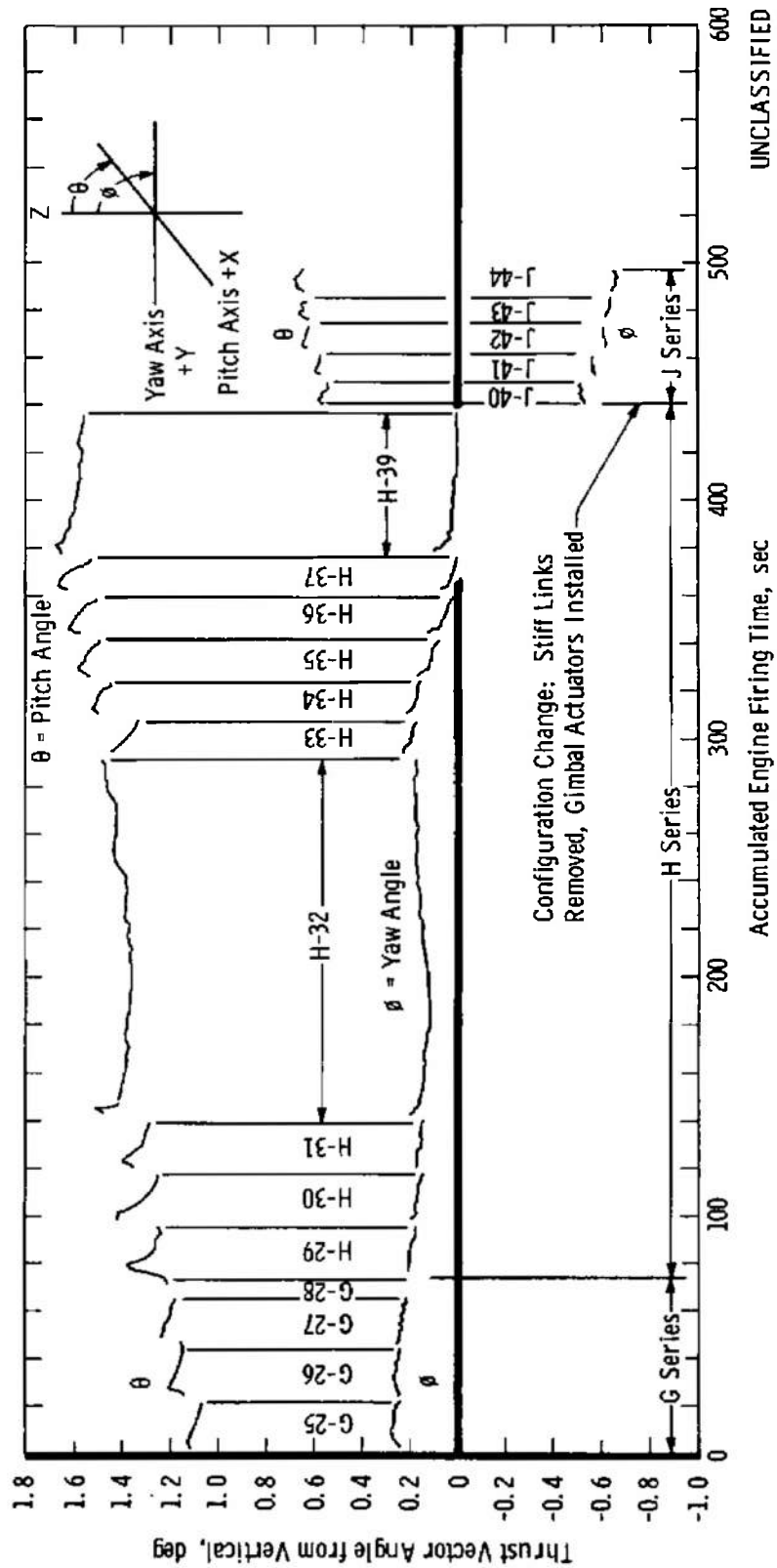

Fig. 29 Thrust Vector History, Engine S/N 11

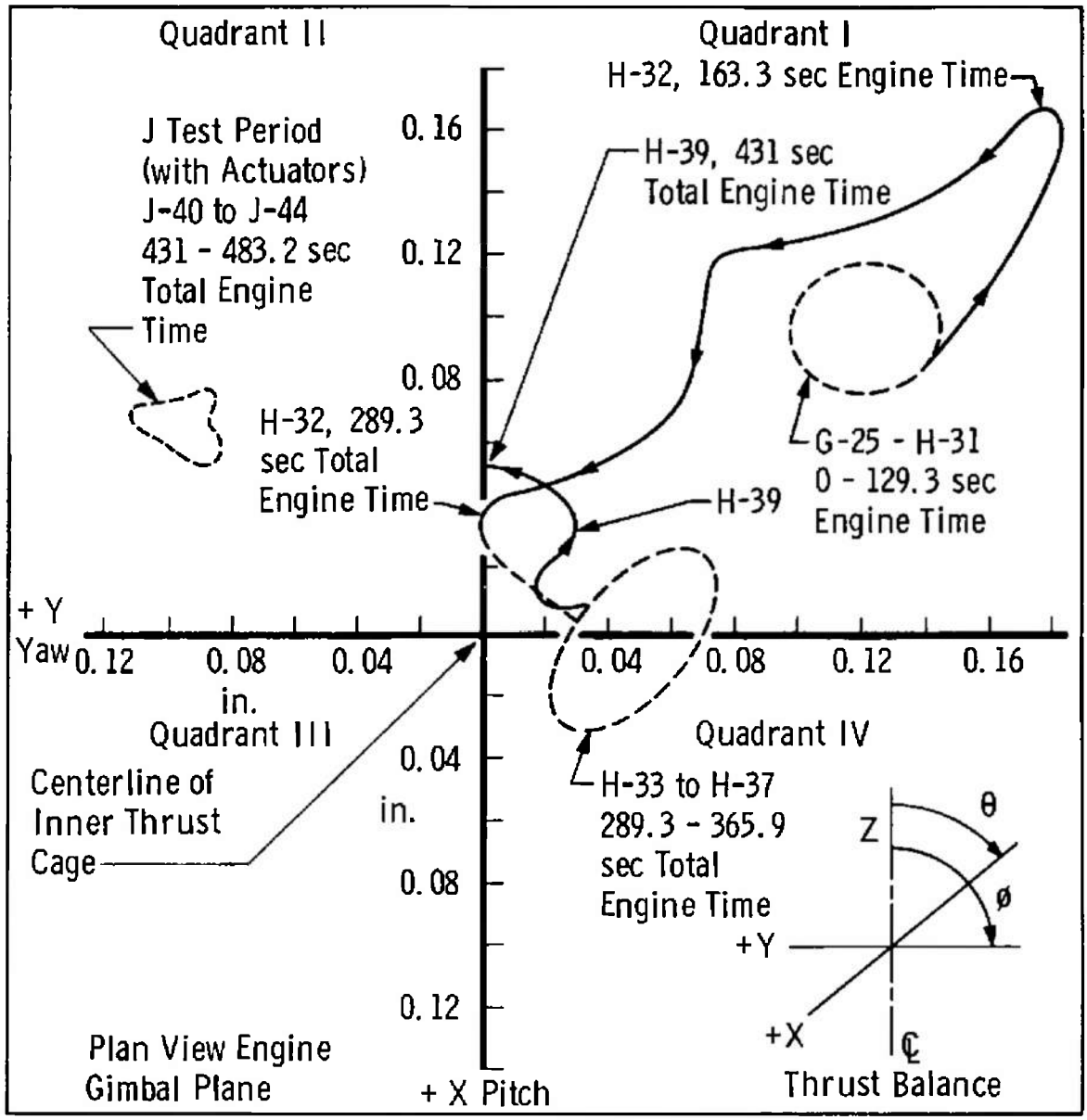

UNCLASSIFIED

Fig. 30 Effect of Ablation on Thrust Vector Intercept Location

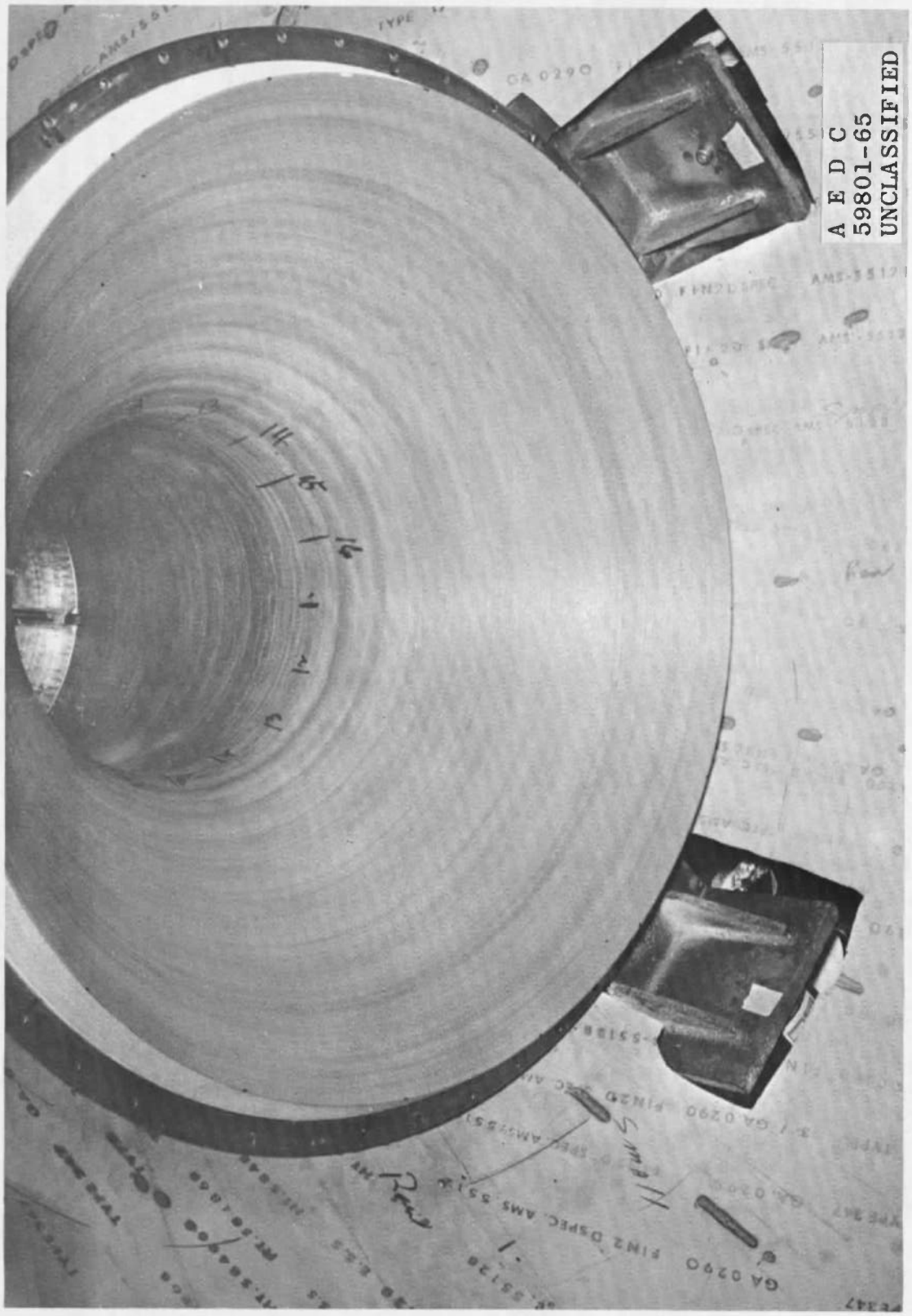

Fig. 31 Engine Combustion Chamber (Pre-Fire)

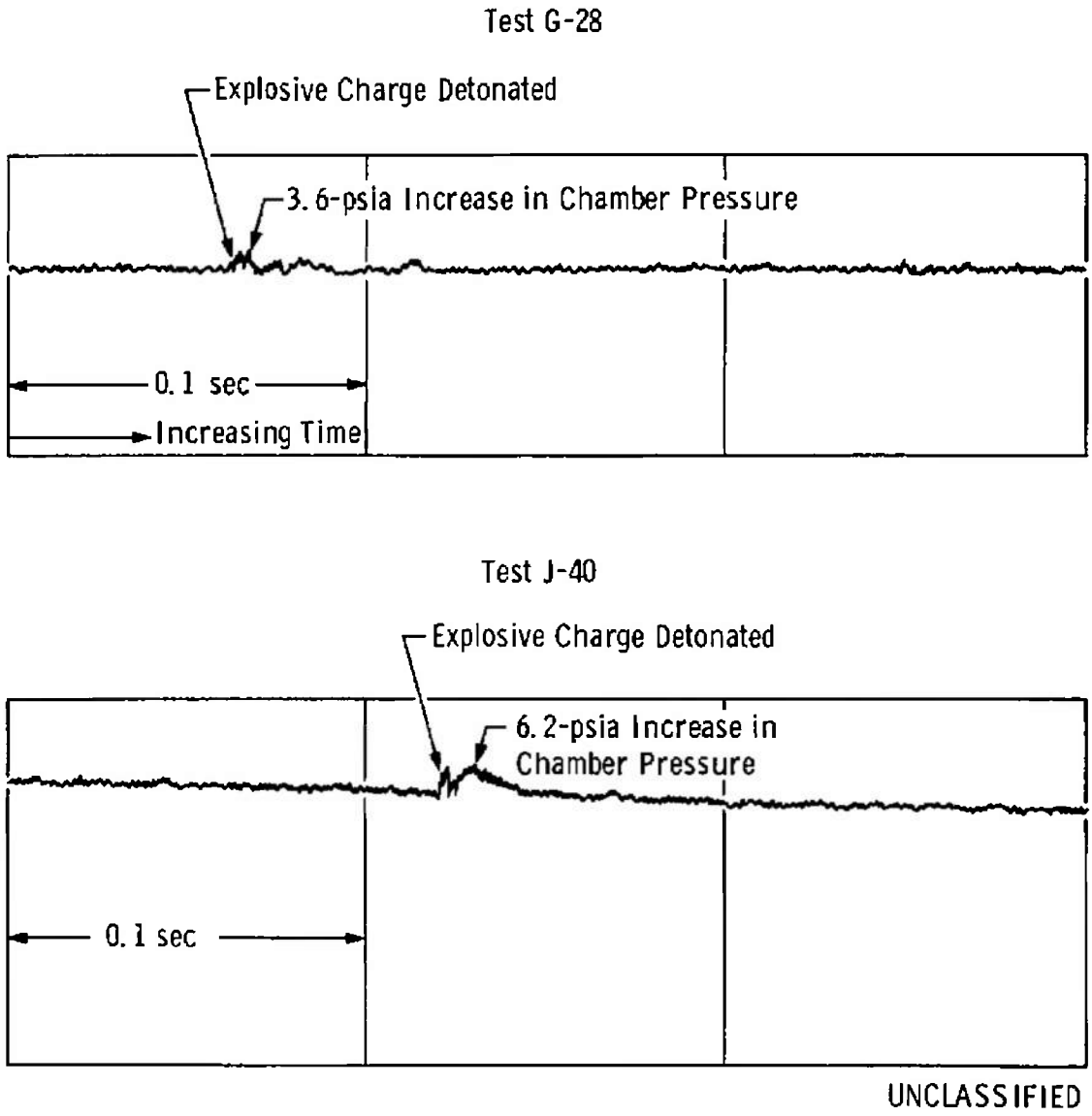

Fig. 32 Oscillograph Data Showing Chamber Pressure Data during Combustion Instability Induced by an Explosive Charge

Fig. 33 Post-Test Nozzle Extension of Test G-28 Showing Slightly Convoluted Columbium Section

TABLE I
DATA ACQUISITION SYSTEMS LIST

Parameter	Range	Data Acquisition System			
		Magnetic Tape		Strip Chart	Oscillograph
		Analog-to-Digital	Analog-to-Frequency		
Axial Thrust Force	0-50,000 lb		x	x	x
Axial Thrust Force	0-50,000 lb		x		x
Yaw Force (2)	0-500 lb		x		x
Pitch Force (2)	0-500 lb		x		x
Roll Force	0-500 lb		x		x
Combustion Chamber Pressure	0-125 psia		x	x	x
Combustion Chamber Pressure	0-125 psia		x		x
Test Cell Pressure	0-30 mm Hg		x		
Test Cell Pressure	0-30 mm Hg			x	
Test Cell Pressure	0-1 psia	x			
Test Cell Pressure	0-1 psia			x	x
Fuel Injector Pressure	0-500 psia		x		x
Oxidizer Injector Pressure	0-500 psia		x		x
Fuel Line Pressure	0-500 psia		x	x	
Fuel Line Pressure	0-500 psia	x			
Oxidizer Line Pressure	0-500 psia		x	x	
Oxidizer Line Pressure	0-500 psia	x			
Fuel TCV Pressure	0-500 psia		x	x	x
Oxidizer TCV Pressure	0-500 psia		x	x	x
Fuel Sump Tank Pressure	0-300 psia			x	
Fuel Sump Tank Pressure	0-300 psia	x			
Fuel Storage Tank Pressure	0-300 psia	x			
Oxidizer Sump Tank Pressure	0-300 psia			x	
Oxidizer Sump Tank Pressure	0-300 psia	x			
Oxidizer Storage Tank Pressure	0-300 psia	x			
Helium Supply Pressure	0-3000 psia			x	
Regulated Helium Pressure (2)	0-500 psia			x	
TCV Actuator Pressure	0-500 psia	x			
Fuel Flow Rate			x		x
Fuel Flow Rate				x	x
Oxidizer Flow Rate			x		x
Oxidizer Flow Rate				x	x
Fuel Temperature Flowmeter	0-180°F		x	x	
Fuel Temperature Engine Line	0-160°F	x			
Oxidizer Temperature Flowmeter	0-180°F		x	x	
Oxidizer Temperature Engine Line	0-160°F	x			
Fuel Storage Tank Temperature (2)	0-200°F	x			
Fuel Sump Tank Temperature (3)	0-200°F	x			
Oxidizer Storage Tank Temperature (2)	0-200°F	x			
Oxidizer Sump Tank Temperature (3)	0-200°F	x			
Chamber Throat Temperature (2)	0-600°F	x			
Chamber Temperature (21)	0-600°F	x			
Injector Temperature (2)	0-400°F	x			
Nozzle Extension Temperature (41)	0-2500°F	x			
Nozzle Extension Stiffener Temperatures (11)	0-2500°F	x			
Nozzle Extension Flange Temperatures (3)	0-2500°F	x			
Test Cell Wall Temperatures (9)	0-250°F	x			
TCV Position Potentiometers (8)	2K				x
Injector Vibration (2)			x		
Injector Vibration-Comb. Stab. Monitor				x	
Chamber Vibration (throat) (2)				x	
Gimbal Ring Vibration (8)				x	
Support Vibration (7)				x	
Gimbal Pitch Position (2)					x
Gimbal Yaw Position (2)					x
Gimbal Pitch Rate					x
Gimbal Yaw Rate					x
Gimbal Pitch Control Signal					x
Gimbal Yaw Control Signal					x
Gimbal Motor Voltage					x
Gimbal Pitch Motor Current (2)					x
Gimbal Yaw Motor Current (2)					x
Gimbal Pitch Clutch Extend Current (2)					x
Gimbal Pitch Clutch Retract Current (2)					x
Gimbal Yaw Clutch Retract Current (2)					x
Gimbal Pitch Input Clutch Current (2)					x
Gimbal Yaw Input Clutch Current (2)					x
TCV Pilot Valve Current (6)					x

TABLE II
GENERAL TEST SUMMARY

Test Number	Date	Duration, sec	Engine Serial Number	Thrust Chamber Valve Bank	Test Objectives
A-1	15 Dec 64	30.1	0	A	Test facility checkout and engine performance.
B-2	17 Dec 64	30.1			
B-3	17 Dec 64	CSM Shutdown 0.6			
C-4	22 Dec 64	30.3			Complete test facility checkout; performance at various mixture ratios.
C-5		39.5			
C-6		39.9			
C-7		40.4			
C-8		40.5			
C-9		39.8			
D-10	29 Jan 65	30.2	0-1		Performance at low, high chamber pressures.
D-11	29 Jan 65	30.3			
E-12	5 Feb 65	39.1		A & B	Performance at various chamber pressures between 80 and 125 psia.
E-13		CSM Shutdown (1.7)			
E-14		39.3			
E-15		40.3			
E-16		40.2			
E-17		39.7			
F-18	19 Feb 65	1.3 (Sequencer Malfunction)		A	Performance at various mixture ratios; obtain gimbal data.
*F-19		40.4			
*F-20		40.2			
*F-21		27.4			
*F-22		40.1			
*F-23		27.8			
*F-24		177.2			
G-25	18 Mar 65	20.4	11		Performance at various mixture ratios.
G-26		20.3			
G-27		20.5			
G-28		6.0			
H-29	25 Mar 65	21.0		B	Performance at various mixture ratios during simulated mission duty cycle.
H-30	25 Mar 65	20.3			
H-31	26 Mar 65	20.8			
H-32		160.0			
H-33		15.1			
H-34		15.2			
H-35		15.5			
H-36		15.5			
H-37		15.2			
H-38		Five Tests 1.00, 1.00, 0.98, 0.90, 1.05			
H-39		60.1			
J-40	7 Apr 65	10.9			Performance repeatability, minimum impulse operation, long-duration test at high chamber pressure, mixture ratio survey, gimbal data.
J-41	8 Apr 65	11.2			
J-42		10.2		A	
J-43		10.3			
J-44		9.6			
J-45	8 Apr 65	Five Tests 0.22, 0.27, 0.22, 0.20, 0.56			
J-46		Five Tests 0.27, 0.57, 0.36, 0.31, 0.44			
J-47		Five Tests 0.39, 0.46, 0.56, 0.56, 0.55			
J-48		Five Tests 0.75, 0.75, 0.76, 0.75, 0.76			
*K-49		110.5			Performance repeatability, minimum impulse operation, long-duration test at high chamber pressure, mixture ratio survey, gimbal data.
K-50		9.6			
K-51		10.4			
K-52		10.6			
K-53		10.8			
K-54		10.0			

*Gimbal Tests

TABLE III
SUMMARY OF ENGINE PERFORMANCE DATA FOR TEST FIRINGS AT DESIGN AND OFF-DESIGN CHAMBER PRESSURE TESTS

a. Engine S/N 9 (Design)

Firing Number	Time for 2-sec Average	F_m, lb_f	P_c, psia	$\dot{W}_o$, lb_m/sec	$\dot{W}_f$, lb_m/sec	P_a, psia	F_v, lb_f	$A_{t_{calc}}$, $in.^2$	MR	I_{sp_v}, lb_f-sec/lb_m	c*, ft/sec	C_{F_v}
A-1	5	21,485	102.27	49.24	23.71	0.1032	22,270	121.64	2.076	305.21	5485.4	1.790
↓	13	21,133	101.22	48.75	23.35	0.1120	21,984	121.35	2.088	304.89	5480.8	1.789
	21	21,021	100.85	48.53	23.23	0.1129	21,880	121.22	2.089	304.86	5480.4	1.789
B-2	7	21,542	102.70	51.10	22.53	0.098	22,294	120.29	2.268	302.77	5396.9	1.805
↓	15	21,320	102.10	50.61	22.45	0.105	22,145	120.21	2.254	303.08	5404.3	1.804
	23	21,255	101.77	50.28	22.39	0.106	22,063	120.06	2.245	303.56	5408.7	1.805
C-4	5	21,422	101.82	47.05	24.46	0.1020	22,198	121.00	1.924	310.37	5542.3	1.801
↓	11	21,199	101.02	47.00	24.06	0.1083	22,014	121.02	1.956	309.54	5531.3	1.800
	17	21,095	100.63	47.05	23.88	0.1093	21,926	121.08	1.971	309.09	5526.1	1.799
	23	21,068	100.50	46.89	23.85	0.1094	21,900	120.94	1.966	309.54	5527.7	1.801
C-5	7	20,900	99.82	43.92	25.43	0.1022	21,677	120.89	1.727	312.53	5597.3	1.795
↓	15	20,549	98.43	43.22	25.17	0.1069	21,362	120.94	1.717	312.31	5599.4	1.794
	23	20,408	97.82	42.63	25.21	0.1065	21,218	120.84	1.691	312.70	5605.1	1.795
	31	20,339	97.51	42.36	25.21	0.1060	21,145	120.64	1.675	313.31	5608.3	1.797
C-6	7	21,198	101.40	45.64	24.99	0.1019	21,973	120.65	1.826	311.04	5572.0	1.796
↓	15	20,793	99.71	44.94	24.50	0.1068	21,605	120.58	1.834	311.08	5569.9	1.796
	23	20,639	98.96	44.45	24.47	0.1065	21,449	120.69	1.816	311.15	5574.8	1.795
	31	20,576	98.64	44.07	24.51	0.1060	21,382	120.80	1.798	311.72	5579.8	1.797
C-7	7	21,158	101.07	46.88	24.07	0.1015	21,930	120.77	1.948	309.04	5534.2	1.796
↓	15	20,756	99.42	46.29	23.59	0.1067	21,567	120.81	1.962	308.56	5530.4	1.795
	23	20,497	98.16	45.70	23.29	0.1062	21,305	120.81	1.962	308.75	5529.2	1.796
	31	20,435	97.76	45.27	23.34	0.1057	21,238	120.79	1.940	309.51	5536.8	1.798
C-8	7	21,523	103.01	49.84	23.31	0.1022	22,301	120.49	2.138	304.86	5459.1	1.796
↓	15	21,224	101.82	49.41	22.97	0.1070	22,038	120.51	2.151	304.43	5453.6	1.796
	23	21,115	101.22	49.03	22.89	0.1068	21,927	120.53	2.142	304.85	5457.4	1.797
	31	21,084	100.94	48.71	22.94	0.1063	21,892	120.61	2.123	305.48	5465.8	1.798
C-9	7	21,295	101.89	49.79	22.86	0.1022	22,072	120.61	2.178	303.76	5441.2	1.796
↓	15	21,043	100.95	49.15	22.71	0.1067	21,854	120.53	2.164	304.09	5447.5	1.798
	23	20,984	100.50	48.77	22.72	0.1068	21,798	120.65	2.146	304.81	5455.5	1.797
	31	20,919	100.06	48.40	22.75	0.1065	21,729	120.77	2.127	305.36	5464.0	1.798

Firing Number	Time for 2-sec Average	F_m, lbf	P_c, psia	$\dot{W}_o$, lb_m/sec	$\dot{W}_f$, lb_m/sec	P_a, psia	F_v, lbf	$A_{t_{calc}}$, $in.^2$	MR	Isp_v, lbf-sec/lb_m	c*, ft/sec	CF_v
E-15	7	20,847	101.10	47.76	23.21	0.1334	21,859	120.73	2.058	307.96	5532.3	1.791
↓	17	20,590	100.26	47.34	23.02	0.1424	21,672	120.68	2.057	308.02	5532.8	1.791
	35	20,511	99.67	46.22	23.42	0.1434	21,600	120.84	1.974	310.17	5564.5	1.793
F-19	5	21,074	100.92	45.20	24.93	0.1205	21,989	120.54	1.817	313.12	5573.3	1.807
↓	13	20,849	100.35	44.42	25.28	0.1355	21,879	120.65	1.757	313.88	5588.8	1.807
	21	20,820	100.33	44.25	25.38	0.1382	21,870	120.64	1.743	314.04	5592.2	1.807
	31	20,818	100.35	44.14	25.41	0.1386	21,872	120.48	1.737	314.50	5593.6	1.809
F-20	5	21,192	101.41	46.62	24.37	0.1192	22,098	120.64	1.913	311.28	5544.8	1.806
↓	11	20,808	100.00	45.60	24.36	0.1319	21,810	120.83	1.872	311.78	5557.4	1.805
	17	20,725	99.74	45.12	24.54	0.1344	21,747	120.83	1.839	312.23	5567.3	1.804
	29	20,658	99.34	44.69	24.65	0.1355	21,688	120.92	1.813	312.83	5574.5	1.805
F-21	7	21,136	101.20	47.05	24.06	0.1261	22,095	120.79	1.955	310.71	5530.3	1.807
↓	11	20,771	99.69	45.57	23.62	0.1318	21,773	120.89	1.971	310.22	5524.6	1.806
	17	20,474	98.37	46.08	23.27	0.1334	21,487	121.00	1.980	309.81	5521.5	1.805
	23	20,439	98.197	45.71	23.43	0.1339	21,457	121.04	1.951	310.38	5531.7	1.805
F-22	7	21,450	102.93	51.13	22.76	0.1316	22,450	120.64	2.246	303.83	5406.7	1.808
↓	15	20,849	100.34	50.22	22.05	0.1379	21,897	120.70	2.277	302.97	5391.1	1.808
	23	20,859	100.19	49.63	22.37	0.1381	21,909	121.07	2.218	304.29	5420.6	1.806
	35	20,846	100.00	48.98	22.59	0.1400	21,910	121.12	2.168	306.10	5444.4	1.809
F-23	5	22,137	105.72	52.04	23.55	0.1232	23,073	120.55	2.210	305.28	5424.7	1.810
↓	13	21,409	102.69	50.81	22.88	0.1378	22,457	120.87	2.220	304.75	5410.7	1.809
	19	21,095	101.37	50.32	22.50	0.1405	22,162	120.82	2.237	304.35	5411.4	1.810
	25	21,095	101.25	49.95	22.69	0.1398	22,157	121.05	2.201	305.05	5428.8	1.808
F-24	11	21,456	102.76	50.31	23.28	0.1392	22,514	121.26	2.161	305.93	5447.7	1.807
↓	19	21,479	102.80	49.34	23.79	0.1422	22,559	121.30	2.074	308.45	5485.4	1.800
	31	21,467	102.57	48.70	24.15	0.1438	22,560	121.60	2.016	309.66	5508.1	1.809
	51	21,444	102.27	48.16	24.36	0.1448	22,544	121.72	1.977	310.85	5522.6	1.811

TABLE III (Continued)

c. Engine S/N 11 (Design)

Firing Number	Time for 2-sec Average	F_m, lbf	P_c, psia	$\dot{W}_o$, lb_m/sec	$\dot{W}_f$, lb_m/sec	P_a, psia	F_v, lbf	$A_{t_{calc}}$, in.^{2}	MR	Isp_v, lbf-sec/lb_m	c*, ft/sec	C_{F_v}
G-25	5	20,162	101.95	48.34	22.32	0.2452	22,026	121.20	2.166	311.73	5626.9	1.782
↓	11	19,972	101.16	48.10	21.89	0.2409	21,803	120.82	2.191	311.27	5614.3	1.783
	17	19,699	100.18	47.55	21.62	0.2406	21,528	120.41	2.199	311.22	5610.5	1.784
G-26	5	20,398	104.91	47.08	24.08	0.2809	22,533	120.46	1.955	316.67	5714.4	1.783
↓	11	20,053	103.90	46.58	23.81	0.2957	22,300	120.31	1.956	318.82	5713.9	1.784
	17	19,812	102.99	46.09	23.59	0.2965	22,065	120.20	1.954	316.62	5715.1	1.782
G-27	5	20,158	103.81	48.42	22.61	0.2731	22,234	119.92	2.142	312.99	5638.2	1.786
↓	11	19,855	102.63	48.04	22.29	0.2832	22,007	119.96	2.155	312.91	5631.8	1.787
	17	19,611	101.59	47.55	22.01	0.2816	21,751	119.82	2.160	312.67	5629.4	1.787
G-28	5	19,989	107.64	44.70	26.79	0.3899	22,953	119.62	1.669	321.10	5795.1	1.783
H-29	5	19,879	101.45	46.73	22.88	0.2170	21,528	120.34	2.042	310.74	5669.6	1.763
↓	11	19,396	99.703	45.97	22.16	0.2343	21,176	120.39	2.074	310.83	5668.6	1.764
	17	19,271	99.095	45.64	22.05	0.2327	21,039	120.38	2.070	310.83	5670.5	1.763
H-30	5	20,338	103.96	46.89	23.58	0.2225	22,029	120.15	1.989	312.61	5703.2	1.763
↓	11	19,764	101.90	45.64	23.33	0.2420	21,602	120.22	1.956	313.23	5715.0	1.763
	17	19,547	101.09	45.15	23.16	0.2455	21,412	120.08	1.949	313.45	5717.5	1.764
H-31	5	21,287	104.06	44.28	25.14	0.0746	21,854	119.74	1.761	314.79	5774.8	1.754
↓	7	21,121	103.33	43.90	25.08	0.0776	21,711	119.89	1.750	314.70	5777.6	1.752
	11	20,908	102.38	43.31	24.93	0.0800	21,516	119.75	1.737	315.32	5780.8	1.755
	15	20,803	101.92	43.14	24.82	0.0808	21,418	119.81	1.738	315.14	5780.5	1.754
	17	20,756	101.73	42.98	24.76	0.0811	21,372	119.66	1.736	315.49	5781.1	1.756
H-32	5	20,693	101.57	46.99	22.28	0.0933	21,401	119.83	2.109	308.96	5653.5	1.758
↓	7	20,659	101.43	46.78	22.28	0.0936	21,369	119.71	2.099	309.47	5657.8	1.760
	9	20,629	101.30	46.72	22.25	0.0938	21,342	119.73	2.099	309.44	5657.7	1.760
	11	20,589	101.10	46.67	22.21	0.0942	21,304	119.78	2.101	309.32	5657.0	1.759
	13	20,573	101.06	46.56	22.24	0.0944	21,290	119.76	2.094	309.48	5660.3	1.759
	15	20,539	100.94	46.50	22.21	0.0945	21,257	119.75	2.094	309.37	5660.2	1.758
	17	20,526	100.93	46.45	22.18	0.0948	21,246	119.63	2.094	309.58	5660.1	1.760
	19	20,505	100.85	46.45	22.15	0.0951	21,227	119.64	2.097	309.43	5659.0	1.759

TABLE III (Continued)

c. Continued

Firing Number	Time for 2-sec Average	F_m, lbf	P_c, psia	$\dot{W}_o$, lb_m/sec	$\dot{W}_f$, lb_m/sec	P_a, psia	F_v, lbf	$A_{t_{calc}}$, $in.^2$	MR	Isp_v, lbf-sec/lb_m	c*, ft/sec	C_{F_v}
H-32	21	20,510	100.91	46.45	22.19	0.0952	21,234	119.68	2.093	309.34	5660.7	1.758
	23	20,501	100.89	46.40	22.18	0.0956	21,228	119.60	2.092	309.55	5661.2	1.759
	25	20,488	100.87	46.40	22.17	0.0959	21,217	119.58	2.093	309.47	5660.6	1.759
	27	20,481	100.86	46.34	22.17	0.0960	21,210	119.52	2.090	309.60	5661.7	1.759
	29	20,478	100.85	46.34	22.17	0.0962	21,209	119.53	2.090	309.59	5661.7	1.759
	31	20,466	100.77	46.39	22.14	0.0965	21,200	119.63	2.095	309.34	5659.5	1.759
	33	20,456	100.75	46.39	22.12	0.0967	21,190	119.61	2.097	309.27	5658.9	1.758
	35	20,453	100.72	46.34	22.12	0.0970	21,190	119.59	2.095	309.51	5660.0	1.759
	37	20,451	100.71	46.29	22.14	0.0974	21,191	119.56	2.091	309.69	5661.6	1.760
	39	20,455	100.72	46.13	22.17	0.0978	21,198	119.40	2.081	310.41	5665.9	1.763
	41	20,447	100.69	46.29	22.12	0.0982	21,193	119.55	2.093	309.79	5661.0	1.761
	43	20,433	100.66	46.24	22.15	0.0987	21,183	119.59	2.088	309.75	5663.2	1.760
	45	20,437	100.71	46.18	22.14	0.0991	21,190	119.42	2.086	310.16	5663.7	1.762
	47	20,424	100.72	46.18	22.14	0.0997	21,182	119.40	2.086	310.04	5663.7	1.761
	49	20,414	100.69	46.24	22.13	0.1000	21,174	119.47	2.089	309.75	5662.1	1.760
	51	20,410	100.71	46.24	22.14	0.1002	21,171	119.49	2.088	309.65	5662.6	1.759
	53	20,402	100.70	46.13	22.11	0.1006	21,166	119.28	2.086	310.19	5663.6	1.762
	55	20,398	100.71	46.13	22.10	0.1013	21,168	119.23	2.087	310.28	5663.0	1.763
H-33	5	20,882	103.32	48.95	21.84	0.1003	21,643	119.04	2.241	305.75	5590.6	1.759
	7	20,769	102.81	48.68	21.74	0.1035	21,556	119.05	2.239	306.10	5591.8	1.761
	9	20,668	102.33	48.51	21.66	0.1055	21,469	119.18	2.240	305.94	5591.2	1.761
	11	20,591	101.97	48.35	21.57	0.1068	21,402	119.17	2.242	306.06	5590.6	1.761
H-34	5	20,410	100.52	47.10	21.63	0.0930	21,116	119.48	2.178	307.25	5622.2	1.758
	7	20,277	100.00	46.88	21.54	0.0984	21,025	119.59	2.176	307.25	5623.0	1.758
	9	20,175	99.589	46.66	21.47	0.1017	20,948	119.61	2.173	307.40	5624.4	1.758
	11	20,095	99.233	46.50	21.38	0.1038	20,883	119.56	2.175	307.63	5623.2	1.760
H-35	5	20,588	101.31	45.68	22.80	0.0933	21,297	119.69	2.004	311.02	5697.4	1.756
	7	20,480	100.90	45.57	22.70	0.0987	21,231	119.79	2.007	310.95	5695.9	1.756
	9	20,360	100.43	45.36	22.61	0.1025	21,139	119.81	2.006	311.04	5696.3	1.757
	11	20,255	99.998	45.14	22.52	0.1054	21,056	119.81	2.004	311.18	5697.1	1.757

TABLE III (Continued)

c. Continued

Firing Number	Time for 2-sec Average	F_m, lbf	P_c, psia	$\dot{W}_o$, lb_m/sec	$\dot{W}_f$, lb_m/sec	P_a, psia	F_v, lbf	At_{calc}, $in.^2$	MR	Isp_v, lbf-sec/lb_m	c*, ft/sec	CF_v
H-36	5	20,567	101.28	44.21	23.72	0.0930	21,273	119.77	1.864	313.19	5745.9	1.754
	7	20,464	100.97	44.16	23.59	0.1005	21,228	119.78	1.872	313.34	5743.5	1.755
	9	20,322	100.51	43.99	23.49	0.1072	21,136	119.86	1.873	313.18	5743.3	1.755
	11	20,211	100.17	43.83	23.41	0.1127	21,067	119.83	1.872	313.30	5743.3	1.755
H-37	5	20,940	103.66	43.33	25.61	0.1022	21,716	119.71	1.692	315.00	5791.1	1.750
	7	20,795	103.36	43.22	25.51	0.1151	21,669	110.68	1.694	315.24	5790.6	1.752
	9	20,525	102.91	43.11	25.37	0.1363	21,561	119.78	1.699	314.80	5789.5	1.749
	11	20,247	102.55	42.90	25.34	0.1636	21,490	119.78	1.693	314.89	5791.0	1.750
H-39	5	21,034	102.72	46.97	22.90	0.0810	21,649	120.04	2.051	309.84	5678.2	1.756
	7	20,974	102.51	46.98	22.77	0.0846	21,617	119.99	2.063	309.92	5673.5	1.757
	9	20,882	102.14	46.92	22.66	0.0865	21,540	120.07	2.071	309.55	5670.2	1.756
	11	20,827	101.90	46.76	22.60	0.0877	21,493	110.99	2.069	309.84	5671.1	1.758
	13	20,788	101.72	46.71	22.54	0.0884	21,460	119.95	2.072	309.91	5669.4	1.759
	15	20,756	101.59	46.66	22.52	0.0889	21,432	120.00	2.072	309.81	5669.9	1.758
	17	20,715	101.42	46.66	22.44	0.0893	21,393	119.99	2.079	309.63	5666.6	1.758
	19	20,686	101.29	46.60	22.42	0.0896	21,367	120.03	2.078	309.55	5667.0	1.757
	21	20,656	101.16	46.55	22.40	0.0898	21,338	120.04	2.078	309.50	5667.0	1.757
	23	20,628	101.04	46.50	22.33	0.0899	21,312	119.93	2.082	309.68	5665.2	1.759
	25	20,611	100.96	46.39	22.33	0.0899	21,294	119.89	2.077	309.91	5667.3	1.759
	27	20,587	100.86	46.44	22.30	0.0899	21,270	120.00	2.083	309.43	5665.2	1.757
	29	20,572	100.77	46.33	22.31	0.0900	21,256	120.00	2.077	309.66	5667.8	1.758
	31	20,557	100.68	46.22	22.28	0.0902	21,242	110.89	2.075	310.06	5668.7	1.760
	33	20,536	100.59	46.28	22.27	0.0905	21,223	120.03	2.078	309.62	5667.1	1.758
	35	20,530	100.53	46.22	22.25	0.0907	21,219	119.99	2.077	309.86	5667.6	1.759
	37	20,516	100.46	46.17	22.27	0.0908	21,206	120.04	2.073	309.84	5669.2	1.758
	39	20,493	100.36	46.17	22.23	0.0909	21,185	120.05	2.077	309.73	5667.6	1.758
	41	20,493	100.35	46.17	22.24	0.0912	21,186	120.10	2.076	309.69	5668.1	1.758
	43	20,484	100.31	46.11	22.21	0.0914	21,178	120.00	2.076	309.94	5668.0	1.759
	45	20,466	100.25	46.11	22.21	0.0917	21,163	120.07	2.076	309.71	5668.0	1.758

TABLE III (Continued)

c. Concluded

Firing Number	Time for 2-sec Average	F_m, lbf	P_c, psia	$\dot{W}_o$, lbm/sec	$\dot{W}_f$, lbm/sec	P_a, psia	F_v, lbf	$A_{t_{calc}}$, in.^{2}	MR	Isp_v, lbf-sec/lbm	c*, ft/sec	C_{F_v}
H-39	47	20,449	100.16	46.11	22.18	0.0918	21,146	120.12	2.079	309.59	5666.9	1.757
↓	49	20,442	100.15	46.01	22.18	0.0919	21,140	119.98	2.074	310.01	5669.0	1.759
	51	20,439	100.15	46.06	22.20	0.0921	21,139	120.08	2.075	309.68	5668.5	1.758
	53	20,420	100.07	46.01	22.17	0.0924	21,121	120.04	2.075	309.79	5668.4	1.758
	55	20,418	100.08	45.95	22.20	0.0926	21,121	120.03	2.070	309.91	5670.6	1.758
	57	20,403	100.03	45.95	22.19	0.0928	21,108	120.04	2.071	309.78	5670.0	1.758
J-40	5	20,523	100.60	46.34	22.06	0.0758	21,097	119.54	2.100	308.43	5656.6	1.754
↓	7	20,407	100.12	46.12	21.97	0.0786	21,001	119.57	2.099	308.44	5656.9	1.754
J-41	5	20,483	100.18	45.58	22.35	0.0748	21,049	119.76	2.039	309.84	5682.3	1.754
↓	7	20,323	99.479	45.21	22.23	0.0777	20,910	119.77	2.034	310.08	5684.5	1.755
J-42	5	20,897	102.05	45.95	23.03	0.0737	21,455	119.73	1.995	311.06	5699.5	1.756
↓	7	20,726	101.31	45.58	22.86	0.0771	21,309	119.67	1.994	311.38	5700.2	1.757
J-43	5	20,778	101.44	45.68	22.95	0.0730	21,330	119.90	1.990	310.79	5701.7	1.754
↓	7	20,605	100.73	45.31	22.80	0.0766	21,184	119.85	1.987	311.04	5702.9	1.755
J-44	5	20,805	101.53	45.52	23.06	0.0731	21,357	119.83	1.974	311.42	5707.8	1.755
K-50	5	21,333	104.26	47.20	23.48	0.0833	21,963	119.96	2.010	310.77	5693.9	1.756
K-51	5	20,704	101.28	43.39	24.51	0.0808	21,315	120.28	1.770	313.94	5771.6	1.750
↓	7	20,744	101.45	43.87	24.29	0.0842	21,381	120.32	1.806	313.68	5761.9	1.752
K-52	5	20,809	101.75	43.27	24.91	0.0810	21,421	120.37	1.737	314.20	5779.8	1.749
↓	7	20,825	101.80	43.60	24.70	0.0845	21,464	120.37	1.765	314.29	5778.0	1.752
K-53	5	20,864	102.15	42.23	25.92	0.0815	21,481	120.33	1.629	315.20	5802.6	1.748
↓	7	21,021	102.80	43.09	25.67	0.0851	21,665	120.43	1.679	315.08	5793.0	1.750
K-54	5	20,614	101.32	40.56	26.81	0.0820	21,234	120.27	1.513	315.20	5820.2	1.742
↓	7	20,643	101.40	40.78	26.66	0.0851	21,286	120.25	1.530	315.68	5818.1	1.746

TABLE III (Concluded)

d. Engine S/N 9-1 and 11 (Off-Design)

ENGINE S/N 9-1

Firing Number	Time for 2-sec Average	F_m, lbf	P_c, psia	$\dot{W}_o$, lb_m/sec	$\dot{W}_f$, lb_m/sec	P_a, psia	F_v, lbf	At_{calc}, $in.^2$	MR	Isp_v, lbf-sec/lb_m	c*, ft/sec	C_{F_v}
D-10	5	27,228	128.41	61.87	29.27	0.124	28,178	121.54	2.113	309.12	5508.8	1.805
↓	11	26,725	127.22	61.21	28.89	0.146	27,839	121.22	2.118	308.97	5506.8	1.805
	17	26,513	126.55	60.93	28.69	0.151	27,660	121.17	2.123	308.61	5504.6	1.803
	25	28,344	125.91	60.44	28.55	0.152	27,501	120.99	2.116	309.03	5507.5	1.805
D-11	5	17,467	83.85	40.40	19.26	0.1031	18,251	121.99	2.097	305.86	5515.9	1.784
↓	11	17,214	83.23	40.12	19.06	0.1175	18,107	121.86	2.104	305.89	5512.9	1.785
	17	17,076	82.77	40.12	18.84	0.1201	17,989	121.82	2.129	305.07	5501.9	1.784
	27	16,949	82.25	40.01	18.57	0.1208	17,854	121.56	2.154	304.74	5490.8	1.785
E-12	9	26,773	128.61	60.08	29.71	0.1521	27,929	120.38	2.021	311.00	5546.5	1.804
↓	17	26,525	127.85	59.27	29.73	0.1606	27,745	120.24	1.993	311.71	5557.1	1.805
	27	26,390	127.33	58.68	29.78	0.1620	27,622	120.19	1.971	312.21	5565.7	1.805
	37	28,293	126.92	58.14	29.85	0.1623	27,526	120.12	1.947	312.79	5573.6	1.806
E-14	7	23,321	112.55	52.82	25.77	0.1363	24,357	120.16	2.049	309.88	5535.7	1.801
↓	17	22,949	111.75	51.70	25.80	0.1473	24,069	119.71	2.003	310.53	5553.4	1.799
	27	22,847	111.09	51.17	25.87	0.1483	23,979	119.91	1.977	311.17	5563.0	1.799
	37	22,785	110.81	50.74	25.95	0.1486	23,914	119.86	1.954	311.79	5571.1	1.800
E-16	7	19,128	92.84	43.37	21.66	0.1270	20,093	120.92	2.001	308.95	5554.1	1.789
↓	17	18,747	91.21	42.73	21.27	0.1345	19,769	121.09	2.008	308.85	5551.7	1.789
	27	18,547	90.28	42.30	21.02	0.1350	19,573	121.02	2.011	309.04	5550.3	1.791
	37	18,470	89.88	42.09	20.95	0.1350	19,496	121.04	2.008	309.21	5551.6	1.792
E-17	7	16,781	81.99	38.65	18.95	0.1177	17,676	120.97	2.039	306.81	5539.7	1.781
↓	17	16,509	80.86	38.33	18.68	0.1235	17,447	121.25	2.054	308.07	5533.8	1.779
	27	16,350	80.07	38.01	18.41	0.1239	17,292	121.12	2.064	306.41	5529.6	1.782
	37	16,270	79.69	38.07	18.24	0.1241	17,213	121.25	2.086	305.62	5520.6	1.781

ENGINE S/N 11

K-49	11	25,295	122.82	55.34	27.77	0.0955	26,018	119.91	1.992	313.02	5700.6	1.766
↓	27	25,265	122.87	56.57	27.12	0.1027	28,043	119.91	2.085	311.14	5662.9	1.767
	39	25,342	123.27	56.79	27.16	0.1039	26,128	119.84	2.090	311.21	5660.9	1.768
	47	25,476	123.92	56.63	27.62	0.1050	26,270	119.99	2.050	311.80	5677.9	1.766

TABLE IV
SUMMARY OF MEASURED OPERATING PARAMETERS

a. Design Chamber Pressure Tests

ENGINE ASSEMBLY 9

Firing No.	Duration, sec	P_{otca}, psia	P_{ftca}, psia	P_{oj}, psia	P_{fj}, psia	P_c, psia	$\dot{W}_o$, lb_m/sec	$\dot{W}_f$, lb_m/sec
A-1	30.1	173.58	168.16	154.37	133.03	100.97	48.53	23.28
B-2	30.1	175.03	163.84	153.49	131.87	101.90	50.45	22.40
C-4	30.3	164.93	165.38	145.40	134.58	100.57	46.95	23.84
C-5	39.5	152.63	169.81	136.82	135.19	98.06	42.85	25.16
C-6	39.9	157.22	165.22	140.30	133.89	99.18	44.67	24.44
C-7	40.4	159.10	159.43	141.65	130.83	98.67	45.98	23.39
C-8	40.5	169.62	159.49	149.67	131.95	101.41	49.25	22.88
C-9	39.8	166.36	157.60	147.29	131.01	100.24	48.51	22.77

ENGINE ASSEMBLY 9-1

E-15	40.3	164.20	166.62	140.37	130.21	100.11	46.91	23.14
F-19	40.4	157.65	178.98	136.14	137.04	100.33	44.25	25.39
F-20	40.2	158.29	173.60	137.70	133.27	99.58	44.90	24.61
F-21	27.4	159.14	165.82	138.88	128.40	98.23	45.81	23.37
F-22	40.1	168.28	162.68	145.50	128.25	100.07	49.14	22.55
F-23	27.8	172.38	163.84	148.55	129.21	101.24	50.22	22.50
F-24	177.2	168.07	174.94	144.87	135.23	102.27	48.16	24.36

ENGINE ASSEMBLY 11

H-31	20.8	158.32	181.92	146.79	160.63	101.92	43.14	24.82
H-32	160.0	164.17	164.26	150.51	147.36	100.69	46.24	22.12
H-33	15.1	172.13	163.71	150.94	147.25	102.33	48.51	21.66
H-34	15.2	163.05	158.23	144.37	142.34	98.94	46.45	21.31
H-35	15.6	160.00	165.35	141.15	147.82	99.71	44.98	22.49
H-36	15.5	156.82	170.55	139.51	151.70	99.83	43.67	23.33
H-37	15.2	157.07	184.56	140.28	162.73	102.20	42.74	25.22
H-39	60.1	165.56	166.55	146.17	149.21	101.29	46.60	22.42
J-40	10.9	165.46	164.47	144.05	146.90	100.12	46.12	21.97
J-41	11.2	162.46	165.14	142.29	147.46	99.48	45.21	22.23
J-42	10.2	165.38	167.34	144.91	151.51	101.31	45.58	22.86
J-43	10.3	163.75	166.90	143.48	150.91	100.73	45.31	22.80
J-44	9.6	163.57	167.48	143.00	151.55	100.84	45.20	22.93
K-50	9.6	173.35	173.47	151.36	157.34	104.22	47.47	23.30
K-51	10.4	160.71	176.50	141.27	158.72	101.45	43.87	24.29
K-52	10.6	160.30	179.56	141.06	161.12	101.80	43.60	24.70
K-53	10.8	160.28	186.53	141.43	166.87	102.80	43.09	25.67
K-54	10.1	153.23	191.63	136.37	170.24	101.40	40.78	26.66

TABLE IV (Concluded)

b. Off-Design Chamber Pressure Tests

ENGINE ASSEMBLY 9

Firing No.	Duration, sec	P_{otca}, psia	P_{ftca}, psia	P_{oj}, psia	P_{fj}, psia	P_c, psia	$\dot{W}_o$, lb_m/sec	$\dot{W}_f$, lb_m/sec
	NO OFF-DESIGN CHAMBER PRESSURE FIRINGS CONDUCTED							

ENGINE ASSEMBLY 9-1

D-10	30.2	227.80	224.80	190.83	169.99	126.19	60.60	28.64
D-11	30.3	128.55	126.11	112.40	101.04	82.42	40.12	18.66
E-12	39.1	226.07	235.96	184.77	175.81	127.62	59.01	29.76
E-14	39.3	187.22	193.62	156.56	148.22	111.51	51.39	25.80
E-16	40.2	143.91	146.71	123.76	116.06	90.66	42.47	21.17
E-17	39.7	123.67	123.94	106.05	100.21	80.36	38.13	18.53

ENGINE ASSEMBLY 11

K-49	110.5	213.26	216.71	185.47	194.20	121.59	55.02	27.36

APPENDIX I
PROPELLANT FLOWMETER AND WEIGH SCALE CALIBRATIONS

I. GENERAL

(U) An in-place flowmeter calibration system was installed in the J-3 stand to calibrate turbine-type flowmeters so that flow rates could be measured within the degree of accuracy required for the Phase II Apollo Service Module Propulsion System tests at AEDC. The in-place calibration system provides the capability of calibrating the flowmeters in their line configuration and at the same temperatures, pressures, and propellant flow rates that exist during an engine test firing. The configuration of the F-3 propellant feed lines (Fig. I-1) does not provide an optimum flowmeter location; therefore, it was deemed necessary to provide for in-place flowmeter calibrations.

(U) Meters were calibrated in propellants with the in-place calibration system and were also calibrated in water at the Engineering Support Facility (ESF), AEDC.

A. Water Calibrations

(U) The fuel and oxidizer flowmeters were calibrated with water in four configurations: a straight pipe, the F-3 propellant feed lines with an in-place calibration "tee," the feed lines with the engine interface, and the feed lines with the engine interface plus a "jumper" extension as shown in Fig. I-2. These four configurations were used to provide characteristics of the flowmeters in water and to compare the line effects between the "tee," the interface, and the "jumper" configurations. The straight line configuration provided a basis for comparing pre- and post-test flowmeter characteristics. The "tee" configuration shown in Figs. I-1 and I-3 is the basic in-place calibration configuration. The interface simulated flow through the engine while the "jumper" simulated flow through the feed line with the engine not installed.

B. In-Place Calibration in Propellant

(U) The J-3 in-place flowmeter calibration system is represented schematically in Fig. I-4. In general, the flowmeter was calibrated by recording its total flow indication during a given time period while the flow was accumulated in a weigh tank on the platform of a beam scale.

(U) Flow was established from the pressurized F-3 sump tank through the diverter valve and into the facility storage tank. After a

steady-state flow was reached, the diverter valve was actuated, and flow was diverted into the weigh tank for a specified time. The diverter valve was then actuated and the flow was diverted back to the storage tank. A scale reading was obtained that represented the total accumulated propellant weight. Total flowmeter signal counts were obtained from magnetic tape and represented the flowmeter output from the time the signal was given to divert the flow into the weigh tank (signal 1, Fig. I-5) until the signal was given to divert the flow to the storage tank (signal 2, Fig. I-5). These total counts were corrected for diverter valve transients using flowmeter output from an oscillograph record. Figure I-5 represents graphically this correction, which provided corrected flowmeter counts that correspond to the total volume of propellant diverted to the weigh tank. A flowmeter constant with the units of lb-H_2O/cycle was determined using the corrected counts, the total weight, and the propellant specific gravity. The above procedure was used on both the oxidizer and fuel systems. The instrumentation used to record the calibrating data is listed in Table I-1.

(U) The oxidizer flowmeter (AEDC 2-1/2 in.-3) was calibrated both through the "tee" and "interface" configurations before the engine was installed in the stand. The fuel flowmeter (AEDC 2 in.-6) was calibrated only after the engine was installed and in the "tee" configuration.

C. Weigh Scale Calibration Procedure

(U) The accumulated propellant weight obtained during the specified time (of a calibration point) was measured with a load cell installed in the linkage of the beam-scale. The load cell was in-place calibrated by applying deadweights to the scale platform and obtaining a sensitivity factor for the load cell. Weights were applied in 400-lb increments from 0 to 3200 lb to determine the linearity and repeatability of the system. Deadweight calibrations of the tank/scale system were also made with various tank internal pressures. The effect on indicated tank weight of various gas pressures in the tank supply and drain lines was thereby established. (Flowmeter calibrations were conducted with tank vents closed to preclude any loss of weight by venting propellant vapors. Propellant filling the weigh tank reduced ullage and caused a rise of tank ullage pressure.)

II. DISCUSSION

A. Water Calibration

(U) The results of the ESF water calibrations are presented in Figs. I-6 and I-7 for four line configurations used with the oxidizer and

fuel flowmeters, respectively. The water calibration constant for the "tee" configuration differs from the constant for the straight pipe configuration by approximately -1.90 percent for the oxidizer meter and 0.26 percent for the fuelmeter. The other line configuration constants are within 0.10 percent of the "tee" configuration. Thus, in water calibrations, the flowmeters show essentially the same flow factor (K) for the three feedline configurations. The flowmeters were recalibrated in the straight line configuration with water after the engine S/N 11 test series. The oxidizer flowmeter constant (K) had increased by 0.857 percent (Fig. I-8a); however, the fuel flowmeter constant remained the same (Fig. I-8b). The shift in the oxidizer flowmeter constant is believed to be the result of the propellant environment on the meter and to have occurred when the meter was first subjected to oxidizer.

B. Oxidizer Flowmeter In-place Calibrations

(U) Five series of oxidizer in-place flowmeter calibrations were made on flowmeter AEDC 2-1/2 in.-3. These calibrations and configurations are tabulated in Table I-2. The data from four calibrations, two through the "interface" and two through the "tee," are shown in Fig. I-9. The flowmeter constant for the calibrations through the "interface" was K = 0.07446 lb-H_2O/cycle with a standard deviation of σ = 0.347 percent. The flowmeter constant for the calibrations through the "tee" was K = 0.07437 with a standard deviation of σ = 0.098 percent. The statistical "t-test" was applied to the means of these two groups of data to evaluate the observed differences. The results of the t-test were that 50 percent of the time a difference this large or larger could be expected from data with the inherent variability shown by the two groups of data.

(U) It was concluded, therefore, that there was no difference in flowmeter constants between the "tee" and the interface configurations. (This repeats the flowmeter characteristics observed from the water calibration.) The data were pooled for an average flowmeter K-constant of K = 0.07442.

(U) Calibration No. 4 was made in the "tee" configuration on January 21, 1965. The data from this calibration gave a flowmeter constant of 0.07430 lb-H_2O/cycle with a standard deviation of σ = 0.215 percent. This is within the expected range of the means, and the established constant of K = 0.07442 lb-H_2O/cycle was used to obtain engine propellant flows for engines S/N 9 and 9-1 testing.

(U) The confidence in the constant is expressed by evaluating the variance in the means of the data. The standard deviation of the means of the data is 0.129 percent.

(U) The constant of 0.07442 was 2.25 percent higher than the flowmeter constant determined from water calibrations in the "tee" configurations.

(U) The fifth calibration was performed prior to the engine S/N 11 test series and after modifications were made to the in-place calibration system. The data are shown in Fig. I-10, and the mean is 0.07471 lb-H_2O/cycle with a standard deviation of 0.220 percent. This value was 0.390 percent higher than the previous constant of 0.07442. The value of K = 0.07471 lb-H_2O/cycle was used to obtain oxidizer flow rates for the engine S/N 11 series. This change is judged to be a result of the calibration system modification. Because the 0.390-percent difference was relatively small, no correction was made for engine S/N 9 data.

C. Fuel Flowmeter In-place Calibrations

(U) Three series of fuel in-place flowmeter calibrations were made on flowmeter S/N AEDC 2 in.-6. These calibrations and configurations are tabulated in Table I-2. All of these calibrations were made with the "tee" configuration. The in-place "interface" calibrations were not conducted on the fuel side because the results of the water calibrations showed no difference in the data from the "interface" and the "tee" configurations.

(U) The data from the first calibration gave a flowmeter constant of 0.03062 lb-H_2O/cycle with a standard deviation of σ = 0.813 percent. Modifications were made to the installation to decrease the dispersion and to improve the data. The average constant from the second calibration was 0.03083 lb-H_2O/cycle with a standard deviation of σ = 0.594 percent. The data from the first two calibrations are shown in Fig. I-11. For the test series on engines S/N 9 and 9-1, the flowmeter constant of K = 0.03068 lb-H_2O/cycle was used. This value is 1.04 percent higher than the value obtained from the calibration with water in the "tee" configuration.

(U) After testing engine S/N 9-1, additional modifications were made to the in-place calibration system valving to preclude trapped propellant; then the third calibration was performed. The constant for this calibration series was K = 0.03066 lb-H_2O/cycle with a standard deviation of σ = 0.136 percent (Fig. I-12). Because of the excellent repeatability and the modifications to the system, the value of K = 0.03066 lb-H_2O/cycle was used to determine propellant flow rates for the engine S/N 11 series. The value of 0.03066 lb-H_2O/cycle is 0.987 percent higher than the flow factor determined from water in the "tee" configuration. The value of 0.03066 lb-H_2O/cycle was 0.05 percent lower than the value used to determine flows for the engines S/N 9 and 9-1 series.

III. SUMMARY OF RESULTS

(U) 1. The oxidizer constant obtained with the in-place calibration system was 2.25 percent higher than the flowmeter constant determined from calibrations with water in the "tee" configuration.

(U) 2. The fuel flowmeter constant obtained with the in-place calibration system was 0.987 percent higher than the constant obtained with water in the "tee" configuration.

(U) 3. The calibration with water showed a 0.857-percent increase in the oxidizer flowmeter constant from prior to engine S/N 9 test series until after the engine S/N 11 test series. This shift probably occurred when the meter was first subjected to the oxidizer environment.

(U) 4. The accuracy of the in-place calibration facilities is determined by evaluating the individual components of the system and combining with this the precision observed in the measured value.

The following table lists the accuracy of the individual components in terms of one standard deviation:

System Component	N_2O_4 Constant, percent	AZ-50 Constant, percent
Deadweights	0.001	0.001
Load Cell and Scale Calibration	0.10	0.10
Pressure Correction	0.075	0.144
Combined System Component Accuracy	0.125	0.175

This component accuracy is combined with the variability of the means of the data from the in-place oxidizer flowmeter calibration of 0.129 percent to give a standard deviation of the oxidizer flowmeter constant of 0.180 percent. The component accuracy is combined with the variability of the means of the data from the in-place fuel flowmeter calibration of 0.085 percent to give a standard deviation of the fuel flowmeter constant of 0.195 percent.

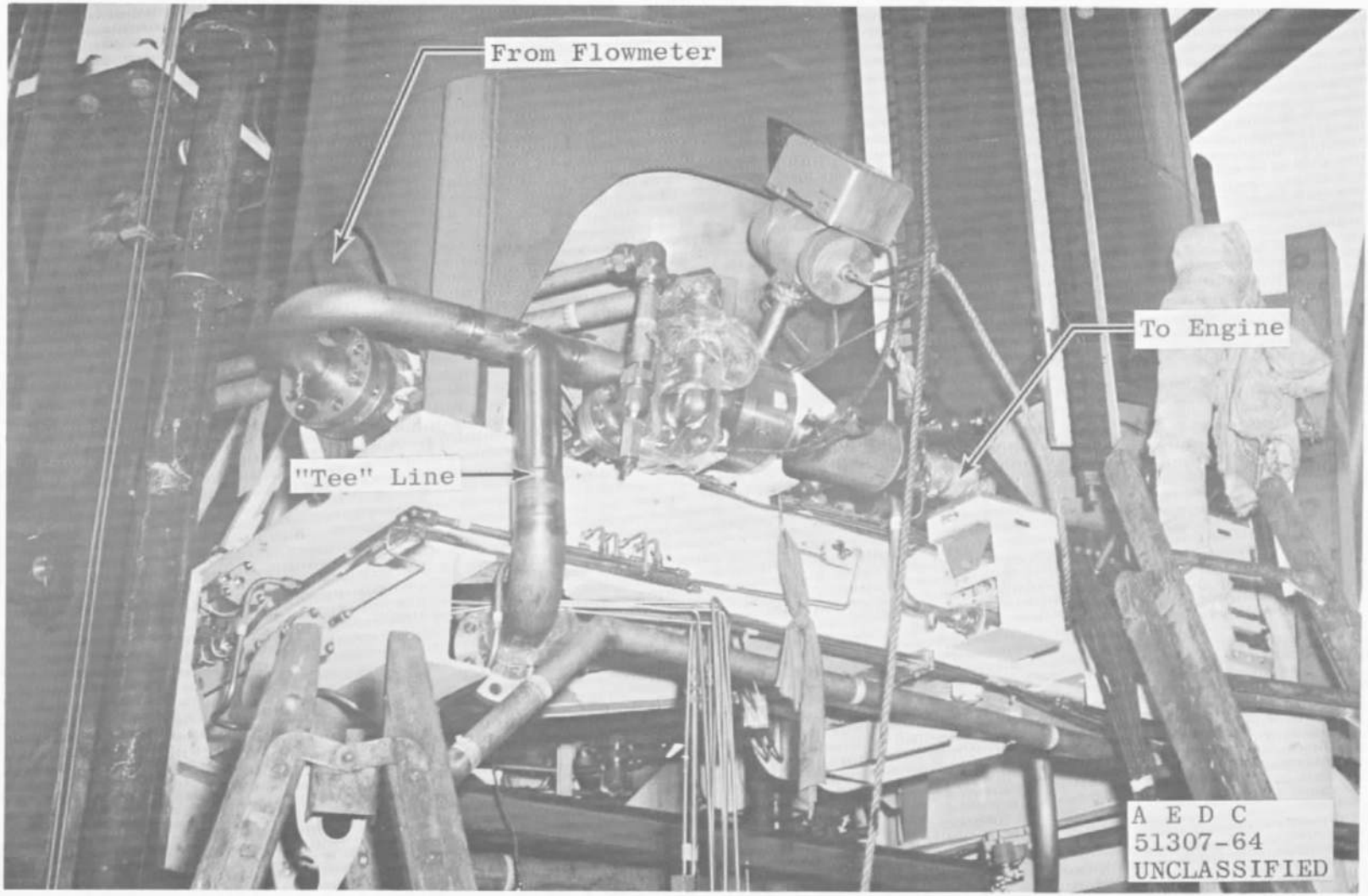

Fig. I-1 Weight Flow System Propellant Line "Tee" (Oxidizer Side)

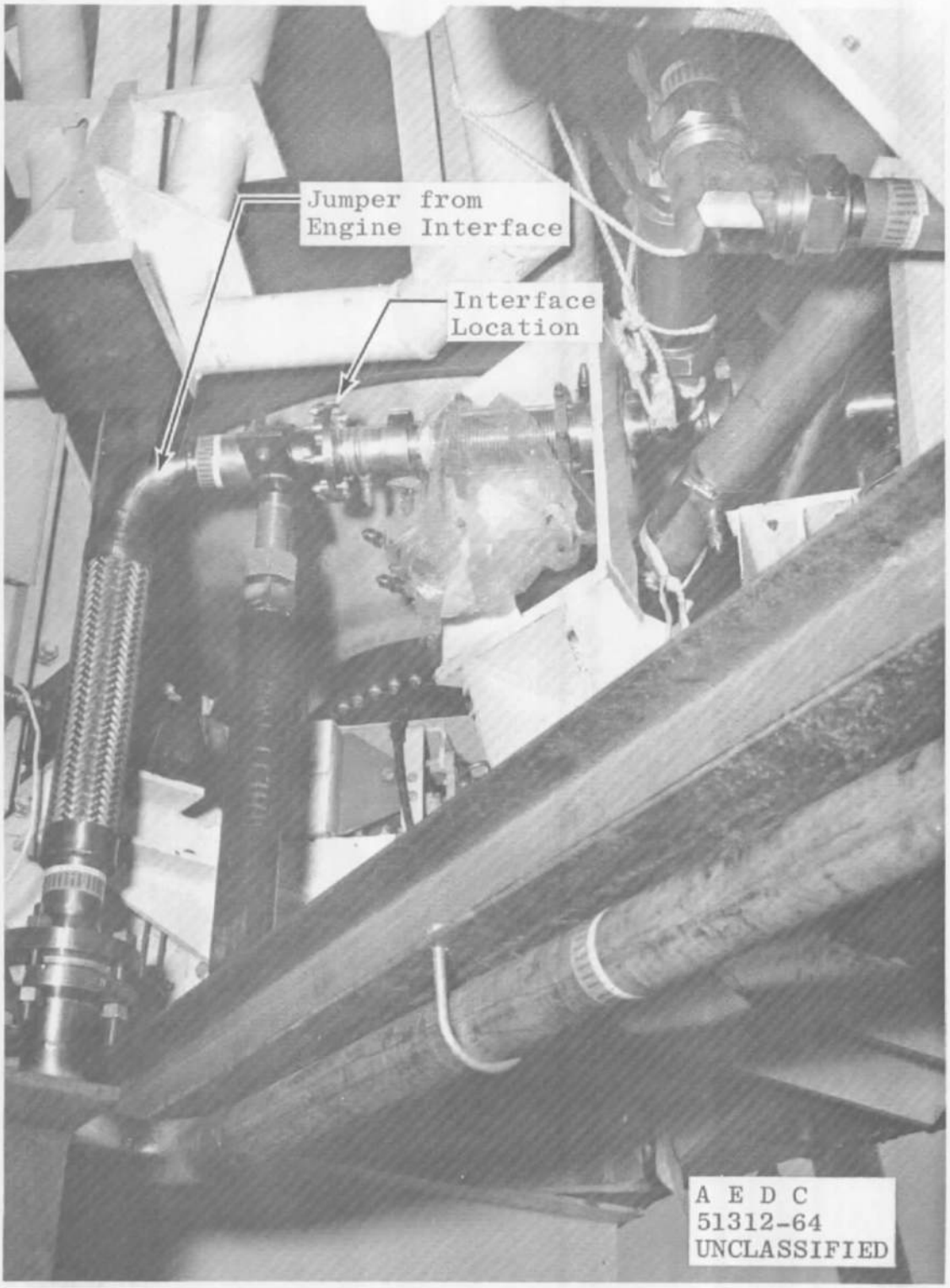

Fig. 1-2 Weight Flow System Jumper Line (Fuel Side)

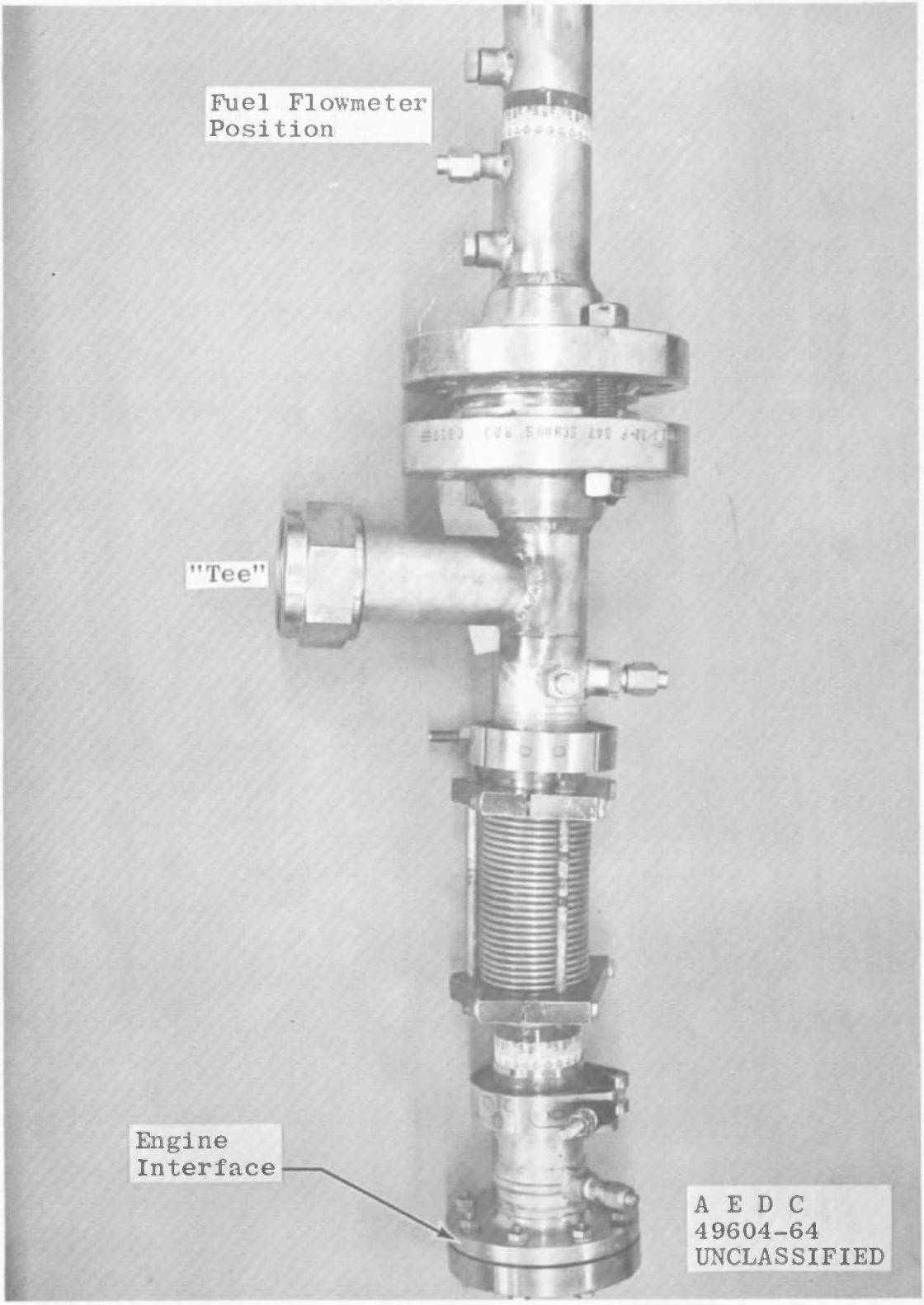

Fig. I-3 Fuel Flowmeter Position and In-Place Calibration "Tee"

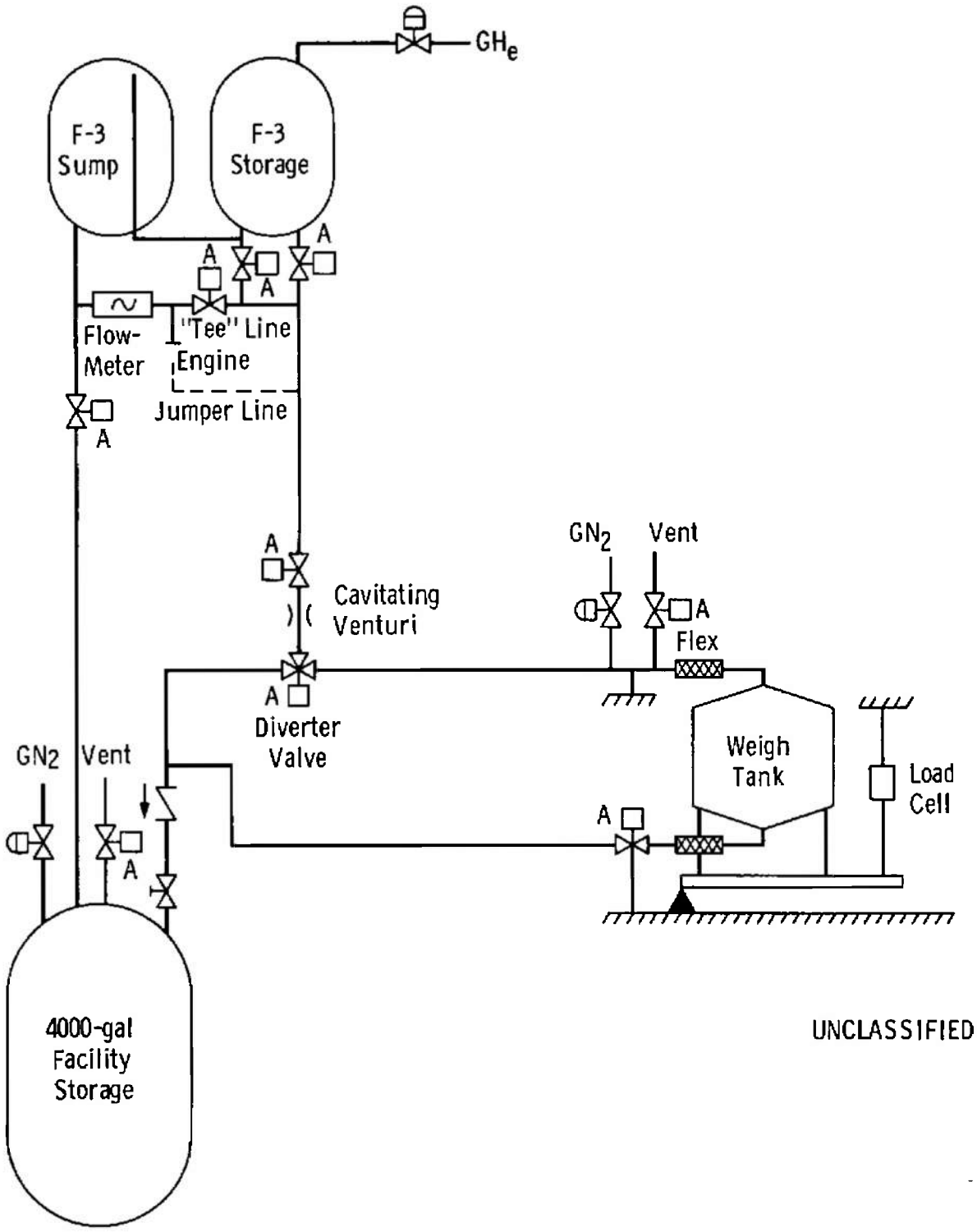

Fig. I-4 Schematic Diagram of Flowmeter In-Place Calibration System

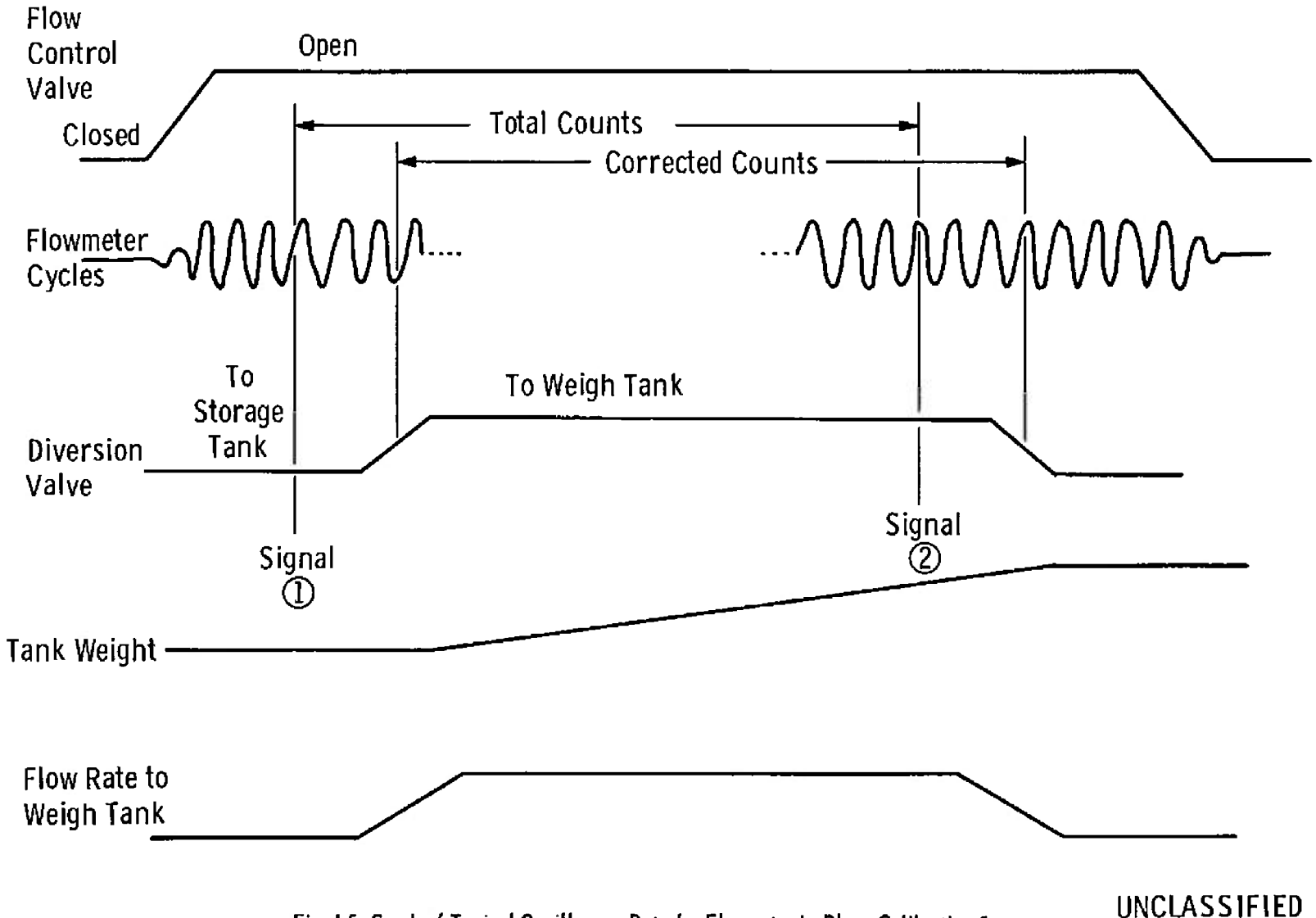

Fig. I-5 Graph of Typical Oscillogram Data for Flowmeter In-Place Calibration System

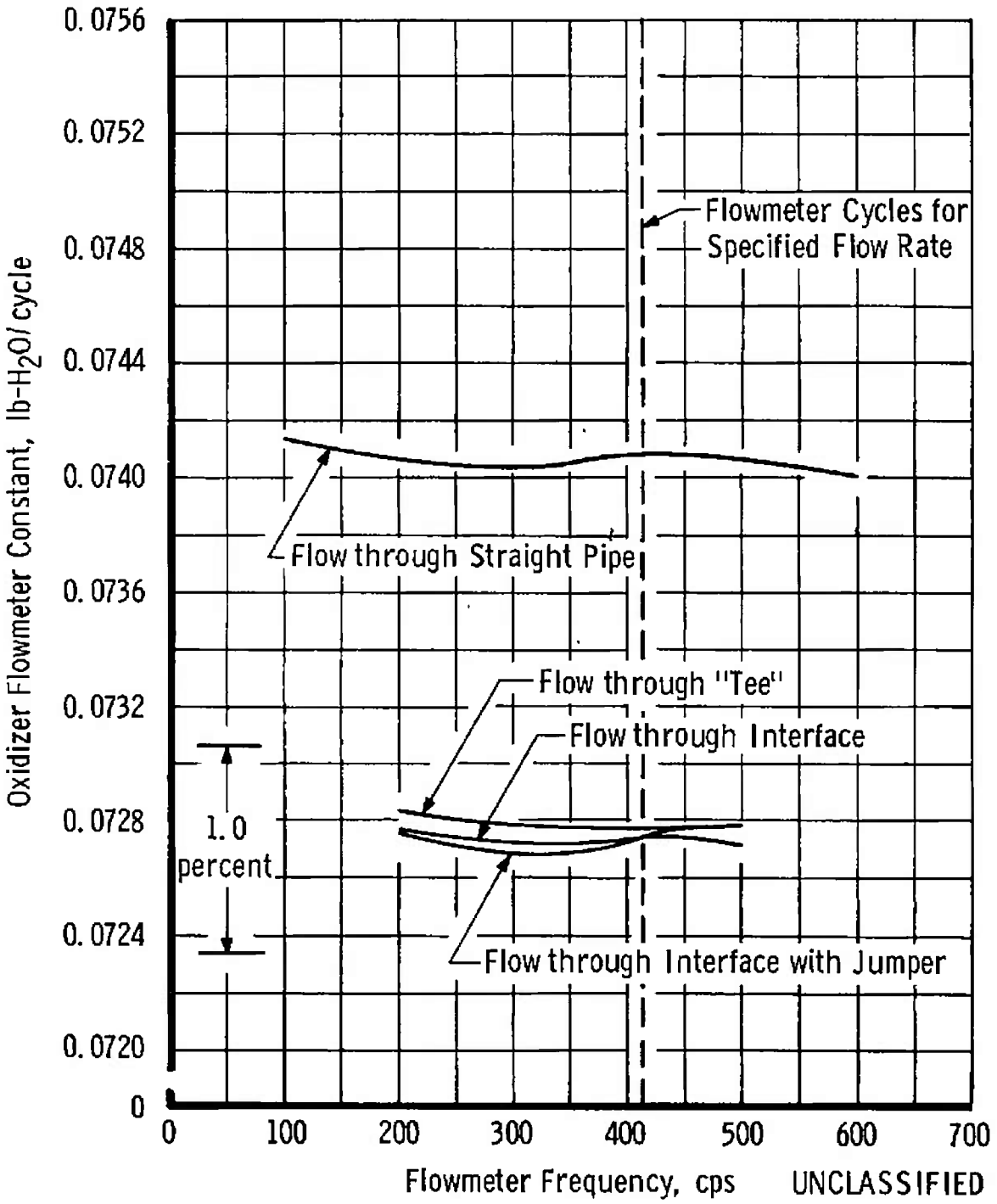

Fig. I-6 Oxidizer Flowmeter Calibration in Water

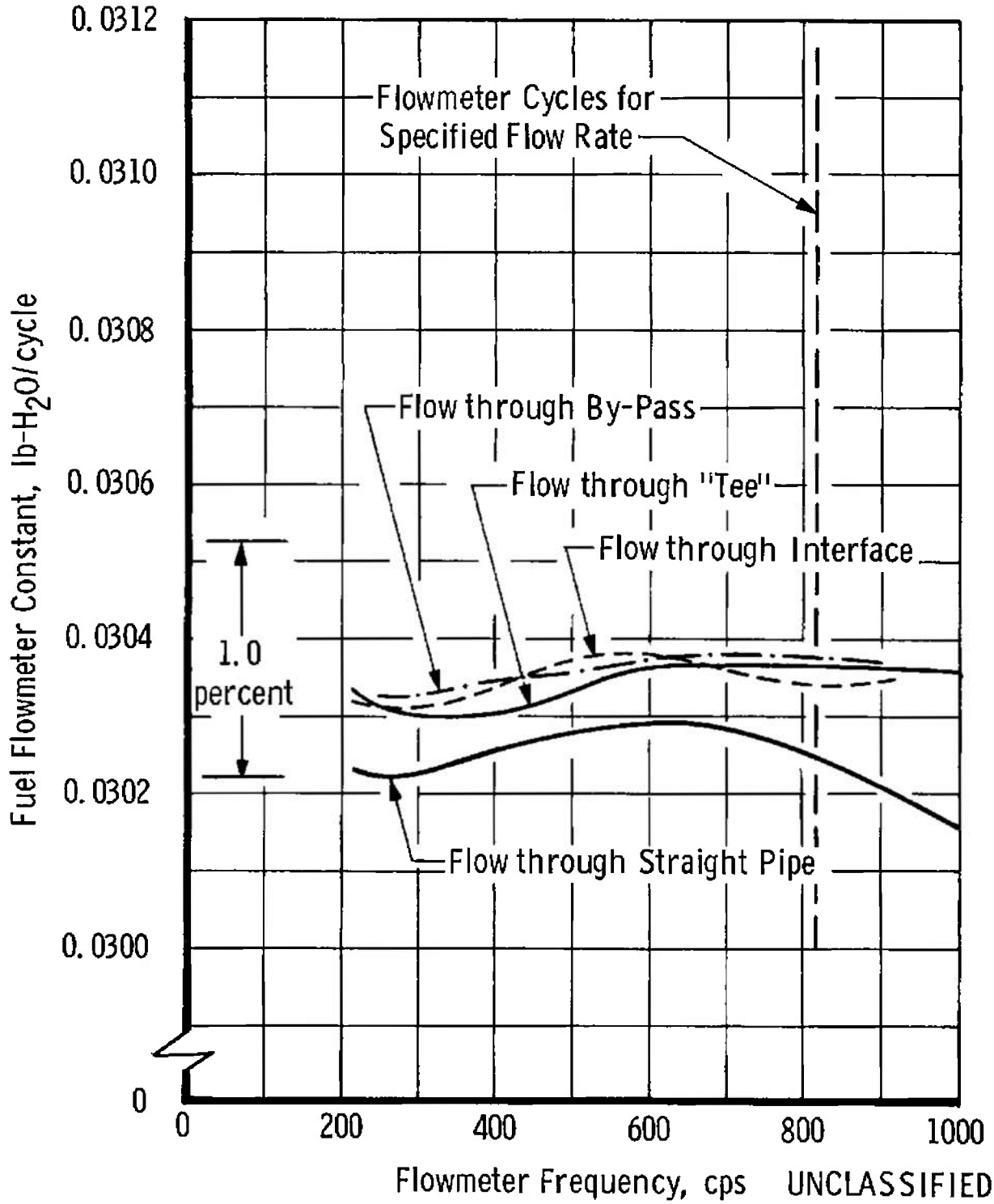

Fig. I-7 Fuel Flowmeter Calibration in Water

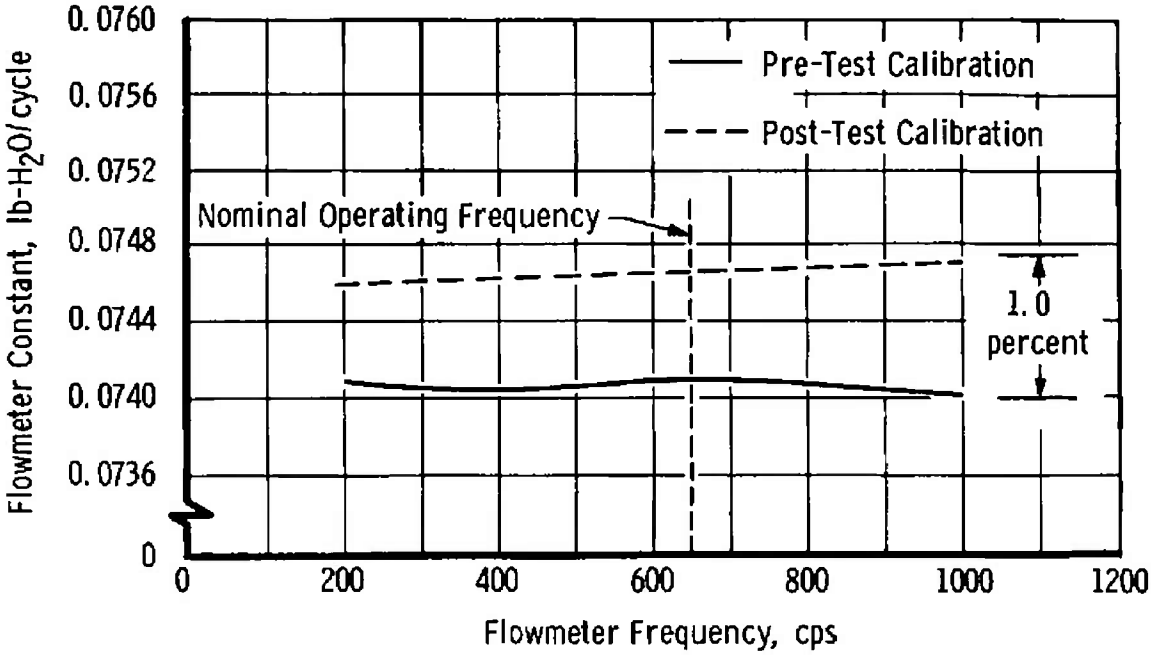

a. Oxidizer Flowmeter Calibration with Water in a Straight Pipe

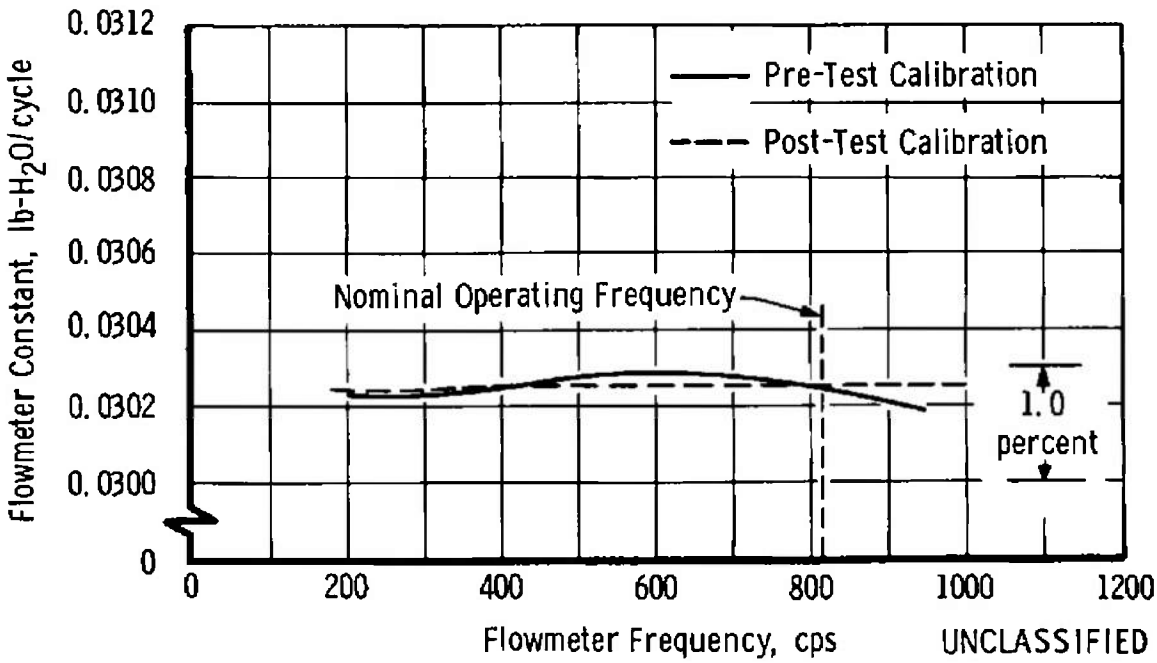

b. Fuel Flowmeter Calibration with Water in a Straight Pipe

Fig. I-8 Flowmeter Calibrations with Water

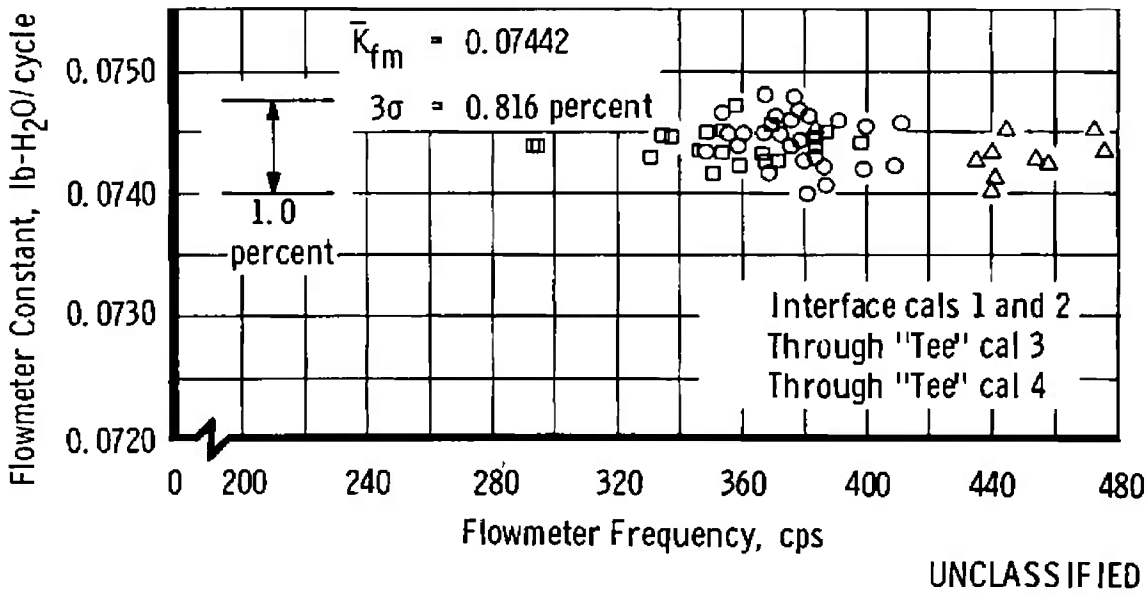

Fig. I-9 Flowmeter In-Place Calibrations with Propellant

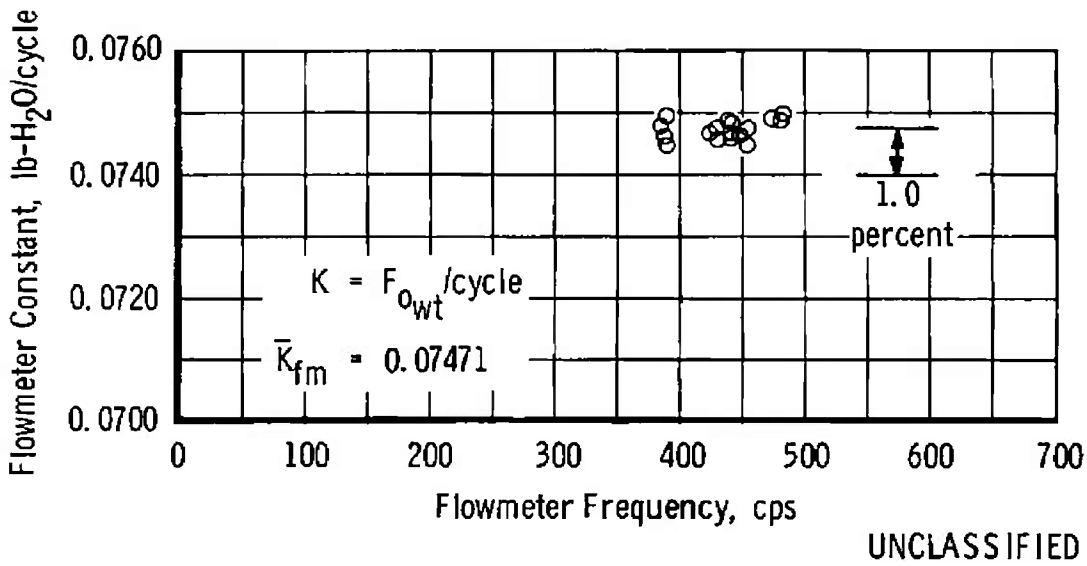

Fig. I-10 Flowmeter In-Place Calibration with Propellant

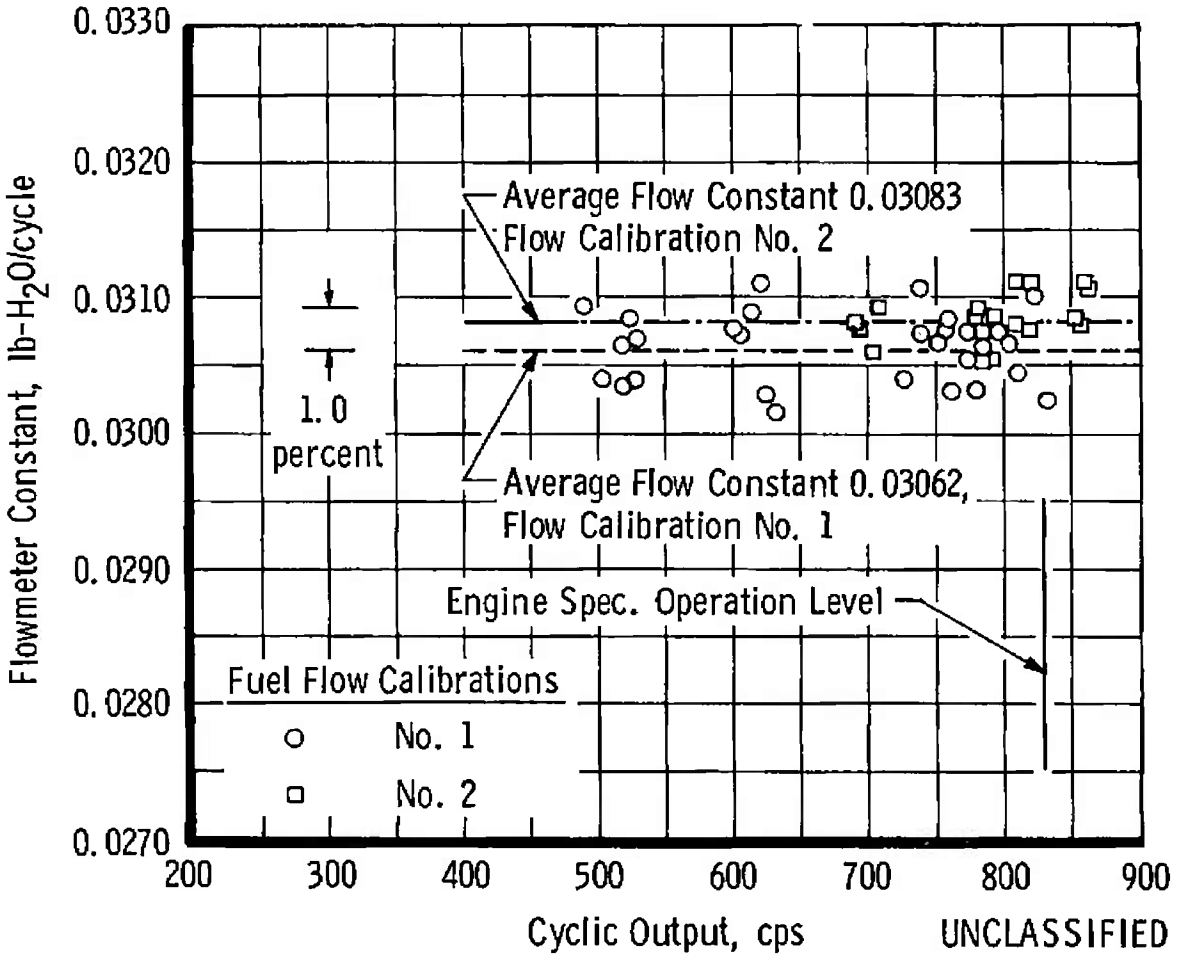

Fig. I-11 Flowmeter In-Place Calibrations with Propellant

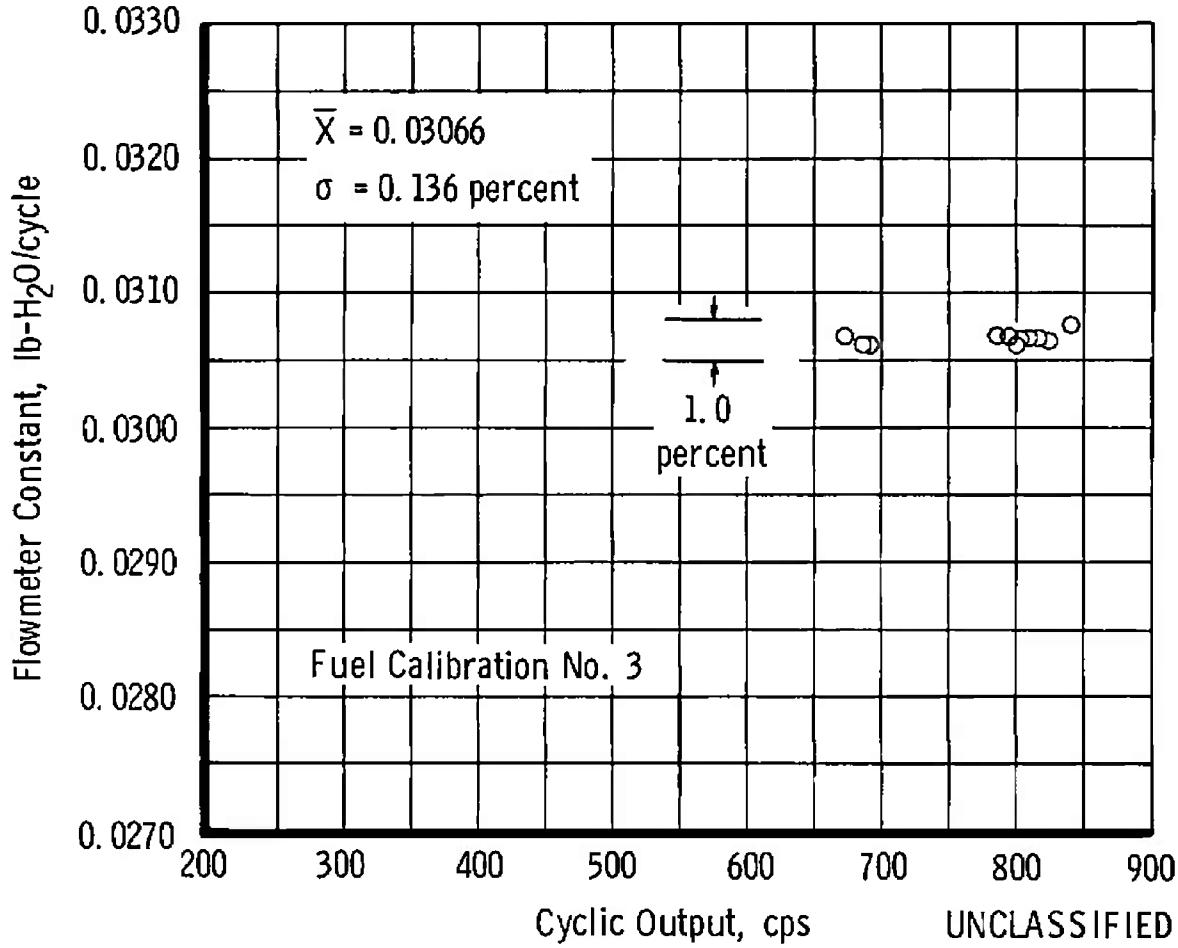

Fig. I-12 Flowmeter In-Place Calibration with Propellant

TABLE I-1
INSTRUMENT RECORDINGS

Parameter	Recorder
Propellant Weight Flowmeter Output	Magnetic Tape - Oscillograph-Counter
Diverter Valve Position	- Oscillograph-Counter
Sump Tank Pressure	- Strip Chart
Diverter Valve Inlet Pressure	
Diverter Valve Outlet Pressure	
Venturi Inlet Pressure	
Weigh Tank Pressure	- Strip Chart
Propellant Temperatures	- Strip Chart

TABLE I-2
OXIDIZER FLOWMETER CALIBRATIONS

Calibration Number	Configuration	Date
1	Interface	11-18-64
2	Interface	11-20-64
3	"tee"	12- 1-64
4	"tee"	1-21-65
5	"tee"	3- 3-65

FUEL FLOWMETER CALIBRATIONS

Calibration Number	Configuration	Date
1	"tee"	12-3-64
2	"tee"	1-14-65
3	"tee"	2-2-65

APPENDIX II
SUMMARY OF TESTS

A-Period (A-1)

(U) The first test firing (A-1) of Apollo Phase II was performed on December 15, 1964. The nozzle extension had been previously used during Apollo Phase I. This nozzle had incurred perforation (in the columbium section) during Phase I (Ref. 2) and had been repaired with a riveted patch. The patch was approximately 1.5 by 4 in. and was located about 12 in. from the mounting flange station. The unbaffled injector was a reconditioned unit that had been tested at the AGC facility. The primary objectives were to provide for propulsion system and test facility checkout and to obtain engine performance data for performance data comparisons.

(U) Propulsion system operation was normal, and no test hardware malfunctions occurred during this test.

B-Period (B-2, B-3)

(U) Completion of the checkout tests and a mixture ratio survey were scheduled for this test period. The period was terminated when test B-3 experienced a combustion stability monitor (CSM) shutdown.

(U) Other than the CSM shutdown, no incident occurred during these two tests.

C-Period (C-4 through C-9)

(U) The primary objectives were to complete the third test cell checkout firing and to evaluate rocket engine performance at various mixture ratios.

(U) Propulsion system operation was normal, and no test hardware malfunctions occurred during this period. Objectives were accomplished.

D-Period (D-10, D-11)

(U) During a preparatory axial thrust calibration at one-atmosphere pressure conditions, the engine thrust chamber propellant valve (TCV) opened inadvertently by a facility malfunction. The propellant lines had been pressurized to normal operating levels and apparently contained some propellant residuals. The resulting engine partial ignition, with

one-atmosphere pressure in the test cell, damaged the engine nozzle extension, the stiff links (installed in place of gimbal actuators), and the yaw link attachment bracket of the thrust/mount cage. The engine was removed from the test cell and rebuilt with a new combustion chamber. The previous chamber fitted the one available nozzle extension which had a J-flange mount. Consequently the engine was rebuilt with a modified J-flange chamber and installed in the cell for the D-Period tests. The same injector used for tests A, B, and C was also employed on this engine.

(U) The test objective was the determination of engine performance at low and high chamber pressure. Propulsion system operation was normal. On test D-10, the TCV closing was slow and was accomplished by the sequenced operation of the test facility auxiliary closing system.

E-Period (E-12 through E-17)

(U) The primary objective was to determine rocket engine performance at various chamber pressures from 80 to 125 psia.

(U) Test E-13 was terminated by the CSM during the ignition transient. With the exception of E-13, propulsion system operation was normal.

(U) Post-test inspection revealed that the yaw bracket was loose and that the AGC fuel line bellows was distorted.

F-Period (F-18 through F-24)

(U) The primary objectives of this period were to determine rocket engine performance at various mixture ratios and to obtain gimbal data. This was the first test (Phase I or Phase II) during which the Apollo engine was gimbaled.

(U) Two attempts were made to fire the engine, but the TCV did not open. These attempts were made using TCV bank B; all subsequent testing was made using TCV bank A.

(U) A power failure to the TCV pilot valves caused F-18 to be terminated approximately 1.3 sec after ignition. During the next tests (F-19 and F-20), propulsion system operation was normal. Test F-21 was terminated after 27 sec because of facility horizontal exhaust duct high temperature (approximately 1100°F). The maximum permissible is 1000°F. During Test F-22, the propulsion system operation was normal. Test F-23 was terminated because of excessive facility

horizontal exhaust duct temperature. For the last test (F-24), propulsion system operation was normal.

(U) The engine fuel line bellows was damaged prior to the start of the F-period. The damaged bellows did not cause any malfunction. The extent of the bellows damage did not increase during F-period operation.

G-Period (G-25 through G-28)

(U) The primary objective of this period was to determine rocket engine performance at various mixture ratios. The one-segment (120 deg) NAA heat shield was installed prior to this period. This was the first period during which the baffled injector and a nozzle extension with the columbium to the 40:1 and titanium to 60:1 area ratios were used.

(U) For Test G-25, an explosive charge was installed in the injector face to test the resistance of the new baffled injector to combustion instability. Stability recovery was satisfactory. Propulsion system operation was normal for tests G-25, 26, and 27.

(U) Test G-28 was terminated at 6 sec because of high test cell pressure. Test cell pressure was higher than normal for the G-period because of test cell leakage from atmosphere and from gaseous nitrogen (GN_2) which was used for instrument cooling. The higher pressure was not detected earlier in the testing cycle because the control room indication of test cell pressure was erroneous. At FS-2 + 3.5 sec, the fuel line pressure had decayed to approximately 10 psia. Post-test leak checks indicated flow through the TCV actuator overboard dump line. Further checks isolated the leakage to the broken 1/4-in. line on the thrust chamber enable valve.

(U) Post-test inspection revealed the nozzle extension to be slightly convoluted in the columbium section.

H-Period (H-29 through H-39)

(U) The primary objective of this test period was to determine rocket engine performance at various mixture ratios and during a simulated mission duty cycle. The 120-deg segment of the NAA heat shield remained for this period.

(U) Test cell pressure was again higher than normal for the first two tests of this period. Testing was temporarily stopped while a test cell inspection was made. This inspection revealed GN_2 leaking into the

test cell from the camera boxes. The GN_2 pressure was decreased, and testing was resumed to complete the period. This difficulty was repaired for the J and K test periods.

(U) For Test H-29, an explosive charge was installed on the injector face to test the ability of the baffled injector to recover from combustion instability. It is suspected that the charge did not detonate; no pressure pulse was noted on the oscillograph record.

(U) For Tests H-29 through 39, the propulsion system operation was normal.

J-K Periods (J-40 through J-48 and K-49 through K-54)

(U) The objectives of these two test periods were performance repeatability, minimum impulse bits, long-duration gimbal operation at high combustion chamber pressure, and mixture ratio (O/F) performance survey.

(U) The explosive charge was installed on the baffled injector face for Test J-40.

(U) Propulsion system operation was normal for all J and K tests. Combustion stability recovery from the explosive pulse charge oscillations was satisfactory.

UNCLASSIFIED DECLASSIFIED UNCLASSIFIED

Security Classification

DOCUMENT CONTROL DATA - R&D

(Security classification of title, body of abstract and indexing annotation must be entered when the overall report is classified)

1 ORIGINATING ACTIVITY (Corporate author)
Arnold Engineering Development Center
ARO, Inc., Operating Contractor
Arnold Air Force Station, Tennessee

2a REPORT SECURITY CLASSIFICATION
[redacted] Unclassified

2b GROUP
[redacted]

3 REPORT TITLE
SIMULATED ALTITUDE TESTING OF THE APOLLO SERVICE MODULE PROPULSION SYSTEM (REPORT I, PHASE II DEVELOPMENT TEST)

4 DESCRIPTIVE NOTES (Type of report and inclusive dates)
Report I, Phase II Development Test

This document has been approved for public release its distribution is unlimited. Per A.F. Letter dated 27 June, 73,

5 AUTHOR(S) (Last name, first name, initial)
Schulz, G. H. and DeFord, J. F., ARO, Inc.

6 REPORT DATE	7a TOTAL NO OF PAGES	7b NO OF REFS
January 1966	136	4

8a CONTRACT OR GRANT NO.	9a ORIGINATOR'S REPORT NUMBER(S)
AF 40(600)-1200	AEDC-TR-65-233
b System 921E	
c	9b OTHER REPORT NO(S) (Any other numbers that may be assigned this report)
d	N/A

10 AVAILABILITY/LIMITATION NOTICES
Qualified users may obtain copies of this report from DDC. ~~Release to foreign governments or foreign nationals must have prior approval of NASA-MSC.~~

11 SUPPLEMENTARY NOTES	12 SPONSORING MILITARY ACTIVITY
N/A	National Aeronautics and Space Administration, Manned Spacecraft Center, Houston, Texas

13 ABSTRACT The Apollo Service Module (S/M) propulsion system, tested at AEDC, consisted of the Aerojet-General Corporation AJ10-137 flight-type rocket engine and a North American Aviation ground test replica of the Apollo S/M propellant system and was subjected to simulated altitudes up to 120,000 ft during engine firing operation. The testing reported herein was conducted with the first three engine assemblies of the AEDC Phase II development program and included fifty-four test firings with an accumulated duration of 1561.2 sec. The primary objectives of the test were to check out system operation, define propulsion system altitude performance, and prove engine structural endurance over ranges of propellant mixture ratio and combustion chamber pressure. Engine gimbaling operations were performed during certain firings. Ballistic performance of the three engine assemblies tested is presented. Engine temperature data, the effect of ablation on the thrust vector, and a discussion of engine gimbal operation are also presented. (U)

DD FORM 1 JAN 64 1473

UNCLASSIFIED

Security Classification

14 KEY WORDS	LINK A		LINK B		LINK C	
	ROLE	WT	ROLE	WT	ROLE	WT
Apollo Service Module rocket engines liquid propellants simulated altitude testing propulsion system performance structural integrity gimballed engines						

INSTRUCTIONS

1. ORIGINATING ACTIVITY: Enter the name and address of the contractor, subcontractor, grantee, Department of Defense activity or other organization *(corporate author)* issuing the report.

2a. REPORT SECURITY CLASSIFICATION: Enter the overall security classification of the report. Indicate whether "Restricted Data" is included. Marking is to be in accordance with appropriate security regulations.

2b. GROUP: Automatic downgrading is specified in DoD Directive 5200.10 and Armed Forces Industrial Manual. Enter the group number. Also, when applicable, show that optional markings have been used for Group 3 and Group 4 as authorized

3. REPORT TITLE: Enter the complete report title in all capital letters. Titles in all cases should be unclassified. If a meaningful title cannot be selected without classification, show title classification in all capitals in parenthesis immediately following the title.

4. DESCRIPTIVE NOTES: If appropriate, enter the type of report, e.g., interim, progress, summary, annual, or final. Give the inclusive dates when a specific reporting period is covered.

5. AUTHOR(S): Enter the name(s) of author(s) as shown on or in the report. Enter last name, first name, middle initial. If military, show rank and branch of service. The name of the principal author is an absolute minimum requirement.

6. REPORT DATE: Enter the date of the report as day, month, year, or month, year. If more than one date appears on the report, use date of publication.

7a. TOTAL NUMBER OF PAGES: The total page count should follow normal pagination procedures, i.e., enter the number of pages containing information.

7b. NUMBER OF REFERENCES: Enter the total number of references cited in the report.

8a. CONTRACT OR GRANT NUMBER: If appropriate, enter the applicable number of the contract or grant under which the report was written.

8b, 8c, & 8d. PROJECT NUMBER: Enter the appropriate military department identification, such as project number, subproject number, system numbers, task number, etc.

9a. ORIGINATOR'S REPORT NUMBER(S): Enter the official report number by which the document will be identified and controlled by the originating activity. This number must be unique to this report.

9b. OTHER REPORT NUMBER(S): If the report has been assigned any other report numbers *(either by the originator or by the sponsor)*, also enter this number(s).

10. AVAILABILITY/LIMITATION NOTICES: Enter any limitations on further dissemination of the report, other than those imposed by security classification, using standard statements such as:

(1) "Qualified requesters may obtain copies of this report from DDC."

(2) "Foreign announcement and dissemination of this report by DDC is not authorized."

(3) "U. S. Government agencies may obtain copies of this report directly from DDC. Other qualified DDC users shall request through

_____."

(4) "U. S. military agencies may obtain copies of this report directly from DDC. Other qualified users shall request through

_____."

(5) "All distribution of this report is controlled. Qualified DDC users shall request through

_____."

If the report has been furnished to the Office of Technical Services, Department of Commerce, for sale to the public, indicate this fact and enter the price, if known.

11. SUPPLEMENTARY NOTES: Use for additional explanatory notes.

12. SPONSORING MILITARY ACTIVITY: Enter the name of the departmental project office or laboratory sponsoring *(paying for)* the research and development. Include address.

13 ABSTRACT: Enter an abstract giving a brief and factual summary of the document indicative of the report, even though it may also appear elsewhere in the body of the technical report. If additional space is required, a continuation sheet shall be attached.

It is highly desirable that the abstract of classified reports be unclassified. Each paragraph of the abstract shall end with an indication of the military security classification of the information in the paragraph, represented as *(TS)*, *(S)*, *(C)*, or *(U)*

There is no limitation on the length of the abstract. However, the suggested length is from 150 to 225 words.

14. KEY WORDS: Key words are technically meaningful terms or short phrases that characterize a report and may be used as index entries for cataloging the report. Key words must be selected so that no security classification is required. Identifiers, such as equipment model designation, trade name, military project code name, geographic location, may be used as key words but will be followed by an indication of technical context. The assignment of links, rules, and weights is optional.